Spectroscopy and Structure of the Alkali Hydride Diatomic Molecules and their Ions

Cite as: Journal of Physical and Chemical Reference Data **20**, 153 (1991); https://doi.org/10.1063/1.555906
Submitted: 25 September 1989 . Published Online: 15 October 2009

William C. Stwalley, Warren T. Zemke, and Sze Cheng Yang

Spectroscopy and Structure of the Alkali Hydride Diatomic Molecules and Their Ions

William C. Stwalley

Center for Laser Science and Engineering, and Departments of Chemistry, and of Physics and Astronomy, University of Iowa, Iowa City, IA 52242

Warren T. Zemke

Department of Chemistry, Wartburg College, Waverly, IA 50677

and

Sze Cheng Yang

Department of Chemistry, University of Rhode Island, Kingston, RI 02881

Received September 25, 1989; revised manuscript received July 3, 1990

All significant experimental measurements and theoretical calculations of the spectroscopy and structure of the alkali hydrides NaH, KH, RbH and CsH, and the corresponding alkali deuterides, are identified and reviewed. Published molecular constant determinations from conventional and laser spectroscopy are evaluated; recommended spectroscopic constants for $X\ ^1\Sigma^+$ and $A\ ^1\Sigma^+$ states are tabulated. RKR and hybrid potential energy curves are evaluated; recommended RKR curves for $X\ ^1\Sigma^+$ and $A\ ^1\Sigma^+$ states are tabulated. Ground state dissociation energy (D_e) estimates are evaluated; recommended $X\ ^1\Sigma^+$ and $A\ ^1\Sigma^+$ state D_e and D_o values are tabulated. Accurate electronic structure calculations (Hartree Fock or better) are listed and described briefly; all excited electronic states considered are included. Experimental and theoretical radiative and dipole properties are noted and discussed. Calculations on the positive and negative ions of the four diatomic alkali hydrides are also listed and described briefly.

Key words: alkali hydride; CsH; CsH^+; CsH^-; dissociation energy; electronic structure calculation; KH; KH^+; KH^-; NaH; NaH^+; NaH^-; potential energy curve; RbH; RbH^+; RbH^-; spectroscopic constant.

Contents

1. Introduction 154
2. NaH 156
   2.1. Conventional Spectroscopy 156
   2.2. Laser Spectroscopy 156
   2.3. Spectroscopic Constants 157
   2.4. Potential Energy Curves 159
   2.5. Dissociation Energy 160
   2.6. Electronic Structure Calculations 160
   2.7. Radiative and Dipole Properties 160
   2.8. Other Properties 163
   2.9. Positive Ions 163
   2.10. Negative Ions 163
   2.11. Other Comments 163
3. KH 164
   3.1. Conventional Spectroscopy 164
   3.2. Laser Spectroscopy 164
   3.3. Spectroscopic Constants 164
   3.4. Potential Energy Curves 165
   3.5. Dissociation Energy 166
   3.6. Electronic Structure Calculations 166
   3.7. Radiative and Dipole Properties 168
   3.8. Other Properties 168
   3.9. Positive Ions 168
   3.10. Negative Ions 168
   3.11. Other Comments 168
4. RbH 168
   4.1. Conventional Spectroscopy 168
   4.2. Laser Spectroscopy 168
   4.3. Spectroscopic Constants 170
   4.4. Potential Energy Curves 170

4.5. Dissociation Energy 171
4.6. Electronic Structure Calculations 171
4.7. Radiative and Dipole Properties 171
4.8. Other Properties 173
4.9. Positive Ions 173
4.10. Negative Ions 173
4.11. Other Comments 173
5. CsH 173
5.1. Conventional Spectroscopy 173
5.2. Laser Spectroscopy 174
5.3. Spectroscopic Constants 174
5.4. Potential Energy Curves 174
5.5. Dissociation Energy 176
5.6. Electronic Structure Calculations 176
5.7. Radiative and Dipole Properties 179
5.8. Other Properties 179
5.9. Positive Ions 180
5.10. Negative Ions 180
5.11. Other Comments 180
6. Discussion and Conclusions 180
6.1. Conventional Spectroscopy 180
6.2. Laser Spectroscopy 180
6.3. Spectroscopic Constants 181
6.4. Potential Energy Curves 181
6.5. Dissociation Energy 182
6.6. Electronic Structure Calculations 182
6.7. Radiative and Dipole Properties 183
6.8. Other Properties 183
6.9. Positive Ions 183
6.10. Negative Ions 183
7. Acknowledgments 183
8. References 183

List of Tables

1.1. Recommended molecular structure constants for the alkali hydrides 155
2.1. Dunham coefficients $Y_{ij}(cm^{-1})$ for NaH $X\,^1\Sigma^+$ 157
2.2. Recommended spectroscopic constants for NaH 157
2.3. RKR potential energy curve of the $X\,^1\Sigma^+$ state of NaH 159
2.4. RKR potential energy curve of the $A\,^1\Sigma^+$ state of NaH 159
2.5. Estimated D_e values for NaH 160
2.6. High quality calculations of NaH 161
2.7. High quality calculations of NaH^+ 162
2.8. High quality calculations of NaH^- 163
3.1. Recommended spectroscopic constants for KH 165
3.2. RKR potential energy curve of the $X\,^1\Sigma^+$ state of KH 165
3.3. RKR potential energy curve of the $A\,^1\Sigma^+$ state of KH 165
3.4. Estimated D_e values for KH 166
3.5. High quality calculations of KH 167
3.6. High quality calculations of KH^+ and KH^- .. 169
4.1. Recommended spectroscopic constants for RbH 170
4.2. RKR potential energy curve of the $X\,^1\Sigma^+$ state of RbH 170
4.3. RKR potential energy curve of the $A\,^1\Sigma^+$ state of RbH 170
4.4. High quality calculations of RbH 172
4.5. High quality calculations of RbH^+ and RbH^- 172
5.1. Recommended spectroscopic constants for CsH 173
5.2. RKR potential energy curve of the $X\,^1\Sigma^+$ state of CsH 174
5.3. RKR potential energy curve of the $A\,^1\Sigma^+$ state of CsH 175
5.4. Estimated D_e values for CsH 175
5.5. High quality calculations of CsH 177
5.6. High quality calculations of CsH^+ and CsH^- . 178
6.1. Range of vibrational levels observed 181
6.2. Energy and derivatives of the adiabatic $X\,^1\Sigma^+$ and $A\,^1\Sigma^+$ state potentials at the two-state ionic-covalent crossing distance R_c 181

List of Figures

1. Potential energy curves of NaH 156
2. RKR potential energy curves of KH, RbH, and CsH 158

1. Introduction

In the past decade there has been a surge in interest in the alkali hydrides. For example, as seen from Tables 1.1 and 2.1, nearly all of the experimental advances occurred in the 1980s; fifty percent of the references cited in this paper are from the past ten years. Although valuable compendia on the alkali hydrides are available [HER 50, GAY 68, ROS 70, HUB 79], their coverage is not confined to the alkali hydrides and does not include the many contributions of the 1980s. Hence the need for this current critical review and exhaustive compilation on the alkali hydrides and their ions.

Initially we sought to include lithium hydride with the other alkali hydrides in this review. However, as we proceeded it became clear that LiH was worthy of a single review paper. For LiH there is a considerably larger and different field of experimental data available in the literature: extensive data are available on the significantly different isotopic combinations ^{6}LiH, ^{6}LiD, ^{7}LiH and ^{7}LiD; spectroscopic data include more than just the $X\,^1\Sigma^+$ ground and first excited $A\,^1\Sigma^+$ electronic states; results of sufficiently high resolution exist to enable detailed investigation of the breakdown of the Born-Oppenheimer approximation. Because of its simple electronic structure, LiH (and LiH^+, LiH^-) is one of the favorite systems for testing different quantum mechanical techniques. The literature contains a multitude of LiH theoretical calculations of varying utility and complexity, often distinct from the types of calculations noted in this review. Our critical

review and bibliography on lithium hydride will be forthcoming.

The next four sections examine in order the four molecular systems NaH and its ions (Sec. 2), KH and its ions (Sec. 3), RbH and its ions (Sec. 4), and CsH and its ions (Sec. 5). The beginning of each section includes the sources of experimental data (Subsecs. 1 and 2 on conventional and laser spectroscopy, respectively) and an analysis of the data; recommended spectroscopic constants for $X\ ^1\Sigma^+$ and $A\ ^1\Sigma^+$ states are identified and tabulated in Subsection 3. Subsection 4 examines available RKR [RYD 31] potential energy curves and tabulates the recommended ones for $X\ ^1\Sigma^+$ and $A\ ^1\Sigma^+$ states; additional hybrid potential energy curves are evaluated as well. Subsection 5 includes a survey and recommendation for the ground state dissociation energy. Because an ionic-covalent avoided crossing between the $X\ ^1\Sigma^+$ and $A\ ^1\Sigma^+$ state potential energy curves is common to all the alkali hydrides, the behavior of each A state is quite anomalous [MUL 36, HER 50, GAY 68]. The typical A state potential curve is flat-bottomed (see Figs. 1 and 2) and highly anharmonic: the anharmonicity constant $\omega_e x_e$ is negative and the vibrational energy levels initially become more rather than less widely separated with increasing v. The shape of the X state potential curve is also influenced by this ionic-covalent avoided crossing interaction. Although this avoided-crossing makes the typical Birge-Sponer extrapolation unreliable for the alkali hydrides [STW 78, YAN 83], for reasons of completeness, we include in our survey estimates of D_e by Birge-Sponer extrapolation.

Next electronic structure calculations are identified in Subsection 6. Radiative and dipole properties are reported in Subsec. 7, as are other noteworthy properties in Subsection 8. Finally, short subsections on positive (9) and negative (10) ion studies are presented; tables of all high quality calculations (at the Hartree-Fock level or better) briefly list details and results of these theoretical studies.

The last section (6) presents an overview of existing studies and conclusions on the alkali hydrides.

Common symbols and definitions used throughout the paper are introduced now; shorthand notations used to describe *ab initio* calculations will be introduced in the appropriate subsection. Common energy units used are cm^{-1} and hartree units: 1 a.u. = 1 hartree $\doteqdot$ 219474.63067 cm^{-1}, 1 eV $\doteqdot$ 8065.541 cm^{-1}. More complete lists are available in [COH 87]. All reduced masses are based on the mass of carbon-12 equaling exactly 12. [HUB 79]. Distance units used are Å and a_o: 1 a_o = 0.529177249 Å. (1 Å = 10^{-10} m.)

The term values are written in the familiar Dunham expansion [HER 50, HUB 79]:

$$T_{vJ} = \sum_{ij} Y_{ij}(v + 1/2)^i[J(J+1)]^j,$$

where the Y_{ij}'s are called Dunham or ij spectroscopic constants. The vibrational energy $G(v) = \sum_{i\geq 1} Y_{i0}(v+1/2)^i$

$$= Y_{10}(v + 1/2) + Y_{20}(v + 1/2)^2 + Y_{30}(v + 1/2)^3 + \ldots$$

$$= \omega_e(v + 1/2) - \omega_e x_e(v + 1/2)^2 + \omega_e y_e(v + 1/2)^3 + \ldots$$

The rotational constant $B_v = \sum_{i\geq 0} Y_{i1}(v + 1/2)^i$

$$= Y_{01} + Y_{11}(v + 1/2) + Y_{21}(v + 1/2)^2 + \ldots$$

$$= B_e - \alpha_e(v + 1/2) + \gamma_e(v + 1/2)^2 + \ldots .$$

The equilibrium internuclear distance R_e is determined from the rotational constant B_e [HER 50].

In all our vibrational energy levels we include the Y_{00} correction, as well as in the zero point energy ZPE (see footnotes, Table 1.1). T_e is the electronic energy calculated from the bottom of the potential well of the $X\ ^1\Sigma^+$ ground state (by definition zero) to the bottom of the potential well of the excited state ($A\ ^1\Sigma^+$ in this paper); ν_{00} is the experimental transition energy from the ground state $v'' = 0$ vibrational energy level to the excited state $v' = 0$ vibrational energy level (with $J'' = J' = 0$). The dissociation energy D_o is defined as the energy of the separated atoms relative to the lowest existing level of the molecule, the ZPE. D_e is defined with respect to the bottom of the potential well; hence $D_e = D_o$ + ZPE.

Common recommended spectroscopic constants and dissociation energies for the $X\ ^1\Sigma^+$ and $A\ ^1\Sigma^+$ states are listed in Table 1.1. Additional constants may be found in the individual sections.

TABLE 1.1. Recommended molecular structure constants for the alkali hydrides

	$X\ ^1\Sigma^+$ state				
Molecule	$D_e''(cm^{-1})$[a]	$D_o''(cm^{-1})$[b]	R_e''(Å)	$\omega_e''(cm^{-1})$	Ref.[c]
NaH	15,900	15,318.	1.8870	1171.759	MAK 89
KH	14,772.7	14,282.6	2.2401	986.651	HUS 86
RbH	14,580	14,115.	2.3668	937.105	MAG 88A
CsH	14,791.2	14,348.2	2.4943	891.251	MAG 88B

	$A\ ^1\Sigma^+$ state					
	$T_e(cm^{-1})$[a]	$D_e'(cm^{-1})$[d]	$D_o'(cm^{-1})$[b]	R_e'(Å)	$\omega_e'(cm^{-1})$	Ref.[c]
NaH	22,713.	10,143.	9,983.	3.1934	317.56	ORT 80
KH	19,060.	8,698.	8,583.	3.7629	222.74	YAN 80
RbH	18,218.	8,941.	8,832.	3.8719	211.74	KAT 85
CsH	17,839.	8,130.	8,042.	3.9819	169.06	HSI 78

[a]Recommended values are described in the tables and text.

[b]$D_o = D_e$ − ZPE, where the zero point energy ZPE = $G(0) + Y_{00}$ with

$$G(0) = \frac{Y_{10}}{2} + \frac{Y_{20}}{4} + \frac{Y_{30}}{8} + \frac{Y_{40}}{16} + \ldots$$

and

$$Y_{00} = \frac{Y_{01}}{4} - \frac{Y_{11}Y_{10}}{12Y_{01}} + \frac{Y_{11}^2Y_{10}^2}{144Y_{01}^3} + \frac{Y_{20}}{4}$$

[c]Values of ZPE, R_e and ω_e are from the reference cited.

[d]$D_e' = D_e'' + [E(np, {}^2P_{1/2}) - E(ns, {}^2S)]$ where atomic transition energy values $E(np, {}^2P_{1/2}) - E(ns, {}^2S)$ can be found in [MOO 71].

2. NaH

2.1. Conventional Spectroscopy

All observations of electronic spectra of NaH involve the $A\ ^1\Sigma^+ - X\ ^1\Sigma^+$ band system. Hori first observed the absorption [HOR 30] and emission [HOR 31] spectrumof NaH in the early 1930s, but assigned incorrect $A\ ^1\Sigma^+$ vibrational quantum numbers. Olsson photographed NaH and NaD in absorption and established the correct vibrational numbering [OLS 35]. Pankhurst photographed NaH in emission, reporting information on 66 bands including $v'' = 0 - 8$ and $v' = 1 - 20$ [PAN 49]. Orth and coworkers extended these results to include $v' = 0$ [ORT 80].

The rotational spectra of NaH and NaD have been studied by Sastry, Herbst and DeLucia [SAS 81, SAS 81A]. The recent studies of Maki and Olson [MAK 89] report observations of vibrational transitions in the infrared ($v'' = 1 \leftarrow 0, 2 \leftarrow 1, 3 \leftarrow 2$).

2.2. Laser Spectroscopy

Initial observations involved the $A\ ^1\Sigma^+ - X\ ^1\Sigma^+$ band system. The first observation of NaH laser-induced fluorescence excitation spectrum was by Dagdigian in a supersonic NaH molecular beam (with a rotational temperature of 230 ± 50 K) [DAG 76]. A portion of the (8, 0) band is displayed but line positions are not reported (two lines in the (11, 0) band were subsequently displayed [DAG 79]). Shortly thereafter, Baltayan, Jourdan and Nedelec reported spectrally resolved fluorescence from $A\ ^1\Sigma^+$ ($v' = 4, J' = 11$) NaH in a high frequency discharge [BAL 76]. Extensive spectrally resolved laser-induced fluorescence measurements are described by Giroud and Nedelec [GIR 80], but unfortunately only the exciting transitions are reported and not the line positions of the fluorescence spectra. Some seven different NaH fluorescent series were excited, involving upper levels $v' = 6 - 14$ fluorescing to $v'' \leq 15$. Also six different NaD fluorescent series were excited, involving $v' = 10 - 15$ fluorescing to $v'' \leq 20$. An additional eight NaH fluorescent series were later reported without line positions [NED 83], involving $v' \leq 21$ fluorescing to $v'' \leq 19$. Emission from $v' = 21$ includes bound-free emission peaking at 705, 717 and 730 nm as well as bound-bound emission for $\lambda \lesssim 700$ nm. Excitation spectra of the (15, 0) band of NaH in a supersonic beam were reported by Brieger *et al.* [BRI 81]. A few NaH impurity lines are shown in the spectrally resolved laser-induced fluorescence spectrum of Na_2 excited by a 351.1 nm argon ion laser [BAH 84].

Leopold *et al.* [LEO 87] obtained rotational spectra in the $v'' = 0$ ($J'' = 7 \leftarrow 6$), 1 ($J'' = 8 \leftarrow 7$) and 2,3 ($J'' = 6 \leftarrow 5$) vibrational levels of the $X\ ^1\Sigma^+$ state of NaH. They used tunable far-infrared radiation generated from the difference frequency between two CO_2 lasers. Magg and Jones [MAG 88] observed a vibration-rotation spectrum for NaH using diode laser spectroscopy. They measured nineteen transitions in the $v'' = 1 \leftarrow 0$ band and seven in the $v'' = 2 \leftarrow 1$ band.

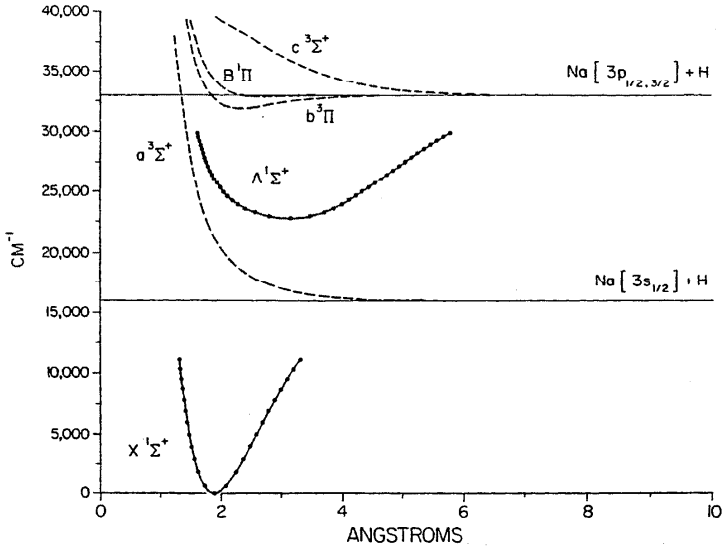

FIG. 1. Potential energy curves of NaH. RKR curves are designated by solid lines connecting the turning points. Dashed lines are *ab initio* curves.

TABLE 2.1. Dunham coefficients Y_{ij} (cm^{-1}) for NaH $X\ ^1\Sigma^+$

ZPE	Y_{00}	Y_{10}	Y_{20}	Y_{30}	10^3Y_{40}	10^4Y_{50}	Y_{01}	Y_{11}	10^3Y_{21}	10^5Y_{31}	Reference
581.42	0.23	1172.2	−19.72	0.160	−5.		4.886	−0.129			PAN 49
582.71	−0.04	1176.1	−21.19				4.890	−0.131			GIR 80
581.48	0.66	1171.4	−19.52	0.148	−5.2		4.902	−0.1386	1.895	−11.6	ORT 80
—	—	1171.2					4.9033622	−0.137061	1.095	−3.2	SAS 81
(583.84)[a]	(−2.67)[a]	1188.22801	−31.95473	3.310086	−359.896	180.9055[b]	—				NED 83
581.59	0.63	1171.750	−19.7405	0.19225	−7.4914		4.90319	−0.13920	1.8993	−10.676	ZEM 84
—	—	—					4.9033634	−0.137092	1.1121	−3.5081	LEO 87
581.52	0.72	1171.0946	−18.99555				4.9033568	−0.137063	1.0949	−3.19	MAG 88
581.80	0.98	1171.40	−19.58	0.175	−11.1	6.4[c]	4.902	−0.1460	6.310	−0.939[d]	PAR 88
581.60	0.59	1171.75909	−19.52352	0.12131	−0.590	−2.235	4.90336382	−0.13709097	1.111351	−3.492	MAK 89[e]

[a]Based on values of Y_{01} and Y_{11} from [GIR 80] plus Y_{10} and Y_{20} from [NED 83].
[b]$Y_{60} = -3.4585 \times 10^{-4}$
[c]$Y_{60} = -2 \times 10^{-5}$
[d]$Y_{41} = 6.2 \times 10^{-5}$, $Y_{51} = -2 \times 10^{-6}$
[e]Recommended values. Other higher order constants include:
$Y_{02} = 0.34347675 \times 10^{-3}$, $Y_{12} = 0.490898 \times 10^{-5}$, $Y_{22} = -0.8895 \times 10^{-7}$,
$Y_{03} = 0.21331016 \times 10^{-7}$, $Y_{13} = 0.1641 \times 10^{-10}$, $Y_{23} = -0.2476 \times 10^{-10}$,
$Y_{04} = -0.185175 \times 10^{-11}$, $Y_{14} = -0.9465 \times 10^{-13}$, $Y_{05} = 0.193516 \times 10^{-15}$,
$Y_{15} = 0.1683 \times 10^{-16}$, $Y_{06} = -0.24844 \times 10^{-19}$.

TABLE 2.2. Recommended spectroscopic constants for NaH[a]

	$X\ ^1\Sigma^+$(MAK 89)	$A\ ^1\Sigma^+$ (ORT 80)
ZPE	581.56[b]	160.35
Y_{00}	0.59	0.86
Y_{10}	1171.75909	317.56
Y_{20}	−19.52352	2.703
Y_{30}	0.12131	0.262
10^3Y_{40}	−0.590	−39.
10^4Y_{50}	−2.235	16.
10^5Y_{60}		−2.4
Y_{01}	4.90336382	1.7121
Y_{11}	−0.13709097	0.09152
10^3Y_{21}	1.111351	−12.3
10^4Y_{31}	−3.492	6.72
10^5Y_{41}		−1.8
10^6Y_{51}		0.18

[a]All entries in cm^{-1} units.
[b]Average of [MAK 89] and [MAG 88].

2.3. Spectroscopic Constants

The spectroscopic constants of the $X\ ^1\Sigma^+$ state of NaH have been determined by many workers [HOR 31, OLS 35, PAN 49, ORT 80, GIR 80, SAS 81, NED 83, LEO 87, MAG 88, PAR 88, MAK 89]. Huber and Herzberg [HUB 79] considered the first three references and recommended the vibrational constants of [PAN 49] and the rotational constants of [OLS 35]. The combined fit of conventional spectra by [ORT 80] provided improved constants, but the two types of new data (moderate precision high v'' data [GIR 80, NED 83] and high precision low v'' data [SAS 81, SAS 81A]) suggested the need for a new combined fit. Such a fit has been carried out [ZEM 84] using all data for $v'' \leq 11$. Higher v'' values [GIR 80, NED 83] were not included in the fit because of the erratic behavior of $B_{v''}$ for these levels. This erratic behavior is presumably a result of measurements with only moderate precision of only a few J'' levels. Jenč and Brandt made a comparison of the ground states of the alkali hydrides with their reduced potential curve (RPC) method [JEN 85, JEN 86]. Their analysis was that the RPC curve based on the NaH constants of [GIR 80] showed significant irregularities at larger distances, consistent with our analysis of the reliability of the $v'' > 11$ data.

The high precision low v'' data of [LEO 87] led to rotational constants in very good agreement with those of [SAS 81]. Magg and Jones [MAG 88] report vibrational and rotational constants, the latter virtually identical to those of [SAS 81]. Their two vibrational constants are based on data [SAS 81] which includes v'' for only the lowest levels ($v'' \leq 3$). Pardo *et al.* [PAR 88] included earlier NaH and NaD data in their analysis and determined both vibrational and rotational constants. Their rotational constants differ slightly from the accurate ones [SAS 81, LEO 87, MAG 88], presumably due to the inclusion of the data up to $v'' \leq 15$ [GIR 80, NED 83]. Maki and Olson [MAK 89] combined their infrared measurements with earlier far infrared [LEO 87] and millimeter wave measurements [SAS 81] and with vibrational spacings $\Delta G(6.5)$ and $\Delta G(7.5)$ [ORT 80] to obtain a very precise set of Dunham coefficients. They did not include any data for $v'' = 9 - 15$ from [GIR 80, NED 83] presumably because of the erratic behavior already noted. They obtained a better fit of the pure rotational transitions when they included the NaD data of [SAS 81] to determine a second set of (isotopically combined) Dunham coeffecients. The isotopically combined five vibrational plus four rotational constants for the $X\ ^1\Sigma^+$ state of NaH [MAK 89] reported in Table 2.2 are the recommended constants for $v'' \leq 8$. Clearly, precise laser fluorescence measurements for high v'' levels (similar to those for KH [HUS 86] and CsH [CRE 84]) should be obtained to reliably extend the range of the spectroscopic constants (and the RKR potentials discussed below).

The spectroscopic constants of the $X\ ^1\Sigma^+$ state of NaD have been determined by [OLS 35, GIR 80, SAS 81]. As in NaH, the new data (moderate precision high v'' data [GIR 80] and high precision low v'' data [SAS 81, SAS 81A]) suggested the need for a new combined fit. However, because of the erratic behavior of $B_{v''}$, especially for high v'', in [GIR 80], we have adopted for the present the limited rotational fit of [SAS 81] which they state gives good agreement with [GIR 80] up to $v'' = 12$, and the vibrational fit of [GIR 80], which is presumably adequate up to $v'' = 19$. The erratic behavior of the $B_{v''}$ values of [GIR 80] suggests significant uncertainties ($\pm$ 1 cm^{-1}?) in some of their $G(v'')$ values as well. However, their low v'' results seem reliable: the $\Delta G(1/2)$ values are 826.10 cm^{-1} [OLS 35], and 825.3 cm^{-1} [GIR 80]; the B_0 and B_1 values are 2.5315 and 2.4795 cm^{-1} [OLS 35] and 2.522 and 2.479 cm^{-1} [GIR 80], respectively.

Because of the numerous measurements and analyses in recent years, we have chosen for the $X\ ^1\Sigma^+$ state of NaH to present a comparison and chronology of the Dunham coefficients found in the literature; see Table 2.1. The agreement in rotational constants (identical precision to the sixth digit in Y_{01} and to the fourth digit in Y_{11}) by four independent investigations [SAS 81, LEO 87, MAG 88, MAK 89] is remarkable! In our opinion, the current recommended values for the dominant vibrational (Y_{10}, Y_{20}) and rotational (Y_{01}, Y_{11}, Y_{21}) constants are highly accurate and very precise. Even the value for the zero point energy seems to have converged to ZPE = 581.56 ($\pm$ 0.04 cm^{-1}). The listed uncertainty is based on the two most precise determinations [MAG 88, MAK 89]. Examination of Table 2.1 identifies two sets of constants [GIR 80, NED 83] that are clearly out of line with the recommended values. Similar extensive comparisons and analyses, whenever possible, have been made for all spectroscopic constants recommended in this paper. For reasons of brevity, we will hereafter give a shorter rationale for our recommendations.

The spectroscopic constants of the $A\ ^1\Sigma^+$ state of NaH have been determined by [OLS 35, PAN 49, ORT 80, PAR 88] (the results of [HOR 31] assume an incorrect A state vibrational numbering). There is apparently a fitting error in the rotational (but not vibrational) constants of [PAN 49] (see [ORT 80]). [PAR 88] report constants that are quite similar to those of [ORT 80]. Although the rotational constants of [PAR 88] reproduce their $B_{v'}$ values, there is an inconsistency between their reported vibrational constants and $G(v')$ values. The constants of [ORT 80] are recommended.

The spectroscopic constants for the $A\ ^1\Sigma^+$ state of NaD have been estimated by mass-reduced scaling [STW 75] of the NaH results. This is necessary since reported NaD results include only $v' = 7 - 17$ [OLS 35] and $v' = 10 - 15$ [GIR 80]. An extrapolation from a limited number of vibrational levels to the minimum of the potential curve would be highly uncertain, more than the uncertainty caused by the Born-Oppenheimer breakdown between NaH and NaD. An estimate of the uncertainty can be obtained by examining the more complete results for LiH (see [VID 82, VID 84, CHA 86] and the references therein).

Based on the observed ν_{00} = 22291.8 cm^{-1} [ORT 80] and the zero point energies for the X and A states (see Table 2.2.), we obtain a recommended value of T_e = 22713.0 cm^{-1} for the $A\ ^1\Sigma^+$ state. The uncertainty should be $\sim$5 cm^{-1} (the uncertainty of the $A\ ^1\Sigma^+$ state zero point energy).

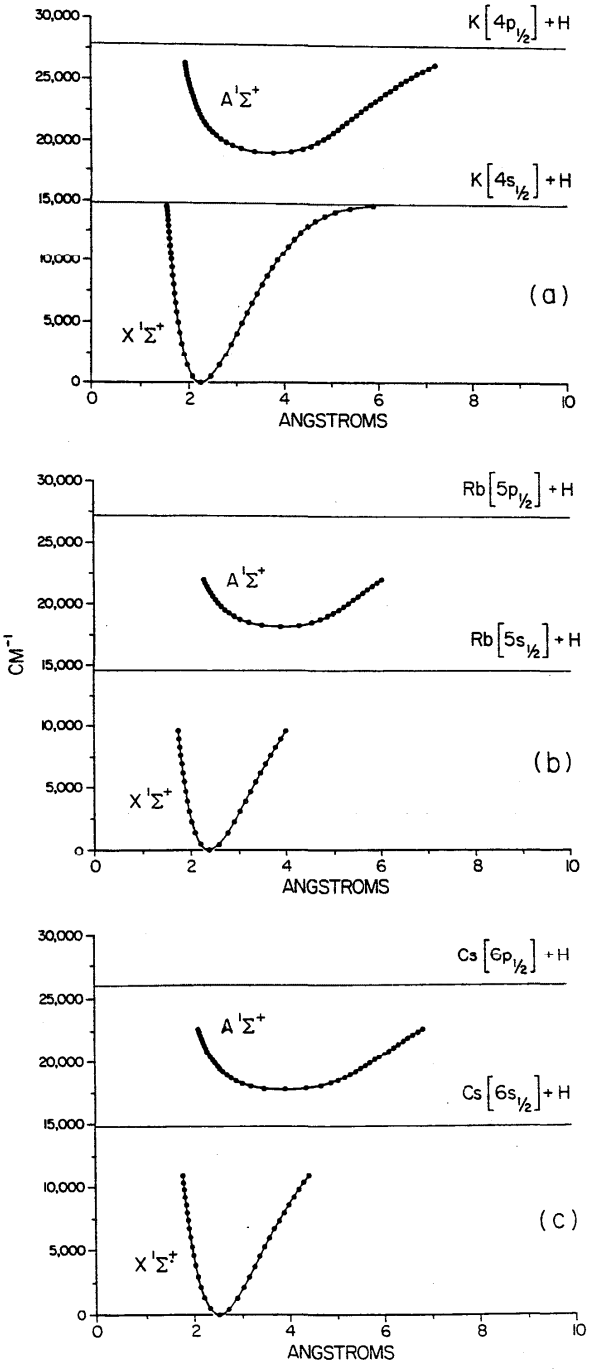

FIG. 2. RKR potential energy curves of KH (a), RbH (b) and CsH (c).

TABLE 2.3. RKR potential energy curve of the $X\ ^1\Sigma^+$ state of NaH [MAK 89]

v	$[G(v) + Y_{00}]$ (cm^{-1})	R_{v-} (Å)	R_{v+} (Å)
0	581.6038	1.7300	2.0777
1	1714.7055	1.6326	2.2433
2	2809.8163	1.5731	2.3729
3	3867.5789	1.5288	2.4889
4	4888.5546	1.4933	2.5981
5	5873.1967	1.4636	2.7035
6	6821.8237	1.4380	2.8070
7	7734.5923	1.4157	2.9098
8	8611.4708	1.3959	3.0129

Reduced mass μ = 0.96549966 for ^{23}NaH [HUB 79].

2.4. Potential Energy Curves

The RKR potential energy curve of the NaH $X\ ^1\Sigma^+$ state has been calculated by [NUM 74, ORT 80, GIR 80, NED 83, ZEM 84, PAR 88]. The results of [ZEM 84] and [PAR 88] agree well with the curve we generated from the mass-reduced Dunham constants of [MAK 89] for $v'' \leq 8$. For the $X\ ^1\Sigma^+$ state of NaH, we recommend the RKR curve generated from the [MAK 89] constants (see Table 2.3). The [ZEM 84] curve goes up to $v'' = 11$. Less accurate results for $v'' > 11$ [NED 83, PAR 88] are also noted.

The RKR potential energy curve of the NaD $X\ ^1\Sigma^+$ state has been calculated previously only by [GIR 80]. We recommend the RKR potential here based on the recommended NaH constants.

The RKR potential energy curve of the NaH $A\ ^1\Sigma^+$ state has been calculated by [JAI 63, ORT 80, PAR 88]. We recommend the [ORT 80] results since they are based on the recommended $A\ ^1\Sigma^+$ constants; the observation of $v' = 21$ [NED 83] has not been incorporated into the [ORT 80] potential curve. As noted by [ORT 80], the rotational constants [PAN 49] used by [JAI 63] appear to be in error and no $v' = 0$ results were then available. The curve of [PAR 88] uses isotopically combined Dunham coefficients and varies slightly from that of [ORT 80].

No separate RKR curve for the NaD $A\ ^1\Sigma^+$ state is given since the recommended constants are simply estimated by mass-reduced scaling from the NaH results.

Hybrid potential energy curves have also been constructed for the $X\ ^1\Sigma^+$ and $A\ ^1\Sigma^+$ states of NaH [ZEM 84, PAR 88]. The [ZEM 84] curves utilize the $X\ ^1\Sigma^+$ and $A\ ^1\Sigma^+$ RKR curves discussed above, up to $v'' = 11$ and $v' = 20$, respectively. An exponential repulsion is used inside the inner turning points R_{11-} and R_{20-}, respectively, and is based on fits to *ab initio* points at 1.75, 2.00 and 2.50 a_0 or at 2.50, 3.00 and 3.25 a_0 [OLS 80A] shifted to join smoothly at R_{11-} or R_{20-}, respectively. The long-range regions ($R > 17\,a_0$ and $R > 20\,a_0$, respectively) are represented as a sum of inverse power terms: $V_{\text{long-range}}(R) = -\sum_n C_n/R^n$, where $n = 6$, 8 and 10. The C_n are dispersion coefficients based on the proper multipole-multipole interactions [PRO 77]. The gap between R_{11+} or R_{20+} and long-range (tied to an assumed asymptote where $D_e'' = 15900$ cm^{-1} or $D_e' = 10137$ cm^{-1}) is filled by slightly scaling the *ab initio* results of [OLS 80A]: in the $X\ ^1\Sigma^+$ state, the *ab initio* binding energies are increased by 4.022%; in the $A\ ^1\Sigma^+$ state, they are increased 4.335%. These curves are recommended for estimates of higher vibrational levels in NaH (or NaD).

The [PAR 88] hybrid potential curves are "PMO-RKR-van der Waals" curves. The minimum of a curve is represented by a perturbed Morse oscillator (PMO, as formulated by [HUF 76, HUF 76A]) described by ten parameters. The RKR region of a curve is based on available vibrational/rotational data (up to $v'' = 15$ and $v' = 20$ [PAR 88]); the turning points are calculated from modified Dunham coefficients which include higher order corrections to the normal Dunham coefficients. The innermost repulsive and outermost attractive regions of a curve are represented by an inverse power series $+\sum_n C_n/R^n$, where $n = 6$, 8, 10 and 12. These C_n constants bear no resemblance (in sign or value) to the normal C_6, C_8 or C_{10} dispersion coefficients [PAR 88] and are obtained from the least-squares fits to the adjacent turning points. It is important to note that the use of the term "van der Waals" [PAR 88] is misleading.

The spectroscopic constants and potential energy curves of all other states of NaH are known only from electronic structure calculations, and hence are discussed in Sec. 2.6.

TABLE 2.4. RKR potential energy curve of the $A\ ^1\Sigma^+$ state of NaH [ORT 80]

v	$[G(v) + Y_{00}]$ (cm^{-1})	R_{v-} (Å)	R_{v+} (Å)
0	160.35	2.8536	3.5144
1	483.98	2.6070	3.7420
2	814.37	2.4484	3.9011
3	1151.60	2.3303	4.0346
4	1495.24	2.2371	4.1547
5	1844.50	2.1612	4.2668
6	2198.34	2.0977	4.3738
7	2555.59	2.0436	4.4777
8	2915.04	1.9967	4.5798
9	3275.51	1.9555	4.6808
10	3635.88	1.9186	4.7814
11	3995.19	1.8854	4.8820
12	4352.61	1.8552	4.9828
13	4707.45	1.8276	5.0840
14	5059.18	1.8022	5.1857
15	5407.38	1.7787	5.2881
16	5751.67	1.7570	5.3912
17	6091.69	1.7371	5.4954
18	6427.00	1.7186	5.6013
19	6756.96	1.7015	5.7096
20	7080.65	1.6856	5.8216

2.5. Dissociation Energy

The dissociation energy of NaH has been estimated from experimental data in a variety of ways. These values are surveyed in [YAN 83] and Table 2.5. The polynomial Birge-Sponer extrapolation D_e value of [NED 83] is a long-range extrapolation. However, the distances involved are too small for a meaningful long-range extrapolation (we suggest $R > 14\ a_o$ in [ZEM 84] while the last turning point in [NED 83] is at 9.0 a_o). We estimate instead $D_e = 15900 \pm 100\ cm^{-1}$ using the comparison of binding energies in our calculated hybrid potential with the experimental binding energies of [NED 83].

TABLE 2.5. Estimated D_e values for NaH

Method	Estimate (cm^{-1})	Reference
Graphical Birge-Sponer Extrapolation, A State	17100 ± 1600	GAY 68
Polynomial Birge-Sponer Extrapolation, X State	16300 ± 500	GIR 80
Polynomial Birge-Sponer Extrapolation, X State (NaD)[a]	16700 ± 500	GIR 80
Extrapolation to Ionic-Covalent Avoided Crossing, X State	15900 ± 500	YAN 82
Extrapolation to Ionic-Covalent Avoided Crossing, A State	16000 ± 400	YAN 83
Observation of $v'' = 19$	>15541.7	NED 83
Polynomial Birge-Sponer Extrapolation, X State	15785 ± 500	NED 83
Binding Energy of $v'' = 19$	15900 ± 100	This work
Recommended	15900 ± 100	

[a]It is estimated that $D_e(NaH) = D_e(NaD) \pm \sim 5\ cm^{-1}$ as in LiH [VID 82, VID 84, CHA 86].

2.6. Electronic Structure Calculations

The first high quality calculations of NaH were those of Cade and Huo at the Hartree-Fock level [CAD 67; see also CAD 69]; a slightly improved Hartree-Fock calculation was carried out many years later by Wilson and Silver [WIL 77]. However, our emphasis here is on more accurate configuration interaction (CI) calculations, e.g. the early valence CI calculations of Lewis, McNamara and Michels [LEW 71]; the multiconfiguration self-consistent field (MCSCF) calculations of Sachs, Hinze and Sabelli [SAC 75, SAC 75A, SAC 75B, SAC 75C, SAC 75D]; the pseudonatural orbital correlated electron pair approximation (PNO/CEPA) calculations of Meyer and Rosmus [MEY 75]; the pseudopotential calculations of Numrich and coworkers [NUM 74, NUM 75, MEL 79], of Fuentealba *et al.* [FUE 87], of Olson and Kimura [OLS 85], of Mó *et al.* [MO 85]; the many body perturbation theory calculations of Silver and coworkers [BAR 76, BAR 76A, WIL 77]; the pseudopotential MCSCF calculations of Karo and coworkers [KAR 78, STE 81]; the core-valence CI calculations of Olson and coworkers [OLS 80A, ZEM 84]; the coupled-pair functional (CPF) calculations of Langhoff *et al.* [LAN 86]; the quantum Monte Carlo calculations of Lester and coworkers [HAM 87]; and the multireference CI calculations (with the inclusion of bond functions) of Barclay and Wright [BAR 88].

Long-range configuration interaction in the $^1\Sigma^+$ states of NaH has been studied by many workers [BAT 56, OLS 71, GRI 74, JAN 76, ADE 77]. Bussery *et al.* [BUS 86] calculated long-range coefficients for $^1\Sigma^+$, $^3\Sigma^+$, $^1\Pi$ and $^3\Pi$ states.

Long-range exchange corresponding to the potential difference between the $X\ ^1\Sigma^+$ and $a\ ^3\Sigma^+$ states of NaH has been studied by [KNO 69].

Less accurate calculations of NaH include [BLU 77, MAR 77, RAY 77, MCA 79, SAK 81].

Electronic structure calculations where NaH is calculated only incidentally as a fragment occurring at asymptotic separations in an overall polyatomic potential energy surface calculation include [RAF 73, BAS 73, RUP 77, PIN 79, BLA 83, SEV 85, JEZ 85]. In general, these calculations are not competitive with the more accurate purely diatomic calculations described above. Also in the category are calculations of the bulk properties of crystalline NaH [KUL 79, PEA 84] and the proton affinity of NaH [DIX 88].

Other theoretical studies examining NaH include [BRU 78, RAY 79, HOE 80, PRE 81, TEL 86].

Fitting of potential energy curves in terms of sets of adjustable parameters was done in [VAR 63, PRA 79, GHO 81, KAU 83, KUM 86, VAR 88].

2.7. Radiative and Dipole Properties

The radiative properties of NaH have not been studied extensively experimentally. There are no reports of relative intensities of various laser-induced fluorescence series. There are, however, a few lifetime measurements in the $A\ ^1\Sigma^+$ state [BAL 76, DAG 76, NED 83], a transition moment measurement in the $X\ ^1\Sigma^+$ state [MAK 89], and measurements of dipole moments in the $X\ ^1\Sigma^+$ [DAG 79] and $A\ ^1\Sigma^+$ [BRI 81] states.

Theoretical calculations of the dipole moment function in the $X\ ^1\Sigma^+$ and $A\ ^1\Sigma^+$ states have been presented in [SAC 75, MEY 75, ZEM 84, LAN 86 (X state only)]. The dipole moment function and vibrationally averaged results of [LAN 86] are nearly identical to those found in [ZEM 84]. As noted in [ZEM 84], their calculations give superior agreement with experiment [DAG 79, BRI 81] compared to earlier dipole moment functions. With regard to $A\ ^1\Sigma^+$ radiative lifetimes, the only calculations are those of [DAG 76, TEL 86] based on extending the results of Sachs, Hinze and Sabelli [SAC 75B]. Selected

TABLE 2.6. High quality calculations of NaH (Hartree-Fock or better), normally calculated at R_e

Method	State	$-E$(a.u.)	D_e(cm^{-1})	$R_e(a_o)$	Range of $V(R)$	Spect. const.	Other properties, comments	Ref.
Hartree-Fock	$X\,^1\Sigma^+$	162.3929 162.3928[E]	7550 7528[E]	3.616 3.566[E]	2 – 5, ∞	√	IP	CAD 67
Valence CI	$X\,^1\Sigma^+$	161.73558[N]	12198[N]	4[N]	4 – 15, ∞	–		LEW 71
	$a\,^3\Sigma^+$	161.6800	–	–	4 – 15, ∞	–	unbound	
	$A\,^1\Sigma^+$	161.64682[N]	9685[N]	5[N]	4 – 15, ∞	–		
	$b\,^3\Pi$	161.60663[N]	865[N]	5[N]	4 – 15, ∞	–		
	$B\,^1\Pi$	161.6026	–	–	4 – 15, ∞	–	unbound	
	$c\,^3\Sigma^+$	161.6027[N]	~2[N]	~12.5[N]	4 – 15, ∞	–		
SCF	$X\,^1\Sigma^+$	162.314134	–	3.603	–	–		RAF 73
SCF	$X\,^1\Sigma^+$	162.33171	–	3.628	–	–		BAS 73
MCSCF (also frozen core approx.)	$X\,^1\Sigma^+$	162.42761	15144	3.609	2 – 20, ∞	√	$\mu(R)$, Q, F, G, μ_v, $D(R)$	SAC 75, SAC 75A,
	$a\,^3\Sigma^+$	162.35861	–	–	3 – 20, ∞	–	unbound, $\mu(R)$, Q, F, G, $D(R)$	SAC 75B, SAC 75C,
	$A\,^1\Sigma^+$	162.32676	9699	6.186	3 – 20, ∞	√	$\mu(R)$, Q, F, G, μ_v, $D(R)$	SAC 75D
	$b\,^3\Pi$	162.28657	878	4.458	3 – 20, ∞	√	$\mu(R)$, Q, F, G, μ_v, $D(R)$	
	$B\,^1\Pi$	162.28261[N]	~7[N]	~8[N]	3 – 20, ∞	–	$\mu(R)$, Q, F, G, $D(R)$	
	$c\,^3\Sigma^+$	162.28257	–	–	3 – 20, ∞	–	unbound, $\mu(R)$, Q, F, G, $D(R)$	
PNO/CEPA/CI	$X\,^1\Sigma^+$	162.428385[N]	15513[N]	3.60[N]	2.8 – 5, ∞	√	$\mu(R)$ (dipole deriv., etc. in BRU 78)	MEY 75
Pseudopotential	$X\,^1\Sigma^+$	–	8751	4.121	–	–	nonadiabatic	NUM 74,
	$a\,^3\Sigma^+$	–	–	–	–	–	nonadiabatic	NUM 75
	$A\,^1\Sigma^+$	–	10509	6.115	–	–	nonadiabatic	
	$b\,^3\Pi$	–	–	–	–	–	nonadiabatic	
	$B\,^1\Pi$	–	–	–	–	–	nonadiabatic	
	$c\,^3\Sigma^+$	–	–	–	–	–	nonadiabatic	
	$C\,^1\Sigma^+$	–	–	–	–	–	nonadiabatic	
	$d\,^3\Sigma^+$	–	–	–	–	–	nonadiabatic	
	$D\,^1\Sigma^+$	–	–	–	–	–	nonadiabatic	
Time-dept. HF pseudopotential	$X\,^1\Sigma^+$	–	–	3.566[E]	–	–	excitation energies and oscillator strengths to next six $^1\Sigma^+$ and five $^1\Pi$ states; polarizabilities	WAT 76
MBPT	$X\,^1\Sigma^+$	162.6449[E]	–	3.566[E]	–	–		BAR 76, BAR 76A
HF	$X\,^1\Sigma^+$	162.39294[E]	–	3.5660[E]	–	–		WIL 77
MBPT	$X\,^1\Sigma^+$	162.6809[E]	–	3.5660[E]	–	–		WIL 77
MCSCF	$X\,^1\Sigma^+$	162.41509	14334[N]	3.75[N]	3.0 – 20, ∞	√		KAR 78
		–	14437	3.622	3.0 – 20, ∞	–		
ECP	$b\,^3\Pi$	–	204[N]	5.5[N]	2 – 11, ∞	–		MEL 79
	$B\,^1\Pi$	–	–	–	2 – 11, ∞	–	unbound	
CVCI	$X\,^1\Sigma^+$	162.436022	15502	3.558	1.5 – 30, ∞	√	(μ in ZEM 84)	OLS 80A
	$a\,^3\Sigma^+$	162.365406	3.5	12.30	1.5 – 30, ∞	√		
	$A\,^1\Sigma^+$	162.333232	9993	5.992	1.5 – 30, ∞	√	(μ in ZEM 84)	
	$b\,^3\Pi$	162.292588	1073	4.497	1.5 – 30, ∞	√		
	$B\,^1\Pi$	162.288251	121	5.30	1.5 – 30, ∞	√		
	$c\,^3\Sigma^+$	162.287709[N]	~2[N]	~20[N]	1.5 – 30, ∞	–		
	$C\,^1\Sigma^+$	162.27222	6348	11.87	1.5 – 30, ∞	√		
Pseudopotential MCSCF	$X\,^1\Sigma^+$	–	15245[N]	3.50[N]	2.75 – 40, ∞	√		STE 81
		–	15204	3.55	2.75 – 40, ∞			
	$a\,^3\Sigma^+$	–	~4[N]	~15[N]	2.75 – 40, ∞	–		

TABLE 2.6. High quality calculations of NaH (Hartree-Fock or better), normally calculated at R_e — Continued

Method	State	$-E$(a.u.)	D_e(cm^{-1})	$R_e(a_o)$	Range of $V(R)$	Spect. const.	Other properties, comments	Ref.
Pseudopotential CI	$X\,^1\Sigma^+$	–	15400	3.55	–	√	μ	FUE 87
CPF	$X\,^1\Sigma^+$	–	15486	3.572	2 – 15	√	$\mu(R)$, μ_v, τ_v	LAN 86
Valence EPC-QMC	$X\,^1\Sigma^+$	–	15760	–	–	–	μ	HAM 87
MRD CI	$X\,^1\Sigma^+$	–	15200	–	2.6 – 6	√	with bond functions	BAR 88
Pseudopotential with one-center wf	$X\,^1\Sigma^+$	–	11300	3.31	1 – 10	–	IP	TAM 89

[N]indicates lowest point, not R_e.
[E]indicates experimental R_e.
∞means asymptotic energy calculation.

TABLE 2.7. High quality calculations of NaH^+ (Hartree-Fock or better), normally calculated at R_e

Method	State	$-E$(a.u.)	D_e(cm^{-1})	$R_e(a_o)$	Range of $V(R)$	Spect. const.	Other properties, comments	Ref.
Hartree-Fock	$X\,^2\Sigma^+$	162.1671$_6$[V]	–	3.566[V]	–	–	vertical NaH IP = 6.14 eV	CAD 67
UHF	$X\,^2\Sigma^+$	–	–	3.60	2.8 – 3.8	–		CLA 70
PNO/CEPA/CI	$X\,^2\Sigma^+$	162.173642	~480	4.900	–	√	adiabatic NaH IP = 6.90 eV	ROS 77, ROS 81
Hellman pseudopotential	$X\,^2\Sigma^+$	–	~160	5.8	–	–	in table only	VAL 78
	$A\,^2\Sigma^+$	–	2712[N]	8.0[N]	5 – 25, ∞	–	in table and figure	
	$B\,^2\Sigma^+$	–	2952[N]	13.0[N]	5 – 25, ∞	–	in table and figure	
	$D\,^2\Sigma^+$	–	–	–	5 – 25, ∞	–	in table and figure, unbound	
	$F\,^2\Sigma^+$	–	282[N]	22.0[N]	5 – 25, ∞	–	in table and figure	
ECP	$X\,^2\Sigma^+$	–	492	5.1	2 – 13, ∞	–		MEL 79
CI/CV or SD	$X\,^2\Sigma^+$	161.17931	492 (±121)	5.1 (±0.2)	3.5 – 30, ∞	√	in table only	OLS 80, LIU 81
	$A\,^2\Sigma^+$	161.87964	3791 (±400)	7.98 (±0.1)	3.5 – 30, ∞	√	in table and figure	
	$B\,^2\Sigma^+$	161.82166[N]	4383[N]	13.0[N]	3.5 – 30, ∞	–	in table and figure	
	$C\,^2\Pi$	~161.8035	~400	~8	3.5 – 20, ∞	–	SCF-in figure only	
	$D\,^2\Sigma^+$	161.79865, ∞	–	–	3.5 – 30, ∞	–	in table and figure, unbound	
	$E\,^2\Pi$	~161.78565, ∞	–	–	3.5 – 20, ∞	–	SCF-in figure only, unbound	
	$F\,^2\Sigma^+$	161.79019[N]	~380[N]	20.0[N]	3.5 – 30, ∞	–	in table and figure	
PVB	$A\,^2\Sigma^+$	–	3146	8.7	–	–	in table and figure	KUB 81
	$B\,^2\Sigma^+$	–	2577[N]	15[N]	2.5 – 40, ∞	–	in table and figure	
	$C\,^2\Pi$	–	–	–	–	–	in figure only	
	$D\,^2\Sigma^+$	–	–	–	2.5 – 40, ∞	–	in table and figure, unbound	
	$E\,^2\Pi$	–	–	–	–	–	in figure only, unbound	
	$F\,^2\Sigma^+$	–	77[N]	22.5[N]	2.5 – 40, ∞	–	in table and figure	
Pseudopotential	$A\,^2\Sigma^+$	–	3710	7.87	–	–	in table and figure	KIM 82, KIM 82A
	$B\,^2\Sigma^+$	–	–	–	–	–	in figure only	
	$C\,^2\Pi$	–	–	–	–	–	in figure only	
	$D\,^2\Sigma^+$	–	–	–	–	–	in figure only, unbound	
	$E\,^2\Pi$	–	–	–	–	–	in figure only	
	$F\,^2\Sigma^+$	–	–	–	–	–	in figure only	
	$G\,^2\Sigma^+$	–	–	–	–	–	in figure only, unbound	
	$H\,^2\Pi$	–	–	–	–	–	in figure only	
Pseudopotential	$X\,^2\Sigma^+$	–	~650	4.86	–	–	with core polarization	FUE 82
Model-potential	$A\,^2\Sigma^+$	–	3710	7.88	2.5 – 30	–	other $^2\Sigma^+$, $^2\Pi$ states in figure only	ALL 86

[V]indicates at neutral ground state R_e.
[N]indicates lowest point, not R_e.
∞means asymptotic energy calculation.

Einstein A coefficients for the $A-X$ bands [SAC 75B] and the purely vibrational transitions in the $X\,^1\Sigma^+$ and $A\,^1\Sigma^+$ states [SAC 75A, ZEM 84] have also been calculated. Given the variety of lifetime measurements now available, careful lifetime calculations are overdue. In addition, adiabatic and nonadiabatic photodissociation calculations have been carried out [KIR 78, SIN 82, SIN 84]. The potentials discussed above have been used in atomic line broadening calculations [MON 85].

2.8. Other Properties

The collisional charge exchange processes ($H + Na \rightarrow Na^+ + H^-$ and $Na^- + H^+$) have been studied [HOW 84]. Sodium line broadening calculations which treat the collision of H and Na with molecular potentials have been performed [LEW 71, ROU 74]. Other properties of NaH which have been studied theoretically include the quadrupole moment, field gradients at nuclei, etc. [SAC 75, SUN 85, GUO 87], the perpendicular and parallel polarizabilities [WAT 76], dipole moment derivatives, atomic anisotropies, etc. [BRU 78], radial $X\,^1\Sigma^+ - A\,^1\Sigma^+$ and $X\,^1\Sigma^+ - C\,^1\Sigma^+$ couplings [MO 85], proton affinity [DIX 88] and magnetic susceptibilities and shielding constants [HOE 80]. Bulk crystalline calculations include [KUL 79, PEA 84].

2.9. Positive Ions

While the NaH^+ ion has not been directly studied experimentally, there is a wide variety of collisional experiments (reviewed in [ALV 81, FRI 84, MOR 85]) which probe the potential energy curves of NaH^+ (e.g. the $A\,^2\Sigma^+$ state which correlates with $H^+ + Na$): [SOL 67, ILI 67, SOL 68, DYA 68, GRU 69, GRU 70, ILI 71, OHA 75, BEA 78, AND 79, DUT 79, NAG 80, HOW 82, NAG 82, BER 84]. Wilkinson [WIL 63] quotes an ionization potential of 6.5 ± 1 eV for NaH.

Theoretical calculations of the NaH^+ ion are numerous. The first high quality calculation (Hartree-Fock) was made by Cade and Huo [CAD 69]. Other accurate calculations include [CLA 70, GAS 75, ROS 77, VAL 78, MEL 79, OLS 80, KUB 81, LIU 81, ROS 81, KIM 82, KIM 82A, FUE 82, ALL 86].

2.10. Negative Ions

While the NaH^- ion has not been directly studied experimentally, there is a variety of collisional experiments (reviewed in [ALV 81, MOR 85]) which probe the potential energy curves of NaH^-: [DYA 72, DIM 74, AND 80, SCH 80, HOW 81, HOW 83, WAN 87].

There are also a number of accurate NaH^- calculations: [JOR 76, JOR 77, JOR 78, ROS 78, KAR 78, OLS 80A, STE 81, OLS 83].

2.11. Other Comments

Various models for the potential energy curves were proposed to reproduce the observed spectroscopic constants [VAR 63, RAY 79, KUL 79, PRA 79, GHO 81, KAU 83, KUM 86, VAR 88]. A modified Rittner model of the ionic adiabatic potential was constructed [YAN

TABLE 2.8. High Quality calculations of NaH^- (Hartree-Fock or better), normally calculated at R_e

Method	State	$-E$(a.u.)	D_e(cm^{-1})	$R_e(a_o)$	Range of $V(R)$	Spect. const.	Other properties, comments	Ref.
EOM	$X\,^2\Sigma^+$	–	13308	3.80	3 – 4.25	√	vert EA(NaH) = 0.36 eV	JOR 76
PNO	$X\,^2\Sigma^+$	162.43914	12233	3.802	–	√	ad EA(NaH) = 0.31 eV	ROS 78
MCSCF	$X\,^2\Sigma^+$	162.42379	10743^N	4.0^N	3 – 20, ∞	√	ad EA(NaH) = 0.278 eV	KAR 78
		–	10888	3.896	3 – 20, ∞			
CI	$X\,^2\Sigma^+$	162.44167	12276	3.851	1.5 – 20, ∞	√	ad EA(NaH) = 0.373 ± 0.02 eV, vert EA(NaH) = 0.336 eV	OLS 80A, OLS 83
	$A\,^2\Sigma^+$	162.41121^N	5590^N	3.7^N	1.5 – 20, ∞	–	barrier at large R	
	$3\,^2\Sigma^+$	162.39718^N	–	3.8^N	1.5 – 20	–	double minimum;	
		?	–	~7	1.5 – 20		asymptote uncertain	
	$4\,^2\Sigma^+$	162.36259^N	–	3.7, 3.8^N	1.5 – 20	–	barrier at large R and double	
		162.35407^N	–	6.0^N	1.5 – 20	–	minimum; asymptote uncertain	
Pseudopotential MCSCF	$X\,^2\Sigma^+$	–	11673	3.74	2.75 – 40, ∞	√	ad EA(NaH) = 0.316 eV	STE 81

^{N}indicates lowest point, not R_e.
∞ means asymptotic energy calculation.

81]. The dissociation energy of NaH was estimated using this ionic potential [YAN 82, YAN 83]. Rotational energy transfer cross sections for NaH ($A\ ^1\Sigma^+$) + H_2 collisions have been measured [GIR 85]. The formation of NaH clusters has been studied experimentally [YAB 80] and theoretically [BAS 73, RUP 77]. For further discussion of this *laser snow*, see Sec. 5.11.

3. KH

3.1. Conventional Spectroscopy

Almy and Hause [ALM 32] photographed the $A\ ^1\Sigma^+ \rightarrow X\ ^1\Sigma^+$ emission in the 410–660 nm region. They reported data on 27 bands that covered v'' from 0 to 4 and v' from 2 to 18 (correct vibrational numbering due to Bartky [BAR 66], see below). Hori [HOR 33] also photographed the $A\ ^1\Sigma^+ \rightarrow X\ ^1\Sigma^+$ emission and identified 62 bands, extending the upper state to $v' = 26$ (correct vibrational numbering due to [BAR 66]). Almy and Beiler [ALM 42] rephotographed the 405–465 nm region in emission. Imanishi [IMA 41] measured the KD emission spectrum in the 415.7–649.5 nm region. [BAR 66] observed the absorption spectrum of KD in the 510–520 nm region and established the correct vibrational numbering for the $A\ ^1\Sigma^+$ state. Hori [HOR 33A] reported a structured continuum resulting from the $B\ ^1\Pi \rightarrow X\ ^1\Sigma^+$ emission transitions. The structure was decomposed [HOR 33A] into contributions primarily from free-bound emission to vibrational levels $v'' = 3$, 4 and 5.

3.2. Laser Spectroscopy

Cruse and Zare [CRU 74] reported the excitation spectrum induced by a nitrogen pumped dye laser (440–470 nm and 480–493 nm) and also observed and assigned the fluorescence spectrum to $v'' = 0$, 1, 2 and 4 excited by an argon ion laser (488.0 nm). They also noted (but did not assign) 496.5 nm excited fluorescence. More extensive fluorescence spectra of KH and KD molecules, generated in a high frequency discharge cell and excited by a nitrogen pumped dye laser, were reported by Giroud and Nedelec [GIR 80]. Vibrational levels up to $v'' = 14$ for KH and $v'' = 16$ for KD were observed. Pardo *et al.* [PAR 83] photographed the fluorescence spectrum of KH excited by an argon ion laser (488.0 nm) and previously seen [CRU 74]. They observed new $v'' = 3$ and $v'' = 5$ lines. Haese *et al.* [HAE 84] measured the vibration-rotation absorption of $v'' = 1 \leftarrow 0$ and $v'' = 2 \leftarrow 1$ transitions of ^{39}KH and ^{41}KH by a diode laser absorption technique. Hussein *et al.* [HUS 86] reported $A\ ^1\Sigma^+$–$X\ ^1\Sigma^+$ fluorescence in ^{39}KH excited by an argon ion laser (488.0 nm). Using high resolution Fourier transform spectrometry, they observed fluorescence from the $v' = 7$, $J' = 6$ level to $v'' = 0$, 1, 2, 4, 5 and 7 levels (visible region) and also $13 \leq v'' \leq 23$ levels (infrared region). Strong K_2 absorption in the intermediate region resulted in the absence of observed levels for $8 \leq v'' \leq 12$.

3.3. Spectroscopic Constants

Bartky [BAR 66] established the correct vibrational numbering in the $A\ ^1\Sigma^+$ state by measuring the absorption spectrum. The early vibrational numbering for KD given by Imanishi [IMA 41] was too low by 3. The numbering for KH given by Almy and Hause [ALM 32] (and used by Hori [HOR 33] and Almy and Beiler [ALM 42]) was too low by 2. [BAR 66] reanalyzed Imanishi's KD data [IMA 41] and Hori's KH data [HOR 33] to obtain unified sets of spectroscopic constants.

With the use of mass-reduced scaling [STW 75] and the reanalyzed data on KH and KD [BAR 66], Yang *et al.* [YAN 80] determined isotopically combined spectroscopic constants for the $X\ ^1\Sigma^+$ state of KH ($0 \leq v'' \leq 4$). [GIR 80] determined separate constants for KH ($0 \leq v'' \leq 14$) and KD ($0 \leq v'' \leq 16$). Although their constants cover a wide range of vibrational levels, it should be noted that the uncertainty for these constants is relatively high in view of the large and irregular scatter in the rotational $B_{v''}$ constants and vibrational $\Delta G(v'')$ spacings. The constants of [HAE 84], based on their data measured by diode laser absorption, are highly accurate representations for KH ($0 \leq v'' \leq 2$), but likely to deviate for higher vibrational energy levels not probed in their experiment. [HUS 86] fit simultaneously their own KH levels and the rotational-vibrational levels of [HAE 84]; they determined eleven vibrational and eleven rotational constants for $0 \leq v'' \leq 23$. [HUS 86] also report $B_{v''}$ and $D_{v''}$ values for $v'' = 4$–5, 7, 13–16, 18 and 20–23.

The recommended spectroscopic constants for the $X\ ^1\Sigma^+$ state of KH are those of [HUS 86] and are listed in Table 3.1. The six vibrational and six rotational constants of [PAR 87A] are based on the data from their own laboratory [PAR 83, PAR 87] and others [ALM 32, ALM 42, BAR 66, GIR 80, HUS 86]. Their most recent constants [PAR 87A] are significantly different than their earlier ones [PAR 83] and the ones we recommend [HUS 86].

Constants for the $A\ ^1\Sigma^+$ state of KH have been determined by [BAR 66, YAN 80, PAR 87A]. The isotopically combined constants of [YAN 80] are based on fits of the experimental $B_{v'}$ and $G(v')$ data for KH and KD found in [BAR 66] and are the recommended constants. The R_e value and the vibrational constants are somewhat uncertain because the $v' = 0$ and 1 levels have not been observed. [PAR 87A] report isotopically combined constants that are slightly different than those of [YAN 80].

The recommended value of $T_e = 19060\ cm^{-1}$ is based on [BAR 66] and $[G(v) + Y_{00}]$ values in Tables 3.2. and 3.3. for $v'' = 3$ and $v' = 2$. This T_e value is somewhat uncertain because the lowest levels for the $A\ ^1\Sigma^+$ state ($v' = 0$, 1 for KH; $v' = 0 - 3$ for KD) were not observed. [YAN 80] give $T_e = 19057\ cm^{-1}$ for KH (19059.9 cm^{-1} for KD), based on [BAR 66]. The uncertainty in T_e due to the extrapolation to the minimum of the potential curve is estimated at $\sim 25\ cm^{-1}$ [YAN 80]. [PAR 87A] give $T_e = 19066 \pm 26\ cm^{-1}$; [HUB 79] give $T_e = 19052.8\ cm^{-1}$.

TABLE 3.1. Recommended spectroscopic constants for KH[a]

	$X\,^1\Sigma^+$ (HUS 86)	$A\,^1\Sigma^+$ (YAN 80)
ZPE	490.0779	115.17
Y_{00}	0.670859	2.05
Y_{10}	986.65055	222.74135
Y_{20}	−15.844615	7.16946996
Y_{30}	0.38533062	−0.3129870308
Y_{40}	−0.09217627	0.0056141654
10^1Y_{50}	0.18413172	0.00048714908
10^2Y_{60}	−0.2385268	
10^3Y_{70}	0.20131181	
10^4Y_{80}	−0.11081649	
10^6Y_{90}	0.38314085	
10^8Y_{100}	−0.75651294	
$10^{10}Y_{110}$	0.64835269	
Y_{01}	3.4189506	1.211900282
10^1Y_{11}	−0.9439438	0.665077733
10^1Y_{21}	0.106325415	−0.068787213
10^2Y_{31}	−0.52310142	0.02580463
10^2Y_{41}	0.14813303	−0.000380005
10^3Y_{51}	−0.248376412	
10^4Y_{61}	0.25605538	
10^5Y_{71}	−0.163822469[b]	
10^7Y_{81}	0.633047058[b]	
10^8Y_{91}	−0.13521347[b]	
$10^{10}Y_{101}$	0.1223840112	

[a]All entries in cm^{-1} units; non-rounded values reported here are important for use in RKR calculations, particularly for highest vibrational levels.

[b]Corrected from originally published numbers; see [ZEM 88].

TABLE 3.2. RKR potential energy curve of the $X\,^1\Sigma^+$ state of KH [HUS 86]

v	$[G(v) + Y_{00}]$ (cm^{-1})	R_{v-} (Å)	R_{v+} (Å)
0	490.0779	2.0701	2.4458
1	1445.9460	1.9636	2.6226
2	2372.0117	1.8977	2.7599
3	3268.9001	1.8485	2.8823
4	4137.1550	1.8088	2.9969
5	4977.3077	1.7754	3.1070
6	5789.8479	1.7466	3.2143
7	6575.1859	1.7213	3.3203
8	7333.6301	1.6989	3.4258
9	8065.3740	1.6789	3.5317
10	8770.4781	1.6609	3.6384
11	9448.8363	1.6444	3.7467
12	10100.1221	1.6293	3.8572
13	10723.7138	1.6154	3.9710
14	11318.5972	1.6026	4.0894
15	11883.2384	1.5910	4.2141
16	12415.4080	1.5804	4.3476
17	12911.9331	1.5709	4.4936
18	13368.3517	1.5623	4.6580
19	13778.4686	1.5547	4.8508
20	14133.8621	1.5482	5.0903
21	14423.4918	1.5432	5.4138
22	14633.7253	1.5393	5.9144
23	14749.3488	1.5273	6.9828

Reduced mass μ = 0.98241434 for ^{39}KH [HUB 79].

TABLE 3.3. RKR potential energy curve of the $A\,^1\Sigma^+$ state of KH [YAN 80]

v	$[G(v) + Y_{00}]$ (cm^{-1})	R_{v-} (Å)	R_{v+} (Å)
0	115.17	3.3629	4.1379
1	351.26	3.0772	4.3895
2	599.04	2.8942	4.5562
3	856.87	2.7570	4.6920
4	1123.26	2.6479	4.8122
5	1396.82	2.5582	4.9237
6	1676.28	2.4827	5.0301
7	1960.46	2.4183	5.1334
8	2248.28	2.3624	5.2350
9	2538.75	2.3136	5.3358
10	2830.97	2.2704	5.4362
11	3124.12	2.2319	5.5367
12	3417.44	2.1972	5.6377
13	3710.26	2.1657	5.7392
14	4001.95	2.1369	5.8416
15	4291.95	2.1104	5.9449
16	4579.74	2.0858	6.0494
17	4864.85	2.0629	6.1551
18	5146.85	2.0414	6.2624
19	5425.34	2.0212	6.3714
20	5699.94	2.0023	6.4825
21	5970.30	1.9845	6.5958
22	6236.09	1.9680	6.7118
23	6496.97	1.9528	6.8310
24	6752.62	1.9390	6.9538
25	7002.71	1.9268	7.0810
26	7246.90	1.9165	7.2134

3.4. Potential Energy Curves

The RKR potentials of the $A\,^1\Sigma^+$ state were constructed by Almy and Beiler [ALM 42] and by Jain and Sah [JAI 63] before the correct vibrational numbering was established [BAR 66]; therefore their potentials are incorrect. Numrich and Truhlar [NUM 74, NUM 75] constructed RKR potentials for the $X\,^1\Sigma^+$ and the $A\,^1\Sigma^+$ states (with correct vibrational numbering). Yang *et al.* [YAN 80] constructed isotopically combined RKR potentials for the $X\,^1\Sigma^+$ and the $A\,^1\Sigma^+$ states. Giroud and Nedelec [GIR 80] extended the $X\,^1\Sigma^+$ RKR potential curve for KH to $v'' = 14$. The $X\,^1\Sigma^+$ state RKR curve of Hussein *et al.* [HUS 86] goes up to $v'' = 23$, which is within 24 cm^{-1} of the dissociation limit. Pardo *et al.* [PAR 87A] determined RKR curves for $X\,^1\Sigma^+$ and $A\,^1\Sigma^+$ states from their reported spectroscopic constants.

The recommended RKR potential energy curve for the KH $X\,^1\Sigma^+$ state is that of [HUS 86]; for the $A\,^1\Sigma^+$ state the recommended RKR curve is that of [YAN 80]. Both RKR curves are based on the recommended spectroscopic constants and are given in Tables 3.2. and 3.3.

A rough estimate of the upper $B\,^1\Pi$ state energy curve of KH was made by Hori [HOR 33A]. In his analysis, the emission structure peaking near 28300, 26700 and 25400 cm^{-1} is interpreted as vertical transitions from inner classical turning points in the upper $B\,^1\Pi$ state to outer classical turning points corresponding to $v'' = 3$, 4 and 5 in the $X\,^1\Sigma^+$ state. Roughly speaking, given the $X\,^1\Sigma^+$ potential curve, one obtains three points on the upper $B\,^1\Pi$

curve: ~31600 cm^{-1} at R_{3+} = 2.88 Å, ~30800 cm^{-1} at R_{4+} = 3.00 Å and ~30400 cm^{-1} at R_{5+} = 3.11 Å. This is intermediate between the *ab initio* calculations of the $B\ ^1\Pi$ and $C\ ^1\Sigma^+$ states [NUM 74, NUM 75, NUM 78, MEL 79], and does not clearly correspond to the $B\ ^1\Pi$ state rather than higher states such as the $C\ ^1\Sigma^+$ state. Further analysis is needed to resolve this uncertainty.

Hybrid potential energy curves have been constructed for the $X\ ^1\Sigma^+$ [PAR 87A, ZEM 88] and $A\ ^1\Sigma^+$ [PAR 87A] states of ^{39}KH. The Zemke and Stwalley [ZEM 88] curve utilizes the $X\ ^1\Sigma^+$ RKR curve of [HUS 86] up to $v'' = 23$. An exponential inner wall, based on the Langhoff *et al.* [LAN 86] *ab initio* points at 2.50, 2.75 and 3.00 a_o, is shifted to join smoothly at the inner R_{22-} turning point. The long-range region of the curve is represented by the $-C_n/R^n$ expansion, where C_6, C_8 and C_{10} are the dispersion coefficients [PRO 77]. This long-range region of the curve ($R \geq 17\ a_o$) fits smoothly onto the outermost R_{23+} turning point (~13.2 a_o).

The [PAR 87A] hybrid potential curves are PMO-RKR-van der Waals curves. A ten-parameter perturbed Morse oscillator (PMO) represents the minimum of the curve (between R_{0+} and R_{0-}). The RKR region [PAR 87A] extends to R_{23+} and R_{23-} (R_{26+} and R_{26-}) for the X (and A) state of KH. The top portion of the curve is represented by an inverse power expansion $+\Sigma\ C_n/R^n$, where n = 6, 8, 10 and 12. These C_n constants bear no resemblance to dispersion coefficients (such as in [ZEM 88]) and are determined by least-squares fits onto the uppermost inner and outer turning points.

The RKR potential energy curve for the KD $X\ ^1\Sigma^+$ state has been calculated only by [GIR 80]. No separate RKR curve for the KD $A\ ^1\Sigma^+$ state is given. [PAR 87A] assume their KH and KD hybrid potential curves are the same and show rather good agreement between experimental and calculated $G(v)$ and B_v values for both X and A states.

The spectroscopic constants and potential energy curves of all other states of KH are known only from electronic structure calculations and are discussed in Sec. 3.6.

TABLE 3.4. Estimated D_e values for KH

Method	Estimate (cm^{-1})	Reference
Graphical Birge-Sponer Extrapolation, A State, plus Linear Birge-Sponer Extrapolation, X State	16160 ± 1200	ALM 42 (see YAN 83)
Polynomial Birge-Sponer Extrapolation, X State	17030 ± 1500	GIR 80
Mass Spectroscopy	16650 ± 1340	FAR 82
Extrapolation to Ionic-Covalent Avoided Crossing, A State	15020 ± 400	YAN 83
Observation of $v'' = 23, J'' = 7$ Predissociation	14777 ± 4	HUS 86
Line Width of $v'' = 23, J'' = 7$	14772.7 ± 0.6	ZEM 88
Recommended	14772.7 ± 0.6	

3.5. Dissociation Energy

Yang *et al.* [YAN 83] obtained the $X\ ^1\Sigma^+$ state dissociation energy as 15020 ± 400 cm^{-1} by an extrapolation of the $A\ ^1\Sigma^+$ state RKR potential curve to the $A\ ^1\Sigma^+ - C\ ^1\Sigma^+$ avoided crossing point. Previous polynomial Birge-Sponer extrapolation of $\Delta G(v)$ [GIR 80] overestimates the dissociation energy because the potential well opens up drastically near the avoided crossing point [YAN 83]. A mass spectroscopic determination [FAR 82] of D_o gave 16160 ± 1340 cm^{-1} (or D_e = 16650 ± 1340 cm^{-1}) which is also too large. Since KH^+ ($X\ ^2\Sigma^+$) is predicted theoretically to be only weakly bound at large internuclear distance (D_e ~ 200–400 cm^{-1}, R_e ~ 5.6–10 a_o), it should not be produced in vertical processes such as photoionization or electron impact ionization (as in [FAR 82]) of unexcited KH. For this reason, we question the reported observation of KH^+ [FAR 82] and do not accept the interpretations of [FAR 82] with regard to D_o(KH) or IP(KH). Recently two very precise values for D_e have been determined by Hussein *et al.* [HUS 86] and Zemke and Stwalley [ZEM 88]. The former value (14776 ± 4 cm^{-1}) is based on the observation that the $v'' = 23, J'' = 7$ quasibound level is predissociating. [ZEM 88] took this observation further; they constructed a hybrid potential based on the RKR potential of [HUS 86] and included proper long range behavior beyond the last turning point. From a comparison of calculated line widths for this quasibound level (for a number of possible dissociation energies) and the experimental line width [HUS 86], [ZEM 88] obtained a value of 14772.7 ± 0.6 cm^{-1}. See Table 3.4.

3.6. Electronic Structure Calculations

Grice and Herschbach [GRI 74] and Adelman and Herschbach [ADE 77] calculated the energy splitting of the $A\ ^1\Sigma^+$ and the $X\ ^1\Sigma^+$ potential curves at the ionic-covalent crossing distance in a two configuration interaction approximation. [ADE 77] also calculated the energy splitting between the $A\ ^1\Sigma^+$ and the $C\ ^1\Sigma^+$ curves at the second ionic-covalent crossing distance.

Numrich and Truhlar [NUM 74, NUM 75, NUM 78] reported adiabatic potential curves for the $X\ ^1\Sigma^+$, $a\ ^3\Sigma^+$, $A\ ^1\Sigma^+$, $b\ ^3\Pi$, $B\ ^1\Pi$, $c\ ^3\Sigma^+$, $C\ ^1\Sigma^+$, $d\ ^3\Sigma^+$ and $D\ ^1\Sigma^+$ states calculated by a one-electron pseudopotential formalism. The last mentioned six states were labeled as $^3\Pi$, $^1\Pi$, $b\ ^3\Sigma^+$, $B\ ^1\Sigma^+$, $c\ ^3\Sigma^+$ and $C\ ^1\Sigma^+$, respectively, in the original article [NUM 75]. They also calculated the coupling matrix elements between electronic states in three different representations. Melius and coworkers [MEL 79] calculated the $B\ ^1\Pi$ and $b\ ^3\Pi$ potential curves. Garrett *et al.* [GAR 81, GAR 81B, GAR 83] calculated the adiabatic potential curves and the nonadiabatic first derivative couplings for the $X\ ^1\Sigma^+$, $A\ ^1\Sigma^+$ and $C\ ^1\Sigma^+$ states.

Stevens *et al.* [STE 81] reported multiconfiguration self-consistent field MCSCF pseudopotential calculations for the $X\ ^1\Sigma^+$ and the $a\ ^3\Sigma^+$ potentials for KH. Jeung *et al.* [JEU 83] studied core-valence correlation effects in

TABLE 3.5. High quality calculations of KH (Hartree-Fock or better), normally calculated at R_e

Method	State	$-E$(a.u.)	D_e(cm^{-1})	$R_e(a_o)$	Range of $V(R)$	Spect. const.	Other properties, comments	Ref.
Time dependent HF pseudopotential	$X\,^1\Sigma^+$	–	–	4.242[E]	–	–	excitation energies and oscillator stengths to next six $^1\Sigma^+$ and five $^1\Pi$ states; polarizabilities	WAT 76
Pseudopotential	$X\,^1\Sigma^+$	–	8025	4.882	–	–	in table and figure	NUM 74, NUM 75
	$a\,^3\Sigma^+$	–	–	–	–	–	in figure only, unbound	
	$A\,^1\Sigma^+$	–	9210	7.505	–	–	in table and figure	
	$b\,^3\Pi$	–	–	–	–	–	in figure only	
	$B\,^1\Pi$	–	–	–	–	–	in figure only	
	$c\,^3\Sigma^+$	–	–	–	–	–	in figure only, unbound	
	$C\,^1\Sigma^+$	–	–	–	–	–	in figure only	
	$d\,^3\Sigma^+$	–	–	–	–	–	in figure only	
	$D\,^1\Sigma^+$	–	–	–	–	–	in figure only	
ECP	$b\,^3\Pi$	–	75[N]	7.0[N]	2 – 11, ∞	–	in table only	MEL 79
	$B\,^1\Pi$	–	15[N]	9.5[N]	2 – 11, ∞	–	in table only	
ECP	$X\,^1\Sigma^+$	–	–	–	–	–	in figure only	GAR 81, GAR 83
	$A\,^1\Sigma^+$	–	–	–	–	–	in figure only	
	$C\,^1\Sigma^+$	–	–	–	–	–	in figure only	
Pseudopotential	$X\,^1\Sigma^+$	–	14447[N]	4.25[N]	3.0 – 40, ∞	√		STE 81
MCSCF		–	14490	4.23	3.0 – 40, ∞	–		
	$a\,^3\Sigma^+$	–	22[N]	12	3.0 – 40, ∞	–		
Pseudopotential	$X\,^1\Sigma^+$	–	12900	4.29	–	√	in table and figure	JEU 83
	$a\,^3\Sigma^+$	–	–	–	–	√	in figure only, unbound	
	$A\,^1\Sigma^+$	–	8710	7.18	–	√	in table and figure	
CPF	$X\,^1\Sigma^+$	–	14437	4.265	2.5 – 15	√	$\mu(R)$, μ_v, τ_v, A_{vJ}	LAN 86
Pseudopotential CI	$X\,^1\Sigma^+$	–	13550	4.30	–	√	μ	FUE 87
Pseudopotential CI	$X\,^1\Sigma^+$	–	14990	4.07	3.75 – 18, ∞	√	in table and figure	ROS 87
	$a\,^3\Sigma^+$	–	465	10.29	3.75 – 18, ∞	√	in table and figure	
	$A\,^1\Sigma^+$	–	8860	6.92	3.75 – 18, ∞	√	in table and figure	
	$b\,^3\Pi$	–	855	5.26	3.75 – 10, ∞	√	in table and figure	
	$B\,^1\Pi$	–	293	5.94	3.75 – 10, ∞	√	in table and figure	
	$c\,3\Sigma^+$	–	–	–	3.75 – 18, ∞	√	in table and figure, unbound	
	$C\,^1\Sigma^+$	–	–	–	3.75 – 18, ∞	√	in table and figure	
	$^3\Sigma^+$	–	954	5.49	3.75 – 18, ∞	√	in table and figure	
	$^3\Pi$	–	1413	5.13	3.75 – 10, ∞	√	in table and figure	
	$^1\Sigma^+$	–	1024	5.66	3.75 – 18, ∞	√	in table and figure	
	$^1\Delta$	–	–	–	3.75 – 10, ∞	√	in table and figure	
	$^3\Delta$	–	380	5.72	3.75 – 10, ∞	√	in table and figure	
	$^1\Pi$	–	285	5.71	3.75 – 10, ∞	√	in table and figure	
	$^3\Sigma^+$	–	–	5.23	3.75 – 18, ∞	√	in table and figure	
	$^1\Sigma^+$	–	1251	5.23	3.75 – 18, ∞	√	in table and figure	
	$^3\Sigma^+$	–	102	8.00	3.75 – 18, ∞	√	in table and figure	
	$^3\Pi$	–	16	5.56	3.75 – 10, ∞	√	in table and figure	
	$^1\Pi$	–	62	5.75	3.75 – 10, ∞	√	in table and figure	
Pseudopotential with one-center wf	$X\,^1\Sigma^+$	–	11600	3.90	1 – 10	–	IP	TAM 89

[N]indicates lowest point, not R_e.
[E]indicates experimental R_e.
∞ means asymptotic energy calculation.

pseudopotential calculations on the $X\,^1\Sigma^+$, $A\,^1\Sigma^+$ and $a\,^3\Sigma^+$ states. Fuentealba *et al.* [FUE 87] determined ground state properties (D_e, R_e, ω_e) with pseudopotential calculations that included core-polarization effects.

Watson *et al.* [WAT 76] performed time dependent Hartree-Fock calculations to obtain the excitation energies and the oscillator strengths for transitions from the ground state at equilibrium bond distance to various excited $^1\Sigma^+$ and $^1\Pi$ states. The $X\,^1\Sigma^+ - a\,^3\Sigma^+$ exchange splitting has been estimated [KNO 69].

Langhoff *et al.* [LAN 86] calculated a complete potential energy curve for the $X\,^1\Sigma^+$ state using their coupled-pair functional (CPF) approach. Bussery *et al.* [BUS 86] calculated long-range multipole expansion coefficients (C_6, C_8, C_{10}) and long-range potential curves for the $X\,^1\Sigma^+, a\,^3\Sigma^+, A\,^1\Sigma^+, b\,^3\Pi, B\,^1\Pi$ and $c\,^3\Sigma^+$ states. Ross *et al.* [ROS 87] report impressive CI pseudopotential calculations on the eighteen lowest-lying molecular states of KH with these symmetries: $^1\Sigma^+$ (ground and four excited states), $^3\Sigma^+$ (five states), $^1\Pi$ (three), $^3\Pi$ (three), $^1\Delta$ (one) and $^3\Delta$ (one).

3.7. Radiative and Dipole Properties

Radiative lifetimes of $A\,^1\Sigma^+$ levels ($5 \leq v' \leq 22$) have been reported [GIR 82]. Langhoff *et al.* [LAN 86] calculated a complete dipole moment function. They report vibrationally averaged dipole moment expectation values, dipole moment absorption matrix elements and Einstein A coefficients for the purely vibrational transitions in the $X\,^1\Sigma^+$ state ($v'' = 0 - 9$ levels).

3.8. Other Properties

The collisions H (or D) + K → H^- + K^+ are reviewed by Alvarez and Cisneros [ALV 81]. Rotational and vibrational energy transfer cross sections for KH ($A\,^1\Sigma^+$) + H_2 collisions have been measured [GIR 82, GIR 85]. [WAT 76] calculated dipole polarizabilities and [GUO 87] determined electronic field gradients in KH. The calculation of bulk properties of crystalline KH has been done [PEA 84].

3.9. Positive Ions

Melius *et al.* [MEL 79] calculated the potential curve of the $X\,^2\Sigma^+$ state of KH^+. Olson *et al.* [OLS 80] calculated the $X\,^2\Sigma^+, A\,^2\Sigma^+, B\,^2\Sigma^+, D\,^2\Sigma^+$ and $F\,^2\Sigma^+$ potential curves of KH^+. Pseudopotential calculations of Fuentealba *et al.* [FUE 82] determined ground state properties (D_e, R_e, ω_e) of KH^+. Potential curves and other properties (especially scattering cross sections) of the higher excited states were calculated by Valance [VAL 78], Kubach and Sidis [KUB 81] and Kimura *et al.* [KIM 82A].

Experimental (scattering) and theoretical studies involving K + H^+ include [SEL 67, INO 72, NAG 82, BER 84]. See the review articles by Alvarez and Cisneros [ALV 81], Fritsch [FRI 84] and Morgan *et al.* [MOR 85]. Farber *et al.* [FAR 82] report an ionization potential based on mass spectroscopy for KH which we consider incorrect (see Sec. 3.5.).

3.10. Negative Ions

Collisional processes (reviewed in [ALV 81, MOR 85]) which probe the negative ion potential curves have been studied [AND 80]. Stevens *et al.* [STE 81] reported an MCSCF pseudopotential calculation on the KH^- $X\,^2\Sigma^+$ state. The calculated spectroscopic constants are referenced in Table 3.6. The calculated electron affinity of KH is 0.316 eV.

3.11. Other Comments

Various models for the potential energy curves were proposed to reproduce the observed spectroscopic constants [VAR 63, RAY 79, KUL 79, PRA 79, GHO 81, KAU 83, KUM 86, VAR 88]. A modified Rittner model of the ionic adiabatic potential was constructed [YAN 82]. The dissociation energy of KH was estimated using this ionic potential [YAN 82, YAN 83].

The quenching cross section of $K(4^2P)$ by muonium was calculated [GAR 81A]. The quenching cross section and rotational energy transfer cross section of KH ($A\,^1\Sigma^+$) by H_2 were measured by Giroud and Nedelec [GIR 82, GIR 85]. Lin and Chang [LIN 89] show that the selective reaction of K*(7s) with H_2 produces KH, while K*(5d) with H_2 does not.

4. RbH

4.1. Conventional Spectroscopy

Gaydon and Pearse [GAY 39A] photographed the RbH emission spectrum in the 468 − 654 nm region. They reported bands that covered $v'' = 0 - 5$ of the $X\,^1\Sigma^+$ state and $v' = 3 - 14$ (mislabeled as 0 − 11 in the original paper) of the $A\,^1\Sigma^+$ state. Bartky [BAR 66A] later photographed RbD in absorption and established that the correct numbering for these v' levels should be 3 − 14. The $v' = 0 - 2$ levels of the $A\,^1\Sigma^+$ state have not been observed.

4.2. Laser Spectroscopy

The laser-excited fluorescence spectrum was observed in the 476 − 847 nm region using the Ar^+ 476.5 nm exciting line [HSI 80]; vibrational levels $v'' = 0 - 12$ of the $X\,^1\Sigma^+$ state were measured. Kato *et al.* [KAT 85] observed $X\,^1\Sigma^+ - A\,^1\Sigma^+$ laser-induced fluorescence in RbD excited by 514.5 and 488.0 nm lines of the Ar^+ laser. In RbH the exciting lines were 476.2, 476.5 and 488.0 nm [KAT 85]. For ^{85}RbD, [KAT 85] lists sixteen $v' = 14, J' = 4 \rightarrow v'', J'' = 3$ and 5 and eighteen $v' = 13, J' = 30 \rightarrow v'', J'' = 29$ and 31 transition frequencies and intensities. Magg *et al.* [MAG 88A] used diode laser spectros-

TABLE 3.6. High quality calculations of KH^+ and KH^- (Hartree-Fock or better), normally calculated at R_e

Method	State	$-E$(a.u.)	D_e(cm^{-1})	R_e(a$_o$)	Range of $V(R)$	Spect. const.	Other properties, comments	Ref.
				KH^+				
Hellman	$X\,^2\Sigma^+$	–	202	10	–	–	in table only	VAL 78
pseudopotential	$A\,^2\Sigma^+$	–	~3950^N	9.0^N	5 – 25, ∞	–	in table and figure	
	$B\,^2\Sigma^+$	–	~2820^N	~14.0^N	5 – 25, ∞	–	in table and figure	
	$D\,^2\Sigma^+$	–	–	–	5 – 25, ∞	–	in table and figure, unbound	
	$F\,^2\Sigma^+$	–	~306^N	23.0^N	5 – 25, ∞	–	in table and figure	
ECP	$X\,^2\Sigma^+$	–	177	6.5	2 – 13, ∞	√		MEL 79
CI/CV or SD	$X\,^2\Sigma^+$	599.51935	435^N	5.75^N	3.5 – 30, ∞	–	in table only	OLS 80
	$A\,^2\Sigma^+$	599.19929^N	4925^N	9.0^N	3.5 – 30, ∞	√	in table and figure	
		–	4952	9.09	3.5 – 30, ∞	–	in table and figure	
	$B\,^2\Sigma^+$	599.15615^N	2208^N	15.0^N	3.5 – 30, ∞	–	in table and figure	
	$D\,^2\Sigma^+$	599.17684$^\infty$	–	–	3.5 – 30, ∞	–	in table and figure, unbound	
	$F\,^2\Sigma^+$	599.11929^N	318^N	25.0^N	3.5 – 30, ∞	–	in table and figure	
PVB	$A\,^2\Sigma^+$	–	3952	9.4	–	–	in table and figure	KUB 81
	$B\,^2\Sigma^+$	–	–	–	2.5 – 40, ∞	–	in table and figure	
	$C\,^2\Pi$	–	–	–	–	–	in figure only	
	$D\,^2\Sigma^+$	–	–	–	2.5 – 40, ∞	–	in table and figure, unbound	
	$E\,^2\Pi$	–	–	–	–	–	in figure only, unbound	
	$F\,^2\Sigma^+$	–	61^N	22.5^N	2.5 – 40, ~∞	–	in table and figure, unbound	
Pseudopotential	$A\,^2\Sigma^+$	–	5485	8.68	–	–	in table and figure	KIM 82A
	$B\,^2\Sigma^+$	–	–	–	–	–	in figure only	
	$C\,^2\Pi$	–	–	–	–	–	in figure only	
	$D\,^2\Sigma^+$	–	–	–	–	–	in figure only, unbound	
	$E\,^2\Pi$	–	–	–	–	–	in figure only	
	$F\,^2\Sigma^+$	–	–	–	–	–	in figure only	
	$G\,^2\Sigma^+$	–	–	–	–	–	in figure only, unbound	
	$H\,^2\Pi$	–	–	–	–	–	in figure only, unbound	
Pseudopotential	$X\,^2\Sigma^+$	–	~400	5.69	–	–	with core polarization	FUE 82
				KH^-				
Pseudopotential	$X\,^2\Sigma^+$	–	11937	4.44	3 – 40, ∞	√	ad EA(KH) = 0.437 eV	STE 81
MCSCF		–	11928^N	4.50^N	3 – 40, ∞			

^{N} indicates lowest point, not R_e.
∞ means asymptotic energy calculation.

copy to obtain a vibration-rotation infrared spectrum of the $X\ ^1\Sigma^+$ state; over forty transitions were measured for the $v'' = 1 \leftarrow 0, 2 \leftarrow 1, 3 \leftarrow 2$ and $4 \leftarrow 3$ bands of ^{85}RbH and ^{87}RbH.

TABLE 4.1. Recommended spectroscopic constants for RbH[a]

	$X\ ^1\Sigma^+$		
	MAG 88A	KAT 85	$A\ ^1\Sigma^+$ (KAT 85)
ZPE	465.2324	465.07	109.12
Y_{00}	0.2375	0.14	1.67
Y_{10}	937.1046	936.94	211.74
Y_{20}	−14.2777	−14.205	6.47
Y_{30}	0.09658	0.0815	−0.253
Y_{40}	−0.000862	–	0.00304
Y_{01}	3.021481	3.0195	1.12898
Y_{11}	−0.07071	−0.07071	0.05133
Y_{21}	0.0003711	−0.000392	−0.005923
10^3Y_{31}	–	0.1147	0.2638
10^5Y_{41}	–	−0.596	−0.481

[a]All entries in cm^{-1} units; non-rounded values reported here are important for use in RKR calculations, particularly for highest vibrational levels.

TABLE 4.2. RKR potential energy curve of the $X\ ^1\Sigma^+$ state of RbH [KAT 85].

v	$[G(v) + Y_{00}]$ (cm^{-1})	R_{v-} (Å)	R_{v+} (Å)
0	465.07	2.1933	2.5759
1	1373.86	2.0838	2.7549
2	2254.98	2.0162	2.8940
3	3108.91	1.9657	3.0179
4	3936.14	1.9248	3.1338
5	4737.17	1.8905	3.2451
6	5512.47	1.8609	3.3536
7	6262.54	1.8348	3.4604
8	6987.87	1.8117	3.5664
9	7688.94	1.7910	3.6723
10	8366.25	1.7726	3.7786

Reduced mass μ = 0.99600357 for ^{85}RbH [HUB 79].

4.3. Spectroscopic Constants

Hsieh *et al.* [HSI 80] determined spectroscopic constants for the $X\ ^1\Sigma^+$ state of RbH. Their vibrational analysis was based on the emission spectrum of [GAY 39A] for $v'' = 0 - 5$, and the laser-induced fluorescence spectrum for $v'' = 6 - 12$ [HSI 80]. Their rotational B_v constants are those of [GAY 39A] (as renumbered by [BAR 66A]). Bartky [BAR 66A] reported the rotational constants of only the $v'' = 1$ band of RbD. Kato *et al.* [KAT 85] adopted the vibrational constants of Bartky [BAR 66A] and determined new rotational constants for RbD ($0 \leq v'' < 15$). Using the relationship $Y_{ij}(\text{RbH}) = Y_{ij}(\text{RbD}) \cdot [\mu(\text{RbD})/\mu(\text{RbH})]^{i/2+j}$, they calculated spectroscopic constants for RbH.

The infrared studies of [MAG 88A] provide highly accurate data on RbH (transitions measured to a nominal accuracy of ± 0.001 cm^{-1}). Their spectroscopic constants for the $X\ ^1\Sigma^+$ state are the most accurate available. However, the range of their constants is limited ($0 \leq v'' \leq 4$), compared to other slightly less accurate results [HSI 80, KAT 85]. Therefore, we list two sets of constants in Table 4.1 [MAG 88A, KAT 85]. The RKR curves calculated with both sets of constants are in good agreement for $v'' = 0 - 4$.

Bartky [BAR 66A] measured the absorption spectrum of RbD and established the numbering for the $A\ ^1\Sigma^+$ state of RbH. Constants for the $A\ ^1\Sigma^+$ state of RbH come from a reanalysis [HSI 80] of the spectroscopic data of Gaydon and Pearse [GAY 39A] and Bartky [BAR 66A]. The corresponding constants for RbD are computed from those for RbH. In addition, [KAT 85] report RbH constants based on RbD constants ($0 \leq v' \leq 20$). They compared observed relative line strengths [KAT 85] for a series of RbH transitions ($v' = 15, J' = 23 \rightarrow v'', J''$ and $v' = 16, J' = 12 \rightarrow v'', J''$) with several calculated ones [BAR 66A, HSI 80, KAT 85]. The best agreement occurred with their mass scaled RbH constants. Hence, we recommend the $A\ ^1\Sigma^+$ state spectroscopic constants of [KAT 85] (see Table 4.1.).

The recommended value of $T_e = 18218$ cm^{-1} is based on [BAR 66A] and $[G(v) + Y_{00}]$ values in Tables 4.2. and 4.3. for $v'' = 3$ and $v' = 3$. This T_e value is somewhat uncertain because $v' = 0 - 2$ levels were not observed. The uncertainty in T_e due to extrapolation to the minumum of the potential curve is estimated at ~30 cm^{-1} [HSI 80]. [BAR 66A] gives $T_e = 18219.8$ cm^{-1} and [HSI 80] give $T_e = 18217$ cm^{-1}. [KAT 85] give 18219.9 cm^{-1} (18219.0 cm^{-1} for RbD).

TABLE 4.3. RKR potential energy curve of the $A\ ^1\Sigma^+$ state of RbH [KAT 85].

v	$[G(v) + Y_{00}]$ (cm^{-1})	R_{v-} (Å)	R_{v+} (Å)
0	109.12	3.4695	4.2595
1	333.00	3.1870	4.5257
2	567.62	3.0076	4.7039
3	811.62	2.8738	4.8490
4	1063.71	2.7676	4.9770
5	1322.64	2.6802	5.0950
6	1587.28	2.6067	5.2066
7	1856.54	2.5436	5.3142
8	2129.41	2.4886	5.4192
9	2404.96	2.4400	5.5225
10	2682.33	2.3966	5.6249
11	2960.72	2.3574	5.7267
12	3239.43	2.3217	5.8285
13	3517.81	2.2889	5.9305
14	3795.30	2.2587	6.0329

4.4. Potential Energy Curves

Gaydon and Pearse [GAY 39B] constructed potential curves of the $X\ ^1\Sigma^+$ and $A\ ^1\Sigma^+$ states using Dunham ex-

pansions. The $A\ ^1\Sigma^+$ potential is incorrect because of the incorrect vibrational numbering. RKR potentials for the $X\ ^1\Sigma^+$ state up to $v'' = 5$ have been constructed by Singh and Jain [SIN 62] and Jain and Sahni [JAI 66]. They also calculated the $A\ ^1\Sigma^+$ state RKR potential but the vibrational numbering was again incorrect. Hsieh *et al.* [HSI 80] constructed the $X\ ^1\Sigma^+$ RKR potential up to $v'' = 12$ based on the laser-induced fluorescence spectrum. [HSI 80] also constructed the $A\ ^1\Sigma^+$ RKR potential up to $v' = 14$. [KAT 85] report RKR potential energy curves for $A\ ^1\Sigma^+$ and $X\ ^1\Sigma^+$ states for both RbH and RbD ($0 \leq v'' \leq 15$ and $0 \leq v' \leq 20$, respectively). Based on the energy range of the experimental RbD data, the range of the RbH RKR curves should be $0 \leq v'' \leq 10$ for the $X\ ^1\Sigma^+$ state and $0 \leq v' \leq 14$ for the $A\ ^1\Sigma^+$ state.

The recommended RKR potential energy curves for the $X\ ^1\Sigma^+$ and $A\ ^1\Sigma^+$ states of ^{85}RbH are those of [KAT 85] but with five rather than three significant figures given (Table 4.2. and Table 4.3., respectively). The RKR curve calculated with the [MAG 88A] constants is in good agreement with that of [KAT 85] up through $v'' = 4$ (differences in $G(v)$ and $R_{v\pm}$ values are ≤ 0.4 cm^{-1} and ≤ 0.0005 Å, respectively).

The RKR potential energy curves for $X\ ^1\Sigma^+$ and $A\ ^1\Sigma^+$ states found in [PAR 87B] are based on the constants of [HSI 80] and are thus identical to those reported earlier [HSI 80] up to $v'' = 12$ and $v' = 14$. Pardo *et al.* [PAR 87B] report the $A\ ^1\Sigma^+$ state RKR curve up to $v' = 18$, although the constants used were for $v' \leq 14$! We suggest caution in the use of an RKR potential energy curve based on an extrapolation beyond the data.

Hybrid potential energy curves have been constructed for the $X\ ^1\Sigma^+$ and $A\ ^1\Sigma^+$ states of RbH [PAR 87B]. The Pardo *et al.* [PAR 87B] curves are PMO-RKR-van der Waals curves. The minimum of a curve is represented by a perturbed Morse oscillator of ten parameters. The RKR region of the $X\ ^1\Sigma^+$ state is based on data [HSI 80] up to $v'' = 12$; for the $A\ ^1\Sigma^+$ state, the RKR curve goes beyond the data [HSI 80] up to $v' = 18$ (see preceding paragraph). The innermost repulsive and outermost attractive regions of a curve are represented by the inverse power series $\sum_n C_n/R^n$ (where n is even and the summation goes from $n = 6$ to $n = 22$) determined by least-squares fits to the uppermost RKR turning points. These C_n constants [PAR 87B] bear no resemblance to the normal dispersion coefficients. We have serious reservations concerning the [PAR 87B] $A\ ^1\Sigma^+$ state hybrid potential energy curve because the upper portion of the curve is based on an extrapolation.

The spectroscopic constants and potential energy curves of all other states of RbH are known only from electronic structure calculations, and hence are discussed in Sec. 4.6.

4.5. Dissociation Energy

Yang *et al.* [YAN 83] obtained the $X\ ^1\Sigma^+$ state dissociation energy as $D_e = 14580 \pm 600$ cm^{-1} by an extrapolation of the $A\ ^1\Sigma^+$ state RKR potential curve to the $A\ ^1\Sigma^+ - C\ ^1\Sigma^+$ avoided crossing point. Linear Birge-Sponer extrapolation [GAY 39B] as well as fitting of empirical potential functions [MUR 83] overestimated the dissociation energy because they did not take into account the sharp change of the slope of the potential curve near the avoided crossing point.

We recommend the value $D_e'' = 14580 \pm 600$ cm^{-1}, but there is an obvious need for further efforts to determine a more precise value.

4.6. Electronic Structure Calculations

Grice and Herschbach [GRI 74] and Adelman and Herschbach [ADE 77] calculated the energy splitting of the $A\ ^1\Sigma^+$ and the $X\ ^1\Sigma^+$ potential curves at the ionic-covalent crossing distance in a two-configuration interaction approximation. [ADE 77] also calculated the energy splitting between the $A\ ^1\Sigma^+$ and the $C\ ^1\Sigma^+$ curves at the second ionic-covalent crossing distance.

Rather than perform an *ab initio* all electron nonrelativistic multiconfiguration self-consistent field calculations on the $X\ ^1\Sigma^+$ state of RbH (such as done by [KAR 78] on NaH), Stevens *et al.* [STE 81] used a pseudopotential to simulate Rb core electrons and reduced the problem to a two-electron multiconfiguration self-consistent-field calculation. [STE 81] also calculated the potential curve of the $a\ ^3\Sigma^+$ state. The $X\ ^1\Sigma^+$ and $a\ ^3\Sigma^+$ splitting was estimated earlier by Knox and Rudge [KNO 69]. Pietro *et al.* [PIE 81] calculated the bond length of the ground state using an extended basis set in a simple (single configuration ?) *ab initio* calculation.

Langhoff *et al.* [LAN 86] calculated a complete potential energy curve for the $X\ ^1\Sigma^+$ state using their coupled-pair functional approach. Bussery *et al.* [BUS 86] calculated long-range multipole expansion coefficients (C_6, C_8, C_{10}) for the $X\ ^1\Sigma^+$, $a\ ^3\Sigma^+$, $A\ ^1\Sigma^+$, $b\ ^3\Pi$, $B\ ^1\Pi$ and $c\ ^3\Sigma^+$ states. Fuentealba *et al.* [FUE 87] calculated ground state properties (D_e, R_e, ω_e, $\omega_e x_e$) by two pseudopotential methods, where valence electron correlation is included by a local spin-density functional or by valence CI (with single and double excitations). Ross *et al.* [ROS 87] report potential energy curves by CI pseudopotential calculations for the eighteen lowest-lying molecular states of RbH with these symmetries: $^1\Sigma^+$ (ground and four excited states), $^3\Sigma^+$ (five states), $^1\Pi$ (three), $^3\Pi$ (three), $^1\Delta$ (one) and $^3\Delta$ (one).

4.7. Radiative and Dipole Properties

Langhoff *et al.* [LAN 86] calculated a complete electric dipole moment function. They report vibrationally averaged dipole moment expectation values, dipole moment absorption matrix elements, lifetimes and Einstein A coefficients for the purely vibrational transitions in the $X\ ^1\Sigma^+$ state ($v'' = 0 - 9$ levels).

TABLE 4.4. High quality calculations of RbH (Hartree-Fock or better), normally calculated at R_e

Method	State	$-E$(a.u.)	D_e(cm^{-1})	$R_e(a_o)$	Range of $V(R)$	Spect. const.	Other properties, comments	Ref.
Pseudopotential	$X\,^1\Sigma^+$	–	14257^N	4.25^N	3.0 – 40, ∞	√		STE 81
MCSCF		–	14294	4.35	3.0 – 40, ∞	–		
	$a\,^3\Sigma^+$	–	~2^N	11^N	3.0 – 40, ∞	–		
CPF	$X\,^1\Sigma^+$	–	14115	4.53	3.0 – 15	√	$\mu(R)$, μ_v, τ_v, A_{vJ}	LAN 86
Pseudopotential CI	$X\,^1\Sigma^+$	–	13227	4.51		√		FUE 87
Pseudopotential CI	$X\,^1\Sigma^+$	–	14100	4.30	4 – 9, ∞	√	in table and figure	ROS 87
	$a\,^3\Sigma^+$	–	–	–	4 – 9, ∞	√	in table and figure, unbound	
	$A\,^1\Sigma^+$	–	8945	7.52	4 – 9, ∞	√	in table and figure	
	$b\,^3\Pi$	–	475	5.80	4 – 9, ∞	√	in table only	
	$B\,^1\Pi$	–	82	6.40	4 – 9, ∞	√	in table only	
	$c\,^3\Sigma^+$	–	–	–	4 – 9, ∞	–	in table and figure, unbound	
	$C\,^1\Sigma^+$	–	–	–	4 – 9, ∞	–	in table and figure, unbound	
	$^3\Pi$	–	1145	5.37	4 – 9, ∞	√	in table only	
	$^3\Sigma^+$	–	485	5.84	4 – 9, ∞	√	in table and figure	
	$^3\Delta$	–	112	6.23	4 – 9, ∞	√	in table only	
	$^1\Delta$	–	114	6.19	4 – 9, ∞	√	in table only	
	$^1\Pi$	–	7	6.36	4 – 9, ∞	√	in table only	
	$^1\Sigma^+$	–	167	5.98	4 – 9, ∞	√	in table and figure	
	$^3\Sigma^+$	–	–	5.61	4 – 9, ∞	√	in table and figure	
	$^1\Sigma^+$	–	473	5.58	4 – 9, ∞	√	in table and figure	
	$^3\Sigma^+$	–	473	8.34	4 – 9, ∞	√	in table and figure	
	$^3\Pi$	–	274	6.09	4 – 9, ∞	√	in table only	
	$^1\Pi$	–	225	6.24	4 – 9, ∞	√	in table only	
Pseudopotential with one-center wf	$X\,^1\Sigma^+$	–	9260	4.25	1 – 10	–	IP	TAM 89

^{N}indicates lowest point, not R_e.
∞ means asymptotic energy calculation.

TABLE 4.5. High quality calculations of RbH^+ and RbH^- (Hartree-Fock or better), normally calculated at R_e

Method	State	$-E$(a.u.)	D_e(cm^{-1})	$R_e(a_o)$	Range of $V(R)$	Spect. const.	Other properties, comments	Ref.
				RbH^+				
Hellman pseudopotential	$X\,^2\Sigma^+$	–	97	13.4	–	–	in table only	VAL 78
	$A\,^2\Sigma^+$	–	4030^N	9.0^N	5 – 25, ∞	–	in table and figure	
	$B\,^2\Sigma^+$	–	~2580^N	~15.0^N	5 – 25, ∞	–	in table and figure	
	$D\,^2\Sigma^+$	–	–	–	5 – 25, ∞	–	in table and figure, unbound	
	$F\,^2\Sigma^+$	–	~370^N	23.0^N	5 – 25, ∞	–	in table and figure	
PVB	$A\,^2\Sigma^+$	–	4436	10.4	–	–	in table and figure	KUB 81
	$B\,^2\Sigma^+$	–	–	–	–	–	in figure only	
	$C\,^2\Pi$	–	–	–	–	–	in figure only	
	$D\,^2\Sigma^+$	–	–	–	–	–	in figure only, unbound	
	$E\,^2\Pi$	–	–	–	–	–	in figure only, unbound	
	$F\,^2\Sigma^+$	–	–	–	–	–	in figure only, unbound	
Pseudopotential	$A\,^2\Sigma^+$	–	5888	8.85	–	–	in table and figure	KIM 82A
	$B\,^2\Sigma^+$	–	–	–	–	–	in figure only	
	$C\,^2\Pi$	–	–	–	–	–	in figure only	
	$D\,^2\Sigma^+$	–	–	–	–	–	in figure only, unbound	
	$E\,^2\Pi$	–	–	–	–	–	in figure only	
	$F\,^2\Sigma^+$	–	–	–	–	–	in figure only	
	$G\,^2\Sigma^+$	–	–	–	–	–	in figure only, unbound	
	$H\,^2\Pi$	–	–	–	–	–	in figure only, unbound	
Pseudopotential	$X\,^2\Sigma^+$	–	350	5.84	–	√	μ	SZE 82

TABLE 4.5. High quality calculations of RbH^+ and RbH^- (Hartree-Fock or better), normally calculated at R_e — Continued

Method	State	$-E$(a.u.)	$D_e(cm^{-1})$	$R_e(a_o)$	Range of $V(R)$	Spect. const.	Other properties, comments	Ref.
				RbH^-				
Pseudopotential	$X\,^2\Sigma^+$	–	11617	4.61	3 – 40, ∞	√	ad EA(RbH) = 0.422 eV	STE 81
MCSCF	$X\,^2\Sigma^+$	–	11579[N]	4.75[N]	3 – 40, ∞			

[N]indicates lowest point, not R_e.
∞ means asymptotic energy calculation.

4.8. Other Properties

The collisions H (or D) + Rb → H^- + Rb^+ are reviewed by Alvarez and Cisneros [ALV 81]. Guo *et al.* [GUO 87] determined electric field gradients in RbH. The calculation of bulk properties of crystalline RbH has been done [PEA 84].

4.9. Positive Ions

Potential energy curves and other properties (especially scattering cross sections) of the higher excited states correlating with Rb + H^+ were calculated by Valence [VAL 78], Kubach and Sidis [KUB 81], and Kimura *et al.* [KIM 82A]. Nagata [NAG 80, NAG 82] studied experimentally the charge transfer reaction Rb + H^+ → Rb^+ + H. Other experimental (scattering) and theoretical studies involving Rb + H^+ (e.g. [SEL 67, GIR 77A]) can be found in review articles [ALV 81, MOR 85]. Pseudopotential calculations by von Szentpály *et al.* [SZE 82] determined ground state properties (D_e, R_e, ω_e) and the dipole moment of RbH^+.

4.10. Negative Ions

Stevens *et al.* [STE 81] calculated the $X\,^2\Sigma^+$ state RbH^- potential energy curve and the electron affinity of RbH. Collisional processes (reviewed by [ALV 81, MOR 85]) which probe the negative ion potential curves have been studied [AND 80].

4.11. Other Comments

Various models for the potential energy curves were proposed to reproduce the observed spectroscopic constants [VAR 63, RAY 79, KUL 79, PRA 79, GHO 81, KAU 83, KUM 86, VAR 88]. *A* modified Rittner model of the ionic diabatic potential was constructed [YAN 82]. The dissociation energy of RbH was estimated using this ionic potential [YAN 82, YAN 83].

The formation of microcrystals of RbH ("laser snow") in an irradiated gaseous mixture of Rb and H_2 has been reported [TAM 75, TAM 77, KAT 85]. See Sec. 5.11. for further discussion of "laser snow".

5. CsH

5.1 Conventional Spectroscopy

Almy and Rassweiler [ALM 38] first photographed the $X\,^1\Sigma^+ - A\,^1\Sigma^+$ absorption spectrum in the region of 455 – 625 nm. Two vibrational levels ($v'' = 0$ and 1) of the $X\,^1\Sigma^+$ state and eighteen vibrational levels ($v' = 3 - 20$, corrected numbering) of the $A\,^1\Sigma^+$ state were observed. Bartky [BAR 66B] and Csaszar and Koczkas [CSA 67] established the correct vibrational numbering for the $A\,^1\Sigma^+$ state by photographing the CsD absorption spectrum. Ringström [RIN 70] photographed absorption from the ground $X\,^1\Sigma^+$ state to the second excited $^1\Sigma^+$ state correlating with the Cs(5*d*) + H separated atom limit. In this review we designate the second excited $^1\Sigma^+$ state as the *C* state instead of the original label given by Ringström (the symbol *B* is reserved for the yet unobserved first excited $^1\Pi$ state). Ringström observed eleven vibrational bands with $v' = (b + 1) - (b + 11)$ where *b* was estimated to be 10 ± 3.

TABLE 5.1. Recommended spectroscopic constants for CsH[a]

	$X\,^1\Sigma^+$		$A\,^1\Sigma^+$ (HSI 78)
	MAG 88B	CRE 84	
ZPE	442.98	442.69	88.10
Y_{00}	0.55	0.18	1.81
Y_{10}	891.251	891.465	169.05833
Y_{20}	−12.8159	−12.943	7.1487519
Y_{30}	0.07701	0.1053	−0.25477119
10^3Y_{40}		−3.19	2.95268
10^5Y_{50}		1.81	
10^6Y_{60}		−6.21	
Y_{01}	2.709011	2.70978	1.0629736
Y_{11}	−0.066948	−0.06153	0.027538611
10^3Y_{21}	0.2317	0.521	−2.1498749
10^5Y_{31}		−4.88	3.8327693
10^6Y_{41}		4.42	
10^7Y_{51}		−1.56	

[a]All entries in cm^{-1} units; non-rounded values reported here are important for use in RKR calculations, particularly for highest vibrational levels.

5.2. Laser Spectroscopy

In 1976 Tam and Happer [TAM 76] reported the first $A\ ^1\Sigma^+ \rightarrow X\ ^1\Sigma^+$ fluorescence spectrum excited by an argon ion laser operating at 457.9 nm. Fifteen vibrational levels ($v'' \leq 14$) of the $X\ ^1\Sigma^+$ state were observed. Using the same 457.9 nm excitation, Ligare *et al.* [LIG 82] observed an additional fluorescence doublet near 1.29 μ. The transition is to a vibrational level very close to the dissociation limit of ground state CsH. Using a krypton ion laser 356.4 nm line, Yang [YAN 82A] excited $C\ ^1\Sigma^+ \rightarrow X\ ^1\Sigma^+$ fluorescence, and P and R doublets for vibrational levels up to $v'' = 24$ for the $X\ ^1\Sigma^+$ state were observed.

In their laser-induced fluorescence, Ferray *et al.* [FER 84] measured ratios of transition probabilities corresponding to the lines $A\ ^1\Sigma^+$ ($v' = 6; J' = 1 - 18$) $\rightarrow X\ ^1\Sigma^+(v'' = 1, 2; J'')$. Crepin *et al.* [CRE 84] pumped the $v'' = 0, J'' = 9$ level of the $X\ ^1\Sigma^+$ state with the 457.9 nm line of the Ar^+ laser to reach the $v' = 19, J' = 10$ level of the $A\ ^1\Sigma^+$ state. They recorded the resulting fluorescence via high-resolution Fourier transform spectrometry. [CRE 84] report over one hundred $A\ ^1\Sigma^+$ ($v' = 19$, $J' = 10$) $\rightarrow X\ ^1\Sigma^+$ (v'', J'') transitions ranging up to $v'' = 25$. The $v'' = 25, J'' = 11$ level was observed to be rotationally predissociated.

The recent vibration-rotation studies of [MAG 88B] give the highly accurate data on twenty-six $X\ ^1\Sigma^+$ state transitions for the $v'' = 1 \leftarrow 0$, $2 \leftarrow 1$ and $3 \leftarrow 2$ bands.

TABLE 5.2. RKR potential energy curve of the $X\ ^1\Sigma^+$ state of CsH [CRE 84]

v	$[G(v) + Y_{00}]$ (cm^{-1})	R_{v-} (Å)	R_{v+} (Å)
0	442.6883	2.3154	2.7067
1	1308.5949	2.2027	2.8887
2	2149.4842	2.1329	3.0294
3	2965.8740	2.0804	3.1543
4	3758.2452	2.0378	3.2708
5	4527.0496	2.0020	3.3823
6	5272.7148	1.9710	3.4907
7	5995.6424	1.9437	3.5973
8	6696.2037	1.9194	3.7028
9	7374.7297	1.8975	3.8079
10	8031.4973	1.8777	3.9131
11	8666.7107	1.8595	4.0190
12	9280.4781	1.8428	4.1261
13	9872.7849	1.8275	4.2348
14	10443.4612	1.8134	4.3457
15	10992.1454	1.8005	4.4598

Reduced mass μ = 1.00024037 for ^{133}CsH [HUB 79].

5.3. Spectroscopic Constants

For the $X\ ^1\Sigma^+$ state, vibrational constants are reported by [TAM 76, YAN 82, CRE 84, MAG 88B, PAR 88A] and rotational constants are reported by [ALM 38, YAN 82, CRE 84, MAG 88B, PAR 88A]. Using the method of [STW 72], Yang determined rotational constants $B_{v'J'}$ and vibrational constants $G_{J'}(v'')$ for the effective potential energy curve of the rotating CsH molecule with $J'' = 15$ [YAN 82]. Pardo *et al.* [PAR 88A] used earlier spectroscopic results on CsH and CsD [ALM 38, BAR 66B, CSA 67, TAM 76] and report isotopically combined spectrosopic constants for $0 \leq v'' \leq 14$. The spectroscopic constants of [MAG 88B] are limited to the range $0 \leq v'' \leq 3$. The constants of [CRE 84] have a larger range, $0 \leq v'' \leq 15$. RKR curves calculated by these last two sets of constants are in good agreement up through $v'' = 3$ (differences in $G(v)$ and $R_{v\pm}$ values are $\leq 0.4\ cm^{-1}$ and ≤ 0.007 Å, respectively). Therefore, we recommend both [CRE 84, MAG 88B] sets of constants (see Table 5.1.).

The spectroscopic constants of the $A\ ^1\Sigma^+$ state recommended by Huber and Herzberg [HUB 79] are those of Bartky [BAR 66B]. The spectroscopic constants by Hsieh *et al.* [HSI 78] are preferred here because they were based on more extensive data. Hsieh *et al.* [HSI 78] reanalyzed the lines reported by Csaszar and Koczkas [CSA 67] and combined them with data reported by Bartky [BAR 66B] and Almy and Rassweiler [ALM 38] in a mass-reduced fit of the spectroscopic constants. [PAR 88A] report isotopically combined constants based on earlier spectroscopic data [ALM 38, BAR 66B, CSA 67, HSI 78].

For the $C\ ^1\Sigma^+$ state the vibrational numbering was unknown. The rotational constants and the vibrational energy spacings for eleven vibrational levels were reported by Ringström [RIN 70].

Ringström [RIN 70] obtained vibrational spacings of the first triplet state that goes to the Cs(5d) + H(1s) asymptote (labeled "$a\ ^3\Delta$" in the original paper and adopted in the tables of [HUB 79]) by analyzing the perturbations in the $C\ ^1\Sigma^+ - X\ ^1\Sigma^+$ absorption spectra. The very recent work of Carnell and Peyerimhoff [CAR 89] identifies this triplet state to be a $^3\Pi$, not a $^3\Delta$ state. Calculations by both [CAR 89] and [JEU 83A] show the $^3\Pi$ state to be bound ($\omega_e = 290\ cm^{-1}$ and $352\ cm^{-1}$, respectively, versus Ringström's $\omega_e = 350\ cm^{-1}$ [JON 90]) and the $^3\Delta$ state to be unbound.

The recommended value of $T_e = 17839\ cm^{-1}$ is based on [ALM 38] and $[G(v) + Y_{00}]$ values in Tables 5.2 and 5.3 for $v'' = 2$ and $v' = 3$. Because the $v' = 0 - 2$ levels of the $A\ ^1\Sigma^+$ state are unobserved, this value must be considered somewhat uncertain. This uncertainty is estimated at $\sim 25\ cm^{-1}$ based on those noted for KH and RbH. [HSI 78] give $17840.9\ cm^{-1}$, [PAR 88A] give $17841.9\ cm^{-1}$ and [BAR 66B] gives $17845.8\ cm^{-1}$.

5.4. Potential Energy Curves

The $A\ ^1\Sigma^+$ RKR vibrational turning points for $v' = 6 - 20$ were first reported by Ringström [RIN 70]. The RKR potential curves of both the $X\ ^1\Sigma^+$ (up to $v'' = 14$) and the $A\ ^1\Sigma^+$ (up to $v' = 20$) states based on more extensive data were calculated by Hsieh *et al.* [HSI 78]. [PAR 88A] also report RKR curves for $X\ ^1\Sigma^+$ ($0 \leq v'' \leq 14$) and $A\ ^1\Sigma^+$ ($0 \leq v' \leq 20$) states. Because the $v' = 0 - 2$ levels for the $A\ ^1\Sigma^+$ state were not observed, the

$A\ ^1\Sigma^+$ state RKR potential is slightly uncertain near the bottom of the potential well. Based on laser-induced fluorescence to higher vibrational levels, Yang [YAN 82A] extended the $X\ ^1\Sigma^+$ state RKR potential curve up to $v'' = 24$.

The recommended RKR potential energy curve for the $X\ ^1\Sigma^+$ state of CsH is based on the spectroscopic constants of [CRE 84] and given in Table 5.2. Although the RKR curve calculated with the [MAG 88B] constants is in good agreement with the one in Table 5.2 for the bottom of the well, it is limited up to only $v'' = 3$. The recommended RKR potential energy curve for the $A\ ^1\Sigma^+$ state is that of [HSI 78]; see Table 5.3.

An RKR potential energy curve for the $2\ ^3\Pi_1$ state of CsH has been reported [JON 90]. After the suggestion of Carnell and Peyerimhoff [CAR 89] (see preceding section), Jong *et al.* [JON 90] reanalyzed the data of Ringström [RIN 70] and determined new Dunham coefficients, from which they constructed a new RKR potential curve ($v = 0$, 1 and 2 in a 912 cm^{-1} deep well). Since this RKR curve is based on a deperturbation analysis and not on direct observation of $2\ ^3\Pi_1$ levels, it is significantly more uncertain than the $X\ ^1\Sigma^+$ and $A\ ^1\Sigma^+$ state RKR potential curves discussed above. Hence the RKR curve is not reported here.

Hybrid potential energy curves have been constructed for the $X\ ^1\Sigma^+$ [YAN 81, TEL 84, ZEM 88, PAR 88A] and the $A\ ^1\Sigma^+$ [YAN 81, TEL 84, PAR 88A] states. The [YAN 81] curves use the $X\ ^1\Sigma^+$ and $A\ ^1\Sigma^+$ RKR curves of [HSI 78] up to $v'' = 14$ and $v' = 20$, respectively. An exponential repulsion is used inside the innermost turning points R_{14-} and R_{20-}, respectively. The long-range regions ($R \geq 18\ a_o$ and $\geq 20\ a_o$, respectively) are represented by $-C_6/R^6 - C_8/R^8$, where C_6 and C_8 are the dispersion constants for CsH. The gap between the RKR outermost turning points and long-range is filled by scaling the *ab initio* results [LAS 81] at 9, 10, 12 and 14 a_o for the X state (only 14 a_o for the A state) to fit smoothly onto R_{14+} (and R_{20+}). Telle [TEL 84] uses hybrid potential curves based on RKR [HSI 78, YAN 82A] and scaled *ab initio* results [LAS 81] for both states. His hybrid curves appear very similar to those just described [YAN 81], but insufficient details are provided to reconstruct them. For both states, the PMO-RKR-van der Waals curves of [PAR 88A] represent the minima of the curves with eleven parameter perturbed Morse oscillators, the middle regions of the curves by RKR curves, and the innermost repulsive and outermost attractive regions by inverse power series $+\sum_n C_n/R^n$ (n is even and goes from 6 to 14). The C_n constants of [PAR 88A] are determined by least-squares fits to the uppermost RKR turning points and bear no resemblance to normal dispersion coefficients.

The Zemke and Stwalley [ZEM 88] hybrid curve for the $X\ ^1\Sigma^+$ state, similar in construction to the earlier one [YAN 81], used newer RKR data [CRE 84, YAN 82A] and three terms in the long-range expansion. The points from [YAN 82A] were scaled to match smoothly onto the R_{15+} outermost turning point [CRE 84]. This extended the well out to 12.5 a_o and no *ab initio* results were needed to fit onto the long-range region. With the [ZEM 88] hybrid curve, the precise line width of the $v'' = 25, J'' = 11$ level could be determined. This curve is recommended for estimating higher vibrational levels in the $X\ ^1\Sigma^+$ state of CsH.

TABLE 5.3. RKR potential energy curve of the $A\ ^1\Sigma^+$ state of CsH [HSI 78]

v	$[G(v) + Y_{00}]$ (cm^{-1})	R_{v-} (Å)	R_{v+} (Å)
0	88.10	3.5505	4.4286
1	270.64	3.2666	4.7426
2	465.27	3.0911	4.9486
3	670.61	2.9609	5.1113
4	885.33	2.8570	5.2502
5	1108.20	2.7708	5.3746
6	1338.03	2.6973	5.4898
7	1573.73	2.6334	5.5989
8	1814.26	2.5772	5.7041
9	2058.66	2.5272	5.8068
10	2306.04	2.4822	5.9081
11	2555.57	2.4416	6.0088
12	2806.52	2.4046	6.1094
13	3058.20	2.3707	6.2104
14	3310.01	2.3395	6.3119
15	3561.40	2.3106	6.4142
16	3811.91	2.2837	6.5175
17	4061.15	2.2586	6.6216
18	4308.80	2.2350	6.7266
19	4554.60	2.2128	6.8324
20	4798.36	2.1917	6.9387

TABLE 5.4. Estimated D_e values for CsH

Method	Estimate (cm^{-1})	Reference
Birge-Sponer Extrapolation, X State	17200 ± 500	TAM 76
Scaled Value from Linear Birge-Sponer Extrapolation, X State	15000 ± 500	STW 78
Fit of Ionic-Covalent Splitting and Avoided Crossing	15300 ± 300	PRA 81
$A - X$ Fluorescence	>14749.3	LIG 82
Fit of Diabatic Ionic Potentials	14500 ± 500	YAN 82
$C - X$ Fluorescence	14805 ± 30	YAN 82A
Extrapolation to Ionic-Covalent Avoided Crossing, A State	14910 ± 400	YAN 83
Observation of $v'' = 25, J'' = 11$ Predissociation	14807 ± 5	CRE 84
Line Width of $v'' = 25, J'' = 11$	14791.2 ± 2.0	ZEM 88
Recommended	14791.2 ± 2.0	

5.5. Dissociation Energy

The common polynomial Birge-Sponer extrapolation of vibrational spacing gives too high an estimate for dissociation energy [STW 78] because the shape of the potential energy curve for the $X\ ^1\Sigma^+$ state near dissociation is influenced by the avoided crossing interaction with the $A\ ^1\Sigma^+$ state. Ligare *et al.* [LIG 82] observed a near-infrared fluorescence from the $A\ ^1\Sigma^+$ state to a high vibrational energy level near dissociation, which therefore allowed them to set a very tight lower limit for a dissociation energy of $D_o > 14303.8\ cm^{-1}$ (or $D_e > 14749.3\ cm^{-1}$). Yang [YAN 82A] observed $C\ ^1\Sigma^+ - X\ ^1\Sigma^+$ fluorescence up to levels quasibound by the centrifugal barrier. The observation in the $A\ ^1\Sigma^+ - X\ ^1\Sigma^+$ fluorescence [CRE 84] that the $v'' = 25, J'' = 11$ quasibound level was predissociating gave a value of $D_e = 14807\ cm^{-1}$, in close agreement with that of [YAN 82A]. Zemke and Stwalley [ZEM 88] took this observation further; they constructed a hybrid potential curve based on the RKR potential [CRE 84, YAN 82A] and included proper long-range behavior beyond the last turning point. From a comparison of calculated line widths for this quasibound level (for a number of possible dissociation energies) and the experimental line width [CRE 84], a precise value of $14791.2 \pm 2.0\ cm^{-1}$ was obtained (see Table 5.4.).

5.6. Electronic Structure Calculations

CsH has been an interesting test case for core-valence correlation and relativistic effects because of the large number of electrons in the Cs atom. Karo *et al.* [KAR 78] performed an *ab initio* all-electron non-relativistic MC-SCF calculation on the $X\ ^1\Sigma^+$ state of CsH. The discrepancies with the spectroscopic data were attributed to the limited basis and the neglect of core-valence correlation [KAR 78, STE 81]. Stevens *et al.* [STE 81] used a pseudopotential to simulate Cs core electrons and therefore the relativistic effects and the atomic core-valence interactions were included empirically. The calculated R_e value for $X\ ^1\Sigma^+$ was too small, perhaps due to the underestimated core polarization effects in CsH. Laskowski and Stallcop [LAS 81] applied a relativistic effective core potential (RECP) method to calculate the potential curves and the dipole moment functions of the $X\ ^1\Sigma^+$ and $A\ ^1\Sigma^+$ states and the $A - X$ transition dipole moment function. CI calculations were performed on the outermost two electrons of CsH. The approximation works well for intermediate and large internuclear distances, but starts to break down for $R \lesssim R_e$. Their well depth of the $A\ ^1\Sigma^+$ potential and shapes of the $A\ ^1\Sigma^+$ and $X\ ^1\Sigma^+$ potential curves agree well with the experimental results [HSI 78, YAN 82A], but the energy gap $\Delta V(R_c)$ at the avoided crossing distance was about 20% too high compared to the gap between the experimental potentials [YAN 82A].

Jeung *et al.* [JEU 83A] calculated the nineteen lowest states of CsH using a relativistic effect core potential method. Langhoff *et al.* [LAN 86] calculated ground state properties (D_e, R_e, ω_e) with their coupled-pair functional approach. Fuentealba *et al.* [FUE 87] also determined ground state properties with their pseudopotential calculations. Bussery *et al.* [BUS 86] calculated long-range multipole expansion coefficients for the $X\ ^1\Sigma^+$, $a\ ^3\Sigma^+$, $A\ ^1\Sigma^+$, $b\ ^3\Pi$, $B\ ^1\Pi$ and $c\ ^3\Sigma^+$ states. Very recently large multireference CI (MRDCI) calculations have been performed on the first seventeen states of CsH [CAR 89, CAR 89A]. Carnell, Peyerimhoff and Hess [CAR 89A] compare relativistic and nonrelativistic potential curves for the $^1\Sigma^+$ states. They report dipole moment functions for the lowest five $^1\Sigma^+$ states, four $^3\Sigma^+$ states, three $^1\Pi$ states and three $^3\Pi$ states. Carnell, Peyerimhoff and Hess [CAR 89A] also report $A - X$, $C - X$ and $C - A$ transition dipole moment functions; these are the first ever transition moments for the $C\ ^1\Sigma^+$ state. Carnell and Peyerimhoff [CAR 89] examine in detail the misassignment by [RIN 70] of the second $^3\Pi$ state (see Jong *et al.* [JON 90]).

Stevens *et al.* [STE 81] calculated the potential curve for the $a\ ^3\Sigma^+$ state. The lowest energy $X\ ^1\Sigma^+ - a\ ^3\Sigma^+$ potential curve splitting was estimated by [KNO 69].

Pyykkö *et al.* [PYY 81] studied the effect of *d* orbitals on relativistic bond-length contractions. They found that 5*d* orbital of Cs is important and it diminishes the usual relativistic bond-length contraction. Laskowski *et al.* [LAS 83] compared ten valence electron relativistic effective core potential and nonrelativistic all electron *ab initio* calculations to examine the relative importance of core-valence correlation and relativistic effects. They found that correlating the Cs (5*s*, 5*p*) electrons leads to a significant bond shortening effect ($\sim 0.15\ a_o$), but relativistic contraction of Cs (6*s*) leads to a bond shortening of only $\sim 0.005\ a_o$.

Other electronic calculations were prompted by the interest in the Cs + H collisional excitation or charge transfer processes. In these studies, the attention is mainly limited to the ionic-covalent configuration mixing. Grice and Herschbach [GRI 74], and Adelman and Herschbach [ADE 77] calculated the energy splitting of the $A\ ^1\Sigma^+$ and the $X\ ^1\Sigma^+$ potential curves at the ionic covalent crossing distance in a two-configuration CI approximation. Adelman and Herschbach [ADE 77] also calculated the energy splitting between the $A\ ^1\Sigma^+$ and the $C\ ^1\Sigma^+$ curves at the second ionic-covalent crossing distance. Olson *et al.* [OLS 76] calculated the $X\ ^1\Sigma^+$, $A\ ^1\Sigma^+$, $B\ ^1\Pi$ and $C\ ^1\Sigma^+$ potentials and the electronic non-adiabatic coupling matrix elements in a two-electron approximation. They calculated the cross section for $Cs^+ + H^- \rightarrow Cs + H$. Olson [OLS 80B] later recalculated the cross section using an empirical coupling matrix element and the RKR curves of Hsieh *et al.* [HSI 78]. Recently Olson *et al.* [OLS 84] made a pseudopotential molecular structure calculation of the lowest five $^1\Sigma^+$ states and two $^1\Pi$ states of CsH. They also calculated the electronic nonadiabatic coupling functions between electronic states in the adiabatic representation. Janev and Radulovic [JAN 78] employed asymptotic wavefunctions in a two-electron approximation to calculate the energy gap $\Delta V(R_c)$ at the avoided crossing point R_c.

TABLE 5.5. High quality calculations of CsH (Hartree-Fock or better), normally calculated at R_e

Method	state	$-E$(a.u.)	D_e(cm^{-1})	$R_e(a_o)$	Range of $V(R)$	Spect. const.	Other properties, comments	Ref.
CI	$X\,^1\Sigma^+$	–	–	–	–	–	in figure only	OLS 76
	$A\,^1\Sigma^+$	–	–	–	–	–	in figure only	
	$B\,^1\Pi$	–	–	–	–	–	in figure only	
	$C\,^1\Sigma^+$	–	–	–	–	–	in figure only	
MCSCF	$X\,^1\Sigma^+$	7554.47132	12545^N	5.5^N	4.0 – 20, ∞	√		KAR 78
			12700	5.26	4.0 – 20, ∞	–		
Pseudopotential	$X\,^1\Sigma^+$	–	15304^N	4.50^N	3.0 – 40, ∞	√		STE 81
MCSCF		–	15384	4.57	3.0 – 40, ∞	–		
	$a\,^3\Sigma^+$	–	437^N	5.0^N	3.0 – 40, ∞	–		
2e$^-$ RECP CI	$X\,^1\Sigma^+$	–	14861^N	4.71^N	4.42 – 25, ∞	–	$\mu(R)$	LAS 81,
10e$^-$ RECP CI		–	14327^N	5.0^N	4.00 – 30, ∞	√		LAS 83
2e$^-$ RECP CI	$A\,^1\Sigma^+$	7554.3419	7598^N	7.525^N	4.42 – 25, ∞	–	$\mu(R)$, $A-X$ transition moment	
Pseudopotential CI	$X\,^1\Sigma^+$	–	15485	4.48	–	√		JEU 82
RECP	$X\,^1\Sigma^+$	–	14518	4.47	4.0 – 21, ∞	√	in table and figure	JEU 83A
	$a\,^3\Sigma^+$	–	–	–	4.0 – 21, ∞	–	in figure only, unbound	
	$A\,^1\Sigma^+$	–	8630	8.10	4.0 – 21, ∞	√	in table and figure	
	$b\,^3\Pi$	–	320	6.25	–	√	in figure only	
	$B\,^1\Pi$	–	80	7.09	–	√	in figure only	
	$c\,^3\Sigma^+$	–	–	–	4.0 – 21, ∞	√	in table and figure, unbound	
	$C\,^1\Sigma^+$	–	2180	6.00	4.0 – 21, ∞	√	in table and figure	
	$^3\Sigma^+$	–	2740	14.8	4.0 – 21, ∞	√	in table and figure	
	$^3\Pi$	–	970	5.66	–	√	in figure only	
	$^3\Delta$	–	~80	6.98	–	√	in figure only	
	$^1\Delta$	–	~80	7.02	–	√	in figure only	
	$^1\Sigma^+$	–	~160	7.04	4.0 – 21, ∞	√	in table and figure	
	$^3\Sigma^+$	–	<8	8.67	4.0 – 21, ∞	√	in table and figure	
	$^1\Sigma^+$	–	~640	6.14	4.0 – 21, ∞	√	in table and figure	
	$^1\Pi$	–	4680	9.97	–	√	in figure only	
	$^3\Sigma^+$	–	~400	7.94	4.0 – 21, ∞	√	in table and figure	
	$^3\Pi$	–	~240	6.75	–	√	in figure only	
	$^1\Pi$	–	4680	6.88	–	√	in figure only	
	$^1\Sigma^+$	–	1940	5.54	4.0 – 21, ∞	√	in table and figure	
Pseudopotential CI	$X\,^1\Sigma^+$	–	–	–	–	–	in figure only	OLS 84
	$A\,^1\Sigma^+$	–	–	–	–	–	in figure only	
	$B\,^1\Pi$	–	–	–	–	–	in figure only	
	$C\,^1\Sigma^+$	–	–	–	–	–	in figure only	
	$^1\Pi$	–	–	–	–	–	in figure only	
	$^1\Sigma^+$	–	–	–	–	–	in figure only	
	$^1\Sigma^+$	–	–	–	–	–	in figure only	
CPF	$X\,^1\Sigma^+$	–	15000	4.78	–	√	$\mu(R)$	LAN 86
Pseudopotential CI	$X\,^1\Sigma^+$	–	13470	4.77	–	√	μ	FUE 87
MRD CI	$2\,^3\Pi$	–	645	5.99	–	√	in table and figure	CAR 89

TABLE 5.5. High quality calculations of CsH (Hartree-Fock or better), normally calculated at R_e – Continued

Method	State	$-E$(a.u.)	D_e(cm^{-1})	$R_e(a_o)$	Range of $V(R)$	Spect. const.	Other properties, comments	Ref.
MRD CI	$X\,^1\Sigma^+$	–	14131	4.81	3.50 – 20, ∞	√	in figure only, $\mu(R)$, $A-X$, $C-X$ transition moment	CAR 89A
	$a\,^3\Sigma^+$	–	–	–	3.50 – 20, ∞	–	in figure only, unbound, $\mu(R)$	
	$A\,^1\Sigma^+$	–	7767	7.46	3.50 – 20, ∞	√	in figure only, $\mu(R)$, $C-A$ transition moment	
	$b\,^3\Pi$	–	–	–	3.50 – 20, ∞	–	in figure only, $\mu(R)$	
	$B\,^1\Pi$	–	–	–	3.50 – 20, ∞	–	in figure only, $\mu(R)$	
	$c\,^3\Sigma^+$	–	–	–	3.50 – 20, ∞	–	in figure only, unbound, $\mu(R)$	
	$C\,^1\Sigma^+$	–	1936	–	3.50 – 20, ∞	√	in figure only, $\mu(R)$, labeled $B\,^1\Sigma^+$	
	$^3\Sigma^+$	–	–	–	3.50 – 20, ∞	–	in figure only, $\mu(R)$	
	$^3\Pi$	–	–	–	3.50 – 20, ∞	–	in figure only, $\mu(R)$	
	$^3\Delta$	–	–	–	3.50 – 20, ∞	–	in figure only, unbound	
	$^1\Delta$	–	–	–	3.50 – 20, ∞	–	in figure only, unbound	
	$^1\Sigma^+$	–	–	–	3.50 – 20, ∞	–	in figure only, $\mu(R)$	
	$^1\Pi$	–	–	–	3.50 – 20, ∞	–	in figure only, $\mu(R)$	
	$^3\Sigma^+$	–	–	–	3.50 – 20, ∞	–	in figure only, $\mu(R)$	
	$^1\Sigma^+$	–	–	–	3.50 – 20, ∞	–	in figure only, $\mu(R)$	
	$^3\Pi$	–	–	–	3.50 – 20, ∞	–	In figure only, $\mu(R)$	
	$^1\Pi$	–	–	–	3.50 – 20, ∞	–	in figure only, $\mu(R)$	
Pseudopotential with one-center wf	$X\,^1\Sigma^+$	–	9240	4.53	1 – 10	–	IP	TAM 89

[N] indicates lowest point, not R_e.
∞ means asymptotic energy calculation.

TABLE 5.6. High quality calculations of CsH^+ and CsH^- (Hartree-Fock or better), normally calculated at R_e

Method	State	$-E$(a.u.)	D_e(cm^{-1})	$R_e(a_o)$	Range of $V(R)$	Spect. const.	Other properties, comments	Ref.
				CsH^+				
CI	$A\,^2\Sigma^+$	–	–	–	–	–	in figure only	OLS 76
	$B\,^2\Sigma^+$	–	–	–	–	–	in figure only, unbound	
	$D\,^2\Sigma^+$	–	–	–	–	–	in figure only	
MCSCF	$X\,^2\Sigma^+$	7554.29351	80[N]	8.0[N]	4 – 20, ∞	–	KAR 78	
PVB	$X\,^2\Sigma^+$	–	–	–	–	–	in figure only	
	$A\,^2\Sigma^+$	–	5487[N]	10.45[N]	–	–	in figure only	SID 78
	$B\,^2\Sigma^+$	–	–	–	–	–	in figure only	
	$C\,^2\Pi$	–	–	–	–	–	in figure only	
	$D\,^2\Sigma^+$	–	–	–	–	–	in figure only, unbound	
	$E\,^2\Pi$	–	–	–	–	–	in figure only	
	$F\,^2\Sigma^+$	–	–	–	–	–	in figure only	
Hellman pseudopotential	$X\,^2\Sigma^+$	–	~240	17.6	–	–	in table only	VAL 78
	$A\,^2\Sigma^+$	–	~5670[N]	9.0[N]	5 – 25, ∞	–	in table and figure	
	$B\,^2\Sigma^+$	–	~2100[N]	~17.0[N]	5 – 25, ∞	–	in table and figure	
	$D\,^2\Sigma^+$	–	–	–	5 – 25, ∞	–	in table and figure, unbound	
	$F\,^2\Sigma^+$	–	~400[N]	23.0[N]	5 – 25, ∞	–	in table and figure	
Pseudopotential	$A\,^2\Sigma^+$	–	6210(±400)	10(±1)	5 – 25, ∞	–	also fit to expt. scat. data	SCH 78
PVB	$A\,^2\Sigma^+$	–	5730	10.4	–	–	in table only	KUB 81
Pseudopotential	$A\,^2\Sigma^+$	–	6940	9.17	–	–	in table and figure	KIM 82A
	$B\,^2\Sigma^+$	–	–	–	–	–	in figure only	
	$C\,^2\Pi$	–	–	–	–	–	in figure only	
	$D\,^2\Sigma^+$	–	–	–	–	–	in figure only, unbound	
	$E\,^2\Pi$	–	–	–	–	–	in figure only	
	$F\,^2\Sigma^+$	–	–	–	–	–	in figure only	
	$G\,^2\Sigma^+$	–	–	–	–	–	in figure only, unbound	
	$H\,^2\Pi$	–	–	–	–	–	in figure only, unbound	
Pseudopotential	$X^2\Sigma^+$	–	282	6.14	–	√	μ	SZE 82

TABLE 5.6. High quality calculations of CsH^+ and CsH^- (Hartree-Fock or better), normally calculated at R_e – Continued

Method	State	$-E$(a.u.)	$D_e(cm^{-1})$	$R_e(a_o)$	Range of $V(R)$	Spect. const.	Other properties, comments	Ref.
				CsH^-				
MCSCF	$X\,^2\Sigma^+$	7554.48276	9700[N]	5.5[N]	4 – 20, ∞	√	ad EA(CsH) = 0.357 eV	KAR 78
			9760	5.62	4 – 20, ∞	–		
Pseudopotential	$X\,^2\Sigma^+$	–	12734[N]	4.713[N]	3 – 40, ∞	√	ad EA(CsH) = 0.438 eV	STE 81
MCSCF		–	12835	4.78	3 – 40, ∞	–		

Comparisons of theoretically calculated and experimentally measured energy gaps $\Delta V(R_c)$ and avoided crossing distances R_c may be found in [YAN 82, YAN 82A, OLS 84]. Dipole moment functions for $X\,^1\Sigma^+$ and $A\,^1\Sigma^+$ states and the $A-X$ transition dipole moment function [LAS 81, CAR 89A] all exhibit strong changes in the curvature of the curves near the avoided crossing distance, reflecting the ionic-covalent configuration interaction in this region. In particular, the $A\,^1\Sigma^+$ state dipole moment function [LAS 81] shows a dramatic change from −1.5 a.u. at short distances (~5 a_o) to +8.5 a.u. at longer distances (~13 a_o) because of the change from Cs^-H^+ polarity at small separations to Cs^+H^- at moderately large separations. Similar behavior was noted in the LiH $A\,^1\Sigma^+$ state dipole moment function [PAR 81].

5.7. Radiative and Dipole Properties

Ferray *et al.* [FER 84] measured relative transition probabilities for the transitions from $A\,^1\Sigma^+$ ($v' = 6; J'$) to $X\,^1\Sigma^+$ ($v'' = 1, 2; J' \pm 1$). They measured radiative lifetimes from several $A\,^1\Sigma^+$ state levels ($J' = 10$ or 11): $v' = 6, 7$ ($\tau = 90$ *ns*), $v' = 12$ ($\tau = 35$ *ns*), $v' = 15$ ($\tau = 27$ *ns*) and $v' = 19$ ($\tau = 30$ *ns*). Other radiative lifetime determinations are based on theoretical calculations.

A radiative lifetime of 84.5 nsec was estimated for the $A\,^1\Sigma^+$ ($v' = 19, J' = 10$) level [YAN 81]. The calculation was based on the theoretical transition dipole moment function [LAS 81] and the experimental RKR potential curves [HSI 78]. The Einstein A coefficients for $A\,^1\Sigma^+$ ($v' = 19, J' = 10$) → $X\,^1\Sigma^+$ ($v'' = 0 - 25, J' = 9, 11$) transitions were calculated. The calculated relative fluorescence intensities agree well with the experimental measurements. These studies also confirm that the assumption of an R-independent transition moment (the Franck-Condon approximation) breaks down badly for these radiative transitions. Carnell *et al.* [CAR 89A] report Einstein A coefficients for the rotationless $A\,^1\Sigma^+$ ($v' = 19$) → $X\,^1\Sigma^+$($v'' = 0 - 10$) transitions.

Telle [TEL 84] calculated improved transition probabilities and lifetimes of the $A\,^1\Sigma^+$ state. In particular, he used the new and improved $X\,^1\Sigma^+$ potential of [YAN 82]. His transition dipole moment function was based on that of [LAS 81], but modified slightly to reproduce experimental intensities [FER 84]. [TEL 84] reports Einstein A coefficients and radiative lifetimes for $v' = 0 - 35$ ($v' = 31, 32, 34$ and 36 were not calculated, but their lifetimes should all be ~31 ns).

These calculations agree reasonably well with prior measurements [YAN 81, FER 84]. The lifetime calculations do not agree quantitatively with the experimental lifetimes of [FER 84], although they are comparable in magnitude and the experimental values are quite uncertain. A simple Landau-Zener calculation [TEL 86] suggests that the lifetimes are not significantly shortened by predissociation. Improved lifetime measurements and an improved $A-X$ transition dipole moment calculation (e.g. without a minimum at 14 a_o) would be desirable.

5.8. Other Properties

There has been very active experimental and theoretical research on the collisional charge exchange process, H (or D) + Cs → H^- + Cs^+, because of its importance to the controlled nuclear fusion technology. The knowledge of the dynamics and the cross section for this charge transfer reaction is useful for the production of intense H^- or (D^-) beams for heating and fueling of magnetically confined plasmas [OLS 80B]. Research in this area prior to 1981 (e.g. [HOO 77, MEY 80]) was reviewed by Alvarez and Cisneros [ALV 81] (see also [MOR 85]). Recently Miethe *et al.* [MIE 82] measured the total cross section for the collision energy range of 0.1 – 5 keV. Pradel *et al.* [PRA 81] measured the angular distribution of the scattered H^- ions.

The cross section is strongly controlled by the electronic nonadiabatic interactions near the avoided crossings of potential energy curves. The controlling factors include the energy gap between the potential curves at the avoided crossing region and the nonadiabatic coupling matrix elements for the adiabatic electronic states. The energy gap for CsH has been obtained by scattering experiments [PRA 81], and by spectroscopic measurement of the $X\,^1\Sigma^+$ and $A\,^1\Sigma^+$ potential energy curves at the avoided crossing region [YAN 82A], and also by theoretical calculations [OLS 84]. LiH is another example for which both the $A\,^1\Sigma^+$ state and the $X\,^1\Sigma^+$ state poten-

tial energy curves in the avoided crossing region were measured accurately [VER 82, CHA 86]. Whenever spectroscopic measurements reach the avoided crossing region, they provide highly accurate potentials and energy gaps.

Hiskes *et al.* [HIS 78] calculated the charge exchange cross-section for $Cs + H \rightarrow Cs^+ + H^-$. Using their theoretical potential curves and electronic nonadiabatic coupling terms, Olson *et al.* [OLS 84] calculated the same cross section for H + Cs (6*s*) and H + Cs* (6*p*) collisions.

5.9. Positive Ions

There are a wide variety of collisional experiments which probe the potential energy curves of CsH^+ [DON 64, ILI 67, SEL 67, BOH 68, SCH 69, GRU 69, GRU 70, SPI 70, SPI 72, PRA 74, TUA 74, MEY 75A, CIS 76, GIR 77A, MEY 77, SCH 78, PRA 79A, MEY 80, NAG 80, KUB 81, NAG 82, NAG 83]. Scheidt *et al.* [SCH 78] measured the elastic scattering of H^+ by Cs and obtained R_e (10 a_o) and well depth (0.77 eV) for the CsH^+ $A\,^2\Sigma^+$ state. There have been several theoretical studies of the $Cs - H^+$ interaction potentials [OLS 76, SCH 78, SID 78, VAL 78, KAR 78, KUB 81, SZE 82]. Note that the interaction potentials correlating with H^+ and Cs are the excited state potentials of CsH^+. The ground state of CsH^+ correlates with $H + Cs^+$. The experimental and theoretical studies on the corresponding collision processes are reviewed by Alvarez and Cisneros [ALV 81], Kubach and Sidis [KUB 81], Kimura *et al.* [KIM 82A], and Morgan *et al.* [MOR 85].

5.10. Negative Ions

Karo *et al.* [KAR 78] reported an MCSCF calculation and Stevens *et al.* [STE 81] reported an MCSCF pseudopotential calculation determining the potential energy curve for the CsH^- $X\,^2\Sigma^+$ state. Collisional processes (reviewed by [ALV 81, MOR 85]) which probe the negative ion potential curves have been studied [SPI 70, LES 71, GIR 77, AND 80, MEY 80, WAN 87A].

5.11. Other Comments

Various models for the potential energy curves were proposed to reproduce the observed spectroscopic constants [VAR 63, PRA 79, KUL 79, GHO 81, KAU 83, KUM 86, VAR 88]. A modified Rittner model of the ionic diabatic potential was constructed [YAN 82].

The photochemical formation of CsH was first reported by Tam *et al.* [TAM 75]. They found that CsH molecules and micrometer-size particles were formed when a gaseous mixture of Cs, H_2 and He was irradiated by an argon ion laser 457.9 nm line which excited the Cs atoms to the $7p_{1/2,3/2}$ states. Several reaction mechanisms were proposed [TAM 75, TAM 77, OMN 80, PIC 80, BHA 81, SAY 81, CRE 84A, GAD 86, VIS 86, GAD 87, LEP 87, RAH 87, GAD 88, LEP 89, TAN 89] including direct photochemical reaction of Cs(7*p*) with H_2 and indirect reactions involving reaction complexes or vibrationally excited H_2 as intermediates. The local concentration of CsH in the laser-illuminated region is well above the equilibrium value so that the CsH vapor condensed to form microcrystals [TAM 75, TAM 77, SAT 82] of various sizes and shapes [TAN 89]. The phenomenon of particle formation, called "laser snow", has been observed not only for Cs atoms excited to the 7*p* state but also for the 6*d* [VIS 83] and the 8*d* [TAM 77] states. Laser snows have also been observed for rubidium [TAM 75, TAM 77, KAT 85] and sodium [YAB 80] when the alkali atoms or the alkali diatomics were photoexcited.

The photochemical enhancement of the alkali hydride concentration has been found to be a useful technique for spectroscopic studies. Most spectroscopic measurements of the alkali hydride molecules were performed with a heated sample cell containing the alkali metal vapor, hydrogen and some buffer gas. The concentration of the alkali hydride in the cell is usually very low because the MH = M + 1/2 H_2 system heavily favors the right side in chemical equilibrium. Photoexcitation of the alkali atoms or molecules significantly increases the alkali hydride concentration of the sample for spectroscopic study. This technique has been applied in the studies of CsH [TAM 76, LIG 82, YAN 82A] and RbH [HSI 80].

Another technique that has been successful in enhancing the concentration of alkali hydrides involves the use of an electrical discharge through an alkali metal and hydrogen gaseous mixture. This technique has been applied in the study of NaH [BAL 76, GIR 80, SAS 81, SAS 81A], KH [GIR 80, GIR 82] and CsH [VIS 82, FER 84].

6. Discussion and Conclusions

6.1. Conventional Spectroscopy

For the four alkali hydrides and deuterides reviewed here, absorption and emission spectra associated with the $A\,^1\Sigma^+ - X\,^1\Sigma^+$ band system have been observed. These studies have already been evaluated in the earlier reviews by [GAY 68, ROS 70, HUB 79]. For KH, a structured continuum associated with $B\,^1\Pi - X\,^1\Sigma^+$ emission was also reported [HOR 33A]; for CsH, absorption spectra associated with the $C\,^1\Sigma^+ - X\,^1\Sigma^+$ system has been photographed [RIN 70]. Very precise vibration-rotation spectra have been observed recently in the $X\,^1\Sigma^+$ state of NaH [SAS 81, SAS 81A, MAK 89].

6.2. Laser Spectroscopy

Laser-induced fluorescence studies have provided additional spectra associated with the $A - X$ and $C - X$ systems already noted above. No new electronic states have been observed. Typically, higher vibrational v'' and v' energy levels have been determined by laser-induced fluorescence than by conventional spectroscopy. In addition,

very precise rotation-vibration studies have recently been published on NaH [LEO 87, MAG 88], KH [HAE 84], RbH [MAG 88A] and CsH [MAG 88B].

TABLE 6.1. Range of vibrational levels observed

Hydrides	$X\,^1\Sigma^+$	Per Cent Well Depth covered	$A\,^1\Sigma^+$	Per Cent Well Depth covered
NaH	0 – 15	86	0 – 21	70
KH	0 – 23	99	2 – 26	83
RbH	0 – 12	66	3 – 16	49
CsH	0 – 24	99	3 – 20	59
Deuterides				
NaD	0 – 20	83	7 – 16	45
KD	0 – 16	65	9 – 23	54
RbD	0 – 15	60	9 – 20	43
CsD	0 – 1	8	8 – 18	38

6.3. Spectroscopic Constants

The data are too sparse to determine spectroscopic constants for the $B\,^1\Pi$ state of KH. A reanalysis [JON 90] of Ringström's data [RIN 70] has provided new term values and rotational constants for the $C\,^1\Sigma^+$ state of CsH and limited information on the $2\,^3\Pi$ state. Spectroscopic constants have been determined for the four alkali hydrides which cover from 66 to 99% of the depth of the potential energy curve for the $X\,^1\Sigma^+$ states (see Table 6.1. and Figs. 1 and 2). Further studies including high v'' energy levels are needed on NaH and particularly RbH.

For the $A\,^1\Sigma^+$ states, vibrational levels observed cover from 49 to 83% of the potential energy curve (see Table 6.1.). More noteworthy, however, is the lack of data for low v' (0, 1 and sometimes 2). Except for NaH [ORT 80], the lowest $v' = 0$ vibrational energy levels and the associated ν_{00} transition energies are unobserved. Clearly, low v' data are needed to properly characterize the $A\,^1\Sigma^+$ potential minimum and very high v' data are needed to determine the uppermost part of the $A\,^1\Sigma^+$ potential in the four alkali hydrides discussed here.

Fits resulting from isotopically combined spectroscopic constants have been reported (e.g. in NaH [MAK 89] and KH [YAN 80]). However, the effect of Born-Oppenheimer breakdown on spectroscopic constants has not yet been treated in the four alkali hydrides reviewed here (unlike LiH [VID 82, VID 84, CHA 86]).

6.4. Potential Energy Curves

Accurate RKR potential energy curves (typically $[G(v) + Y_{00}]$ values to ≤ 0.01 cm^{-1} and $R_{v\pm}$ values to ≤ 0.001 Å) for $X\,^1\Sigma^+$ and $A\,^1\Sigma^+$ states for the four alkali hydrides have been determined (see Figs. 1 and 2, and Tables 2.3, 2.4, 3.2, 3.3, 4.2, 4.3, 5.2, 5.3). Clearly precise laser fluo-

TABLE 6.2. Energy and derivatives of the adiabatic $X\,^1\Sigma^+$ and $A\,^1\Sigma^+$ state potentials at the two-state ionic-covalent "crossing" distance R_c (where $\frac{dV_X}{dR} = \frac{dV_A}{dR}$).

			$V(R_c)$ (cm^{-1})		$\left.\frac{dV}{dR}\right\|_{R_c}$	$\left.\frac{d^2V}{dR^2}\right\|_{R_c}$	
		R_c (Å)	with respect to $V(R_e)$	with respect to $M^+ + H^-$	(cm^{-1}/Å)	(cm^{-1}/Å^2)	Ref.
NaH	$X\,^1\Sigma^+$	{4.0461}	14420.5	−36846.	{2739.0}	−4503.1	ZEM 84
	$A\,^1\Sigma^+$		1182.9	−27370.		2705.4	ORT 80
KH	$X\,^1\Sigma^+$	{4.7366}	13550.7	−30148.7	{2182.6}	−3429.6	HUS 86
	$A\,^1\Sigma^+$		951.8	−23688.		2377.4	YAN 80
RbH	$X\,^1\Sigma^+$	{4.8432}	13772.2	−28416.	{1824.8}	−2933.1	LAN 86
	$A\,^1\Sigma^+$		1824.9	−22145.		2187.2	KAT 85
CsH	$X\,^1\Sigma^+$	{5.3300}	13777.0	−26337.8	{1823.9}	−3634.8	ZEM 88
	$A\,^1\Sigma^+$		1025.1	−21250.		1766.2	HSI 78

rescence measurements for high v'' values in NaH and RbH are needed to reliably extend the range of the spectroscopic constants and the RKR potential energy curves.

Hybrid potential curves that extend beyond the outermost RKR turning points have been constructed for the four $X\,^1\Sigma^+$ and four $A\,^1\Sigma^+$ states. These curves are useful estimates for the determination of higher vibrational levels, until the RKR curves themselves can be extended. However, hybrid curves that are not firmly based on experimental data, that are just extrapolations beyond the observed data, are of unknown reliability and should be avoided. The RbH $A\,^1\Sigma^+$ state hybrid curve [PAR 87A] has already been identified as such an example.

The ionic-covalent curve crossing in the alkali hydrides has a long history [MUL 36]. We will not discuss this here in detail; the interested reader is referred to [YAN 82] for further discussion. However, we feel it useful to summarize (Table 6.2.) the nominal crossing distance, R_c, and $X\,^1\Sigma^+$ and $A\,^1\Sigma^+$ state potentials and derivatives at R_c which are obtained from the recommended potentials in this review. It should be noted that the changes from earlier results, e.g. from the corresponding experimental values in [YAN 82], are significant. Note that the analysis involves simply finding the two-state "crossing" internuclear distance, R_c, in each alkali hydride at which

$$\left.\frac{dV_X(R)}{dR}\right|_{R_c} = \left.\frac{dV_A(R)}{dR}\right|_{R_c}.$$

The potential energy in each state is then reported not only with respect to $V(R_e)$ but also with respect to the ion pair asymptote, i.e. the asymptote $M^+ + H^-$, calculated using the D_e values in Table 1.1, the alkali atomic ionization potential [MOO 71] and the electron affinity of the hydrogen atom (6083.10 cm^{-1} [HOT 85]). The potential energy curves used are RKR potentials except for hybrid potentials for the $X\,^1\Sigma^+$ states of NaH and CsH and an *ab initio* potential for the $X\,^1\Sigma^+$ state of RbH.

The ionic-covalent crossing is an example of potentially severe breakdown of the Born-Oppenheimer approximation. Nevertheless, LiH results (e.g. [CHA 86]), including non-negligible Born-Oppenheimer breakdown terms in adiabatic potential energy curves, support a purely adiabatic approximation even for $X\,^1\Sigma^+$ and $A\,^1\Sigma^+$ levels with significant vibrational amplitude in the region of the ionic-covalent crossing. Similar results are expected for the $X\,^1\Sigma^+$ and $A\,^1\Sigma^+$ levels of the other four alkali hydrides. However, fully nonadiabatic calculations (e.g. based on the nonadiabatic coupling potentials of Numrich and Truhlar [NUM 74, NUM 75, NUM 78]) might reveal observable nonadiabatic processes such as electronic predissociation

$$MH(A\,^1\Sigma^+, v, J) \rightarrow M + H,$$

especially for v, J levels with turning points near R_c.

6.5. Dissociation Energy

The present status of the alkali hydrides is that ground state dissociation energies for LiH [VID 84], KH [ZEM 88] and CsH [ZEM 88] are known to within 2 cm^{-1}. The uncertainties in D_e'' values for NaH (± 100 cm^{-1}) and RbH (± 600 cm^{-1}) demonstrate where further studies are needed to obtain precise D_e'' values.

Because the minima of the $A\,^1\Sigma^+$ state potential curves of KH, RbH and CsH are significantly uncertain (25 – 30 cm^{-1}), the associated T_e values for these three hydrides are also. Dissociation energies for the $A\,^1\Sigma^+$ states can be determined from the energy-balance formula $D_e' = D_e'' + [E(np, {}^2P_{1/2}) - E(ns, {}^2S)] - T_e$. Thus, since the atomic transition energies $[E(np, {}^2P_{1/2}) - E(ns, {}^2S)]$ are precisely known (≤ 0.01 cm^{-1} [MOO 71]), D_e' values can only be as precise as the corresponding T_e or D_e'' values. For example, although D_e'' for KH is uncertain by 0.6 cm^{-1} [ZEM 88], T_e is uncertain by 25 cm^{-1} [YAN 80]; hence $D_e' = 8698 \pm 25$ cm^{-1} (see Table 1.1). The other D_e' values in Table 1.1 are less certain than for KH. The determination of the minimum of an $A\,^1\Sigma^+$ state curve would improve the precision of T_e and D_e' significantly.

6.6. Electronic Structure Calculations

The literature contains numerous electronic structure calculations on the four alkali hydrides reviewed here. Some calculations focus on the long-range portion of the potential curve [PRO 77, BUS 86]; some calculate energy splittings at the ionic-covalent curve crossing distance [GRI 74, ADE 77]; some calculate oscillator strengths [WAT 76]; and some report ground state properties (D_e, R_e, ω_e) only, while testing various theoretical models [FUE 87]. Many, however, calculate complete potential energy curves [MEY 75, NUM 75, SAC 75, KAR 78, MEL 79, OLS 80A, LAS 81, STE 81, JEU 83A, LAN 86, ROS 87, CAR 89A]. For example, the CPF calculations of [LAN 86] determine accurate $X\,^1\Sigma^+$ state potential energy curves and dipole moment functions for NaH, KH and RbH. The [LAN 86] calculations virtually match the RKR potential for NaH. Because the calculated [LAN 86] potential curve is in very good agreement with the lower RKR portion of the potential energy curve for RbH, and because the *ab initio* calculation characterizes the complete curve (calculated D_e'' value agrees with the experimental D_e'' value, within the cited 600 cm^{-1} uncertainty), the theoretical potential curve is very useful for further studies on the $X\,^1\Sigma^+$ state of RbH. Moreover, [LAN 86] report a complete dipole moment function, lifetimes and dipole moment absorption matrix elements for the lower vibrational states of the $X\,^1\Sigma^+$ state.

The best theoretical $A\,^1\Sigma^+$ state potential curves appear to be those of [OLS 80A] for NaH, [ROS 87] for KH and RbH, and [JEU 83A, CAR 89A] for CsH.

Significantly, the predominant sources of information about potential energy curves for states other than the $X\,^1\Sigma^+$ and $A\,^1\Sigma^+$ states are *ab initio* electronic structure calculations. Several calculations are very impressive: potential energy curves and spectroscopic constant calculations of [ROS 87] (the lowest eighteen electronic states for KH and RbH) and [JEU 83A, CAR 89A] (the lowest nineteen and seventeen electronic states, respectively, for

CsH). These high quality and complete calculations should provide a valuable assist for further spectroscopic studies. An example where reliable theoretical calculations were of importance to clarify the experimental situation can be found in the very recent work of [CAR 89] where, based on their own accurate calculations and those of [JEU 83A], they corrected the misassignment [RIN 70] of the second $^3\Pi$ state of CsH (see Subsec. 5.3.).

Because of the availability of experimental potential energy curves, the alkali hydrides have been ideal test cases for various theoretical models. Various types of CI calculations and pseudopotential calculations have been performed; see Tables 2.6, 3.5, 4.4 and 5.5 for a brief summary. In particular, CsH has been a valuable test case for pseudopotential calculations and relativistic effects. For example, Laskowski and co-workers [LAS 81, LAS 83] used a relativistic electron core potential (RECP) method to calculate potential curves and dipole moment functions for $X\,^1\Sigma^+$ and $A\,^1\Sigma^+$ states of CsH. Initially they performed RECP two valence electron CI calculations [LAS 81]; later, they performed RECP ten valence electron CI calculations to examine the relative importance of core-valence correlation and relativistic effects [LAS 83].

6.7. Radiative and Dipole Properties

The radiative properties of the alkali hydrides discussed here have not been studied extensively experimentally. There are a few lifetime measurements in the $A\,^1\Sigma^+$ state for NaH [BAL 76, DAG 76, NED 83], KH [GIR 82], and CsH [FER 84]. Relative emission intensity measurements have been made only in CsH [YAN 81, FER 84]. Theoretical lifetime calculations (NaH [SAC 75B, DAG 76, TEL 86] and CsH [YAN 81, TEL 84]) and relative intensity calculations (NaH [SAC 75B] and CsH [YAN 81, TEL 84, CAR 89A]) depend upon the availability of $A-X$ transition dipole moment functions, such as found for NaH [SAC 75B] and CsH [LAS 81, CAR 89A]. Just as common appears to be the calculation of electronic dipole moment functions and the corresponding Einstein A coefficients for purely vibrational $X\,^1\Sigma^+$ bands (NaH [SAC 75A, ZEM 84], KH [LAN 86] and RbH [LAN 86]) and $A\,^1\Sigma^+$ bands (NaH [SAC 75A, ZEM 84]). There is a clear need for further experimental lifetime determinations and theoretical transition dipole moment function calculations.

6.8. Other Properties

A variety of other properties have been studied theoretically: quadrupole moments, field gradients at nuclei, polarizabilities, dipole moment derivatives, radial couplings, etc. Both experimental and theoretical studies have examined the collisional atomic charge exchange process (for example $H + Cs \rightarrow H^- + Cs^+$) and the cross sections have been reported. The papers by Alvarez and Cisneros [ALV 81] and Morgan *et al.* [MOR 85] review research in this area.

6.9. Positive Ions

Experimental studies on the potential curves of the positive ions of the alkali hydrides are confined to collisional experiments. Theoretical calculations are numerous and include the determination of potential curves for a number of electronic states; scattering cross sections are sometimes calculated also. See Tables 2.7, 3.6, 4.5 and 5.6 for a summary of the calculations for NaH^+, KH^+, RbH^+ and CsH^+, respectively, and also reviews by Alvarez and Cisneros [ALV 81] and Morgan *et al.* [MOR 85].

The best potential energy curve calculations are those of [OLS 81, LIU 81] for NaH^+ and [OLS 81] for KH^+.

6.10. Negative Ions

Experimental studies on the negative ions of the alkali hydrides are confined to collisional experiments, which are reviewed by [ALV 81, MOR 85]. Theoretical potential curve calculations have been performed for all four ions only by Karo and co-workers [KAR 78, STE 81] for the $X\,^2\Sigma^+$ state. In the case of NaH^-, several excited electronic state potential curves have also been calculated [OLS 80A, OLS 83].

7. Acknowledgments

The review presented here was aided by literally hundreds of discussions/correspondences with scientific colleagues over the last decade and a half. We particularly wish to thank: A. Amiot, J. T. Bahns, R. F. Barrow, N. D. Bhaskar, P. J. Dagdigian, F. Jenč, N. N. Haese, W. Happer, D. R. Herschbach, J. Hinze, J. R. Hiskes, Y. K. Hsieh, K. P. Huber, K. D. Jordan, A. M. Karo, H. Kato, S. R. Langhoff, B. C. Laskowski, M. Ligare, K. C. Lin, B. Liu, A. M. Lyyra, A. G. Maki, O. Nedelec, D. D. Nelson, R. E. Olson, F. B. Orth, A. Pardo, H. Partridge, S. D. Peyerimhoff, T. R. Proctor, N. H. Sabelli, E. S. Sachs, K. M. Sando, R. P. Saxon, A. S. Schlachter, W. J. Stevens, A. C. Tam, D. G. Truhlar, D. K. Watson, K. K. Verma, C. R. Vidal and T. Yabuzaki.

This work was supported in part by the Critical Compilation Program of the National Bureau of Standards (now the National Institute of Standards and Technology) and by the National Science Foundation.

8. References

ADE 77 Adelman, S. A., and D. R. Herschbach, Mol. Phys. 33, 793 (1977).

ALL 86 Allan, R. J., J. Phys. B **19**, 321 (1986).

ALM 32 Almy, G. M., and C. D. Hause, Phys. Rev. **42**, 242 (1932).

ALM 38 Almy, G. M., and M. Rassweiler, Phys. Rev. **53**, 890 (1938).

ALM 42 Almy, G. M., and A. C. Beiler, Phys. Rev. **61**, 476 (1942).

ALV 81 Alvarez, I. T., and C. G. Cisneros, Rev. Mex. Fisica **27**, 179 (1981).

AND 79 Anderson, C. J., A. M. Howald and L. W. Anderson, Nucl. Instrum. Methods **165**, 583 (1979).

AND 80 Anderson, C. J., R. J. Girnius, A. M. Howald and L. W. Anderson, Phys. Rev. A **22**, 822 (1980).

BAH 84 Bahns, J. T., and W. C. Stwalley, Appl. Phys. Lett. **44**, 826 (1984).

BAL 76 Baltayan, P., A. Jourdan and O. Nedelec, Phys. Lett. **58A**, 443 (1976).

BAR 66 Bartky, I. R., J. Mol. Spectrosc. **20**, 299 (1966).

BAR 66A Bartky, I. R., J. Mol. Spectrosc. **21**, 1 (1966).

BAR 66B Bartky, I. R., J. Mol. Spectrosc. **21**, 25 (1966).

BAR 76 Bartlett, R. J., and D. M. Silver, J. Chem. Phys. **64**, 4578 (1976).

BAR 76A Bartlett, R. J., and D. M. Silver, Phys. Rev. A **13**, 912 (1976).

BAR 88 Barclay, V. J., and J. S. Wright, Chem. Phys. **121**, 381 (1988).

BAS 73 Baskin, C. P., C. F. Bender and P. A. Kollman, J. Am. Chem. Soc. **95**, 5868 (1973).

BAT 56 Bates, D. R., and T. J. M. Boyd, Proc. Phys. Soc. (London) **69**, 910 (1956).

BEA 78 Bearman, G. H., S. D. Alspach and J. J. Leventhal, Phys. Rev. A **18**, 68 (1978).

BER 84 Berkowitz, J. K., and J. C. Zorn, Phys. Rev. A **29**, 611 (1984).

BHA 81 Bhaskar, N. D., J. Campiro, M. Ligare and W. Happer, Phys. Rev. A **46**, 1387 (1981).

BLA 83 Blais, N. C., D. G. Truhlar and B. C. Garrett, J. Chem. Phys. **78**, 2956 (1983).

BLU 77 Blustin, P. H., J. Chem. Phys. **66**, 5648 (1977).

BOH 68 Bohlen, H., G. Clausnitzer and H. Wilsch, Z. Physik **208**, 159 (1968).

BRI 81 Brieger, M., A. Hese, A. Renn and A. Sodeik, Chem. Phys. Lett. **78**, 153 (1981).

BRU 78 Bruns, R. E., and R. E. Brown, J. Chem. Phys. **68**, 880 (1978).

BUS 86 Bussery, B., M. Aubert-Frécon and M. Saute, Chem. Phys. **109**, 39 (1986).

CAD 67 Cade, P. E., and W. M. Huo, J. Chem. Phys. **47**, 649 (1967).

CAD 69 Cade, P. E., R. F. W. Bader, W. H. Henneker and I. Keaveny, J. Chem. Phys. **50**, 5313 (1969).

CAR 89 Carnell, M., and S. D. Peyerimhoff, Chem. Phys. Lett. **154**, 484 (1989).

CAR 89A Carnell, M., S. D. Peyerimhoff and B. A. Hess, Z. Phys. **D 13**, 317 (1989).

CHA 86 Chan, Y. C., D. R. Harding, W. C. Stwalley and C. R. Vidal, J. Chem. Phys. **85**, 2436 (1986).

CIS 76 Cisneros, C., I. Alvarez, C. F. Barnett and J. A. Ray, Phys. Rev. A **14**, 76 (1976).

CLA 70 Claxton, T. A., and D. McWilliams, Trans. Faraday Soc. **66**, 513 (1970).

COH 87 Cohen, E. R., and B. N. Taylor, Rev. Mod. Phys. **59**, 1121 (1987).

CRE 84 Crépin, C., J. Vergès and C. Amiot, Chem. Phys. Lett. **112**, 10 (1984).

CRE 84A Crépin, C., J. L. Picqué, G. Rahmat, J. Vergès, R. Vetter, F. X. Gadéa, M. Pelissier, F. Spiegelmann, and J. P. Malrieu, Chem. Phys. Lett. **110**, 395 (1984).

CRU 74 Cruse, J. A., and R. N. Zare, J. Chem. Phys. **60**, 1182 (1974).

CSA 67 Császár, M. L., and E. Koczkás, Acta Phys. Acad. Sci. Hung. **23**, 211 (1967).

DAG 76 Dagdigian, P. J., J. Chem. Phys. **64**, 2609 (1976).

DAG 79 Dagdigian, P. J., J. Chem. Phys. **71**, 2328 (1979).

DIM 74 Dimov, G. I., and G. V. Roslyakov, Prib. Tech Eksp. **3**, 31 (1974).

DIX 88 Dixon, D. A., J. L. Gole and A. Komornicki, J. Phys. Chem. **92**, 2134 (1988).

DON 64 Donnally, B. L., T. Clapp, W. Sawyer and M. Schultz, Phys. Rev. Lett. **12**, 502 (1964).

DUT 79 Dutta, N., R. Tkach, D. Frohlich, C. L. Tang, H. Mahr and P. L. Hartman, Phys. Rev. Lett. **42**, 175 (1979).

DYA 68 D'yachkov, B. A., and V. I. Zinenko, Atom. Energ. **24**, 18 (1968).

DYA 72 D'yachkov, B. A., V. I. Zinenko and M. A. Pavlii, Sov. Phys. – Tech. Phys. **16**, 1868 (1972).

FAR 82 Farber, M., R. D. Srivastava and J. W. Moyer, J. Chem. Thermo. **14**, 1103 (1982).

FER 84 Ferray, M., J. P. Visticot, H. Telle and B. Sayer, J. Chem. Phys. **81**, 191 (1984).

FRI 84 Fritsch, W., Phys. Rev. A **30**, 1135 (1984).

FUE 82 Fuentealba, P., H. Preuss, H. Stoll and L. von Szentpály, Chem. Phys. Lett. **89**, 418 (1982).

FUE 87 Fuentealba, P., O. Reyes, H. Stoll and H. Preuss, J. Chem. Phys. **87**, 5338 (1987).

GAD 86 Gadéa, F. X., F. Spiegelmann, M. Pelissier and J. P. Malrieu, J. Chem. Phys. **84**, 4872 (1986).

GAD 87 Gadéa, F. X., and J. Durup, Chem. Phys. Lett. **138**, 43 (1987).

GAD 88 Gadéa, F. X., J. M. L'Hermite, G. Rahmat and R. Vetter, Chem. Phys. Lett. **151**, 183 (1988).

GAR 81 Garrett, B. C., M. J. Redmon, D. G. Truhlar and C. F. Melius, J. Chem. Phys. **74**, 412 (1981).

GAR 81A Garrett, B. C., D. G. Truhlar and C. F. Melius, Phys. Rev. A **24**, 2853 (1981).

GAR 81B Garrett, B. C., and D. G. Truhlar, *Theoretical Chemistry: Advances and Perspectives*, **6A**, D. Henderson, ed. (Academic Press, New York, 1981), p. 215.

GAR 83 Garrett, B. C., D. G. Truhlar and C. F. Melius, *Energy Storage and Redistribution in Molecules*, J. Hinze, ed. (Plenum Press, New York, 1983), p. 375.

GAS 75 Gáspár, R., and I. Tamássey-Lentei, Acta Phys. Hung. **38**, 3 (1975).

GAY 39A Gaydon, A. G., and R. W. B. Pearse, Proc. Roy. Soc. **173**, 28 (1939).

GAY 39B Gaydon, A. G., and R. W. B. Pearse, Proc. Roy. Soc. **173**, 37 (1939).

GAY 68 Gaydon, A. G., *Dissociation Energies and Spectra of Diatomic Molecules*, 3rd edition (Chapman and Hall Ltd., London, 1968).

GHO 81 Ghodgaonkar, A. M., and K. Ramani, J. Chem. Soc. Faraday Trans. II **77**, 209 (1981).

GIR 77 Girnius, R. J., C. J. Anderson and L. W. Anderson, Phys. Rev. A **16**, 2225 (1977).

GIR 77A Girnius, R. J., L. W. Anderson and E. Staab, Nucl. Instrum. Methods **143**, 505 (1977).

GIR 80 Giroud, M., and O. Nedelec, J. Chem. Phys. **73**, 4151 (1980).

GIR 82 Giroud, M., and O. Nedelec, J. Chem. Phys. **77**, 3998 (1982).

GIR 85 Giroud, M., and O. Nedelec, Chem. Phys. **93**, 127 (1985).

GRI 74 Grice, R., and D. R. Herschbach, Mol. Phys. **27**, 159 (1974).

GRU 69 Grübler, W., P. A. Schmelzbach, V. König , and P. Marmier, Phys. Lett. **A29**, 440 (1969).

GRU 70 Grübler, W., P. A. Schmelzbach, V. König, and P. Marmier, Helv. Phys. Acta **43**, 254 (1970).

GUO 87 Guo, K., W. L. Jarrett and L. G. Butler, Inorg. Chem. **26**, 3001 (1987).

HAE 84 Haese, N. N., D. J. Liu and R. S. Altman, J. Chem. Phys. **81**, 3766 (1984).

HAM 87 Hammond, B. L., P. J. Reynolds and W. A. Lester, J. Chem. Phys. **87**, 1130 (1987).

HER 50 Herzberg, G., *Spectra of Diatomic Molecules*, 2nd edition (Van Nostrand Reinhold, New York, 1950).

HIS 78 Hiskes, J. R., A. M. Karo, P. A. Willmann and W. J. Stevens, Phys. Lett. A **68**, 221 (1978).

HOE 80 Höller, R., and H. Lischka, Mol. Phys. **41**, 1041 (1980).

HOO 77 Hooper, E. B., Jr., and P. A. Willmann, J. Appl. Phys. **48**, 1041 (1977).

HOR 30 Hori, T., Z. Phys. **62**, 352 (1930).

HOR 31 Hori, T., Z. Phys. **71**, 478 (1931).

HOR 33 Hori, T., Mem. Ryojun Coll. Eng. **6**, 1 (1933).

HOR 33A Hori, T., Mem. Ryojun Coll. Eng. **6**, 115 (1933).

HOT 85 Hotop, H., and W. C. Lineberger, J. Phys. Chem. Ref. Data **14**, 731 (1985).

HOW 81 Howald, A. M., L. W. Anderson and C. C. Lin, Phys. Rev. A **24**, 44 (1981).

HOW 82 Howald, A. M., R. E. Miers, J. S. Allen, L. W. Anderson and C. C. Lin, Phys. Lett. **92A**, 328 (1982).

HOW 83 Howald, A. M., L. W. Anderson and C. C. Lin, Phys. Rev. Lett. **51**, 2029 (1983).

HOW 84 Howald, A. M., R. E. Miers, J. S. Allen, L. W. Anderson and C. C. Lin, Phys. Rev. A **29**, 1083 (1984).

HSI 78 Hsieh, Y. K., S. C. Yang, A. C. Tam and W. C. Stwalley, J. Chem. Phys. **68**, 1448 (1978).

HSI 80 Hsieh, Y. K., S. C. Yang, A. C. Tam, K. K. Verma and W. C. Stwalley, J. Mol. Spectrosc. **83**, 311 (1980).

HUB 79 Huber, K. P., and G. Herzberg, *Constants of Diatomic Molecules*, (Van Nostrand Reinhold, New York, 1979).

HUF 76 Huffaker, J. N., J. Chem. Phys. **64**, 3175 (1976).

HUF 76A Huffaker, J. N., J. Chem. Phys. **64**, 4564 (1976).

HUS 86 Hussein, K., C. Effantin, J. d'Incan, J. Vergès and R. F. Barrow, Chem. Phys. Lett. **124**, 105 (1986).

ILI 67 Il'in, R. N., V. Oparin, E. S. Solov'ev and N. V. Fedorenko, Sov. Phys.-Tech. Phys. **11**, 921 (1967).

ILI 71 Il'in, R. N., V. A. Oparin, I. T. Serenkov, E. S. Solovyov and N. V. Fedorenko, in *Electronic and Atomic Collisions* (abstracts of papers of the VIIth International Conference on the Physics of Electronic and Atomic Collisions), L. M. Branscomb *et al.*, editors (North Holland, Amsterdam, 1971), p. 793.

IMA 41 Imanishi, S., Sci. Pap. Inst. Phys. Chem. Res. Japan **39**, 45 (1941).

INO 72 Inoue, N., Nucl. Fusion **12**, 130 (1972).

JAI 63 Jain, D. C., and P. Sah, J. Chem. Phys. **38**, 1553 (1963).

JAI 66 Jain, D. C., and R. C. Sahni, Proc. Phys. Soc. **88**, 495 (1966).

JAN 76 Janev, R. K., J. Chem. Phys. **64**, 1891 (1976).

JAN 78 Janev, R. K., and Z. M. Radulovic, Phys. Rev. A **17**, 889 (1978).

JEN 85 Jenč, F., and B. A. Brandt, J. Chem. Phys. **83**, 5486 (1985).

JEN 86 Jenč, F., and B. A. Brandt, J. Chem. Phys. **85**, 3702 (1986).

JEU 82 Jeung, G. H., J. P. Malrieu and J. P. Daudey, J. Chem. Phys. **77**, 3571 (1982).

JEU 83 Jeung, G. H., J. P. Daudey and J. P. Malrieu, J. Phys. B **16**, 699 (1983).

JEU 83A Jeung, G. H., F. Spiegelmann, J. P. Daudey and J. P. Malrieu, J. Phys. B **16**, 2659 (1983).

JEZ 85 Jeziorek, D., and B. Zurawski, Intl. J. Quantum Chem. **28**, 297 (1985).

JON 90 Jong, G., W. C. Stwalley and W. T. Zemke, J. Mol. Spectrosc., **143**, 336 (1990).

JOR 76 Jordan, K. D., K. M. Griffing, J. Denney, E. L. Andersen and J. Simons, J. Chem. Phys. **64**, 4730 (1976).

JOR 77 Jordan, K. D., J. Chem. Phys. **66**, 3305 (1977).

JOR 78 Jordan, K. D. and J. J. Wendoloski, Mol. Phys. **35**, 223 (1978).

KAR 78 Karo, A. M., M. A. Gardner and J. R. Hiskes, J. Chem. Phys. **68**, 1942 (1978).

KAT 85 Kato, H., Y. Toyosaka and T. Suzuki, Bull. Chem. Soc. Japan **58**, 562 (1985).

KAU 83 Kaur, A. J., P. C. Jain, P. S. Bakhshi and J. Shanker, Indian J. Chem. **22A**, 595 (1983).

KIM 82 Kimura, M., R. E. Olson and J. Pascale, Phys. Rev. A **26**, 1138 (1982).

KIM 82A Kimura, M., R. E. Olson and J. Pascale, Phys. Rev. A **26**, 3113 (1982).

KIR 78 Kirby, K., and A. Dalgarno, Astrophys. J. **224**, 444 (1978).

KNO 69 Knox, H. O., and M. R. H. Rudge, Mol. Phys. **17**, 377 (1969).

KUB 81 Kubach, C., and V. Sidis, Phys. Rev. A **23**, 110 (1981).

KUL 79 Kulkarni, S. V., and L. K. Sharma, Indian J. Phys. **53A**, 616 (1979).

KUM 86 Kumar, M., A. J. Kaur and J. Shanker, J. Chem. Phys. **84**, 5735 (1986).

LAN 86 Langhoff, S. R., C. W. Bauschlicher and H. Partridge, J. Chem. Phys. **85**, 5158 (1986).

LAS 81 Laskowski, B. C., and J. R. Stallcop, J. Chem. Phys. **74**, 4883 (1981).

LAS 83 Laskowski, B. C., S. P. Walch and P. A. Christiansen, J. Chem. Phys. **78**, 6824 (1983).

LEO 87 Leopold, K. R., L. R. Zink, K. M. Evenson and D. A. Jennings, J. Mol. Spectrosc. **122**, 150 (1987).

LEP 87 Lepetit, B., M. LeDourneuf, J. M. Launay and F. X. Gadéa, Chem. Phys. Lett. **135**, 377 (1987).

LEP 89 Lepetit, B., J. M. Launay and M. LeDourneuf, Chem. Phys. **134**, 93 (1989).

LES 71 Leslie, T. E., K. P. Sarver and L. W. Anderson, Phys. Rev. A **4**, 408 (1971).

LEW 71 Lewis, E. L., L. F. McNamara and H. H. Michels, Phys. Rev. A **3**, 1939 (1971).

LIG 82 Ligare, M., Z. Wu, N. D. Bhaskar and W. Happer, J. Chem. Phys. **76**, 3480 (1982).

LIN 89 Lin, K. C., and H. C. Chang, J. Chem. Phys. **90**, 6151 (1989).

LIU 81 Liu, B., R. E. Olson and R. P. Saxon, J. Chem. Phys. **74**, 4216 (1981).

MAG 88 Magg, U., and H. Jones, Chem. Phys. Lett. **146**, 415 (1988).

MAG 88A Magg, U., H. Birk and H. Jones, Chem. Phys. Lett. **151**, 503 (1988).

MAG 88B Magg, U., and H. Jones, Chem. Phys. Lett. **148**, 6 (1988).

MAK 89 Maki, A. G., and W. B. Olson, J. Chem. Phys. **90**, 6887 (1989).

MAR 77 Marsh, F. J., and M. S. Gordon, Chem. Phys. Lett. **45**, 255 (1977).

MCA 79 McAdon, M. H., and D. D. Konowalow, J. Chem. Phys. **71**, 3089 (1979).

MEL 79 Melius, C. F., R. W. Numrich and D. G. Truhlar, J. Phys. Chem. **83**, 1221 (1979).

MEY 75 Meyer, W., and P. Rosmus, J. Chem. Phys. **63**, 2356 (1975).

MEY 75A Meyer, F. W., and L. W. Anderson, Phys. Lett. A **54**, 333 (1975).

MEY 77 Meyer, F. W., C. J. Anderson and L. W. Anderson, Phys. Rev. A **15**, 455 (1977).

MEY 80 Meyer, F. W., J. Phys. B **13**, 3823 (1980).

MIE 82 Miethe, K., T. Dreiseidler and E. Salzborn, J. Phys. B **15**, 3069 (1982).

MO 85 Mo, O., A. Riera and M. Yáñez, Phys. Rev. A **31**, 3977 (1985).

MON 85 Monteiro, T. S., A. S. Dickinson and E. L. Lewis, J. Phys. B **18**, 3499 (1985).

MOO 71 Moore, C. E., *Atomic Energy Levels*, vol. I-III, NSRDS-NBS 35 (U.S. Government Printing Office, Washington, DC, 1971).

MOR 85 Morgan, T. J., R. E. Olson, A. S. Schlachter and J. W. Gallagher, J. Phys. Chem. Ref. Data **14**, 971 (1985).

MUL 36 Mulliken, R. S., Phys. Rev. **50**, 1017, 1028 (1936).

MUR 83 Murthy, N. S., T. Manisekaran and N. S. Bapat, J. Quant. Spectrosc. Rad. Transfer **29**, 183 (1983).

NAG 80 Nagata, T., J. Phys. Soc. Japan **48**, 2068 (1980).

NAG 82 Nagata, T., Mass. Spectrosc. (Japan) **30**, 153 (1982).

NAG 83 Nagata, T., J. Phys. Soc. Japan **52**, 4 (1983).

NED 83 Nedelec, O., and M. Giroud, J. Chem. Phys. **79**, 2121 (1983); **80**, 2987(E) (1984).

NUM 74 Numrich, R. W., Ph.D. Thesis, University of Minnesota, Minneapolis, 1974.

NUM 75 Numrich, R. W., and D. G. Truhlar, J. Phys. Chem. **79**, 2745 (1975).

NUM 78 Numrich, R. W., and D. G. Truhlar, J. Phys. Chem. **82**, 168 (1978).

OHA 75 O'Hare, B. G., R. W. McCullough and H. B. Gilbody, J. Phys. B **8**, 2968 (1975).

OLS 35 Olsson, E., Z. Phys. **93**, 206 (1935).

OLS 71 Olson, R. E., F. T. Smith and E. Bauer, Appl. Optics **10**, 1848 (1971).

OLS 76 Olson, R. E., E. J. Shipsey and J. C. Browne, Phys. Rev. A **13**, 180 (1976).

OLS 80 Olson, R. E., R. P. Saxon and B. Liu, J. Phys. B **13**, 297 (1980).

OLS 80A Olson, R. E., and B. Liu, J. Chem. Phys. **73**, 2817 (1980).

OLS 80B Olson, R. E., Phys. Lett. **77A**, 143 (1980).

OLS 83 Olson, R. E., *Energy Storage and Redistribution in Molecules*, J. Hinze, ed. (Plenum Press, New York, 1983), p. 185.

OLS 84 Olson, R. E., M. Kimura and H. Sato, Phys. Rev. A **30**, 1692 (1984).

OLS 85 Olson, R. E., and M. Kimura, Phys. Rev. A **32**, 3092 (1985).

OMN 80 Omnès, R., J. Phys. Lett. **41**, L63 (1980).

ORT 80 Orth, F. B., W. C. Stwalley, S. C. Yang and Y. K. Hsieh, J. Mol. Spectrosc. **79**, 314 (1980).

PAN 49 Pankhurst, R. C., Proc. Phys. Soc. (London) Ser. A **62**, 191 (1949).

PAR 81 Partridge, H., S. R. Langhoff, W. C. Stwalley and W. T. Zemke, J. Chem. Phys. **75**, 2299 (1981).

PAR 83 Pardo, A., J. M. L. Poyato, M. S. Guijarro and J. I. Fernandez-Alonso, J. Mol. Spectrosc. **97**, 248 (1983).

PAR 87 Pardo, A., J. M. L. Poyato and J. J. Camacho, Spectrochim. Acta **43A**, 679 (1987).

PAR 87A Pardo, A., J. J. Camacho, J. M. L. Poyato and E. Martin, Chem. Phys. **117**, 149 (1987).

PAR 87B Pardo, A., J. J. Camacho, J. M. L. Poyato and E. Martin, Spectrochim. Acta **43A**, 887 (1987).

PAR 88 Pardo, A., J. J. Camacho, J. M. L. Poyato and E. Martin, Chem. Phys. **121**, 41 (1988).

PAR 88A Pardo, A., J. J. Camacho, J. M. L. Poyato and E. Martin, Spectrochim. Acta **44A**, 951 (1988).

PEA 84 Pearson, E. W., M. D. Jackson and R. G. Gordon, J. Phys. Chem. **88**, 119 (1984).

PIC 80 Picqué, J. L., J. Vergès and R. Vetter, J. Phys. Lett. **41**, L305 (1980).

PIE 81 Pietro, W. J., E. S. Blurock, R. T. Hout, W. J. Hehre, D. J. deFrees and R. F. Stewart, Inorg. Chem. **20**, 3650 (1981).

PIN 79 Pineda, J., O. Novaro, J. P. Daudey and E. Blaisten-Barojas, J. Chem. Phys. **71**, 5124 (1979).

PRA 74 Pradel, P., F. Roussel, A. S. Schlachter, G. Spiess and A. Valance, Phys. Rev. A **10**, 797 (1974).

PRA 79 Prasad, S. C., N. N. Singh and K. P. Thakar, J. Chem. Soc. Faraday Trans. II **75**, 1717 (1979).

PRA 79A Pradel, P., G. Spiess, V. Sidis and A. Valance, J. Phys. B **12**, 1485 (1979).

PRA 81 Pradel, P., M. El Maddarsi and A. Valance, J. Phys. B **14**, 541 (1981).

PRE 81 Preuss, H., H. Stoll, U. Wedig and T. Krüger, Intl. J. Quantum Chem. **19**, 113 (1981).

PRO 77 Proctor, T. R., and W. C. Stwalley, J. Chem. Phys. **66**, 2063 (1977).

PYY 81 Pyykkö, P., J. G. Snijdero and E. J. Baerends, Chem. Phys. Lett. **83**, 432 (1981).

RAF 73 Raffenetti, R. C., and K. Ruedenberg, J. Chem. Phys. **59**, 5978 (1973).

RAH 87 Rahmat, G., F. Spiegelmann, J. Vergès and R. Vetter, Chem. Phys. Lett. **135**, 459 (1987).

RAY 77 Ray, N. K., S. P. Mehandru and J. D. Switalski, Chem. Phys. **47**, 562 (1977).

RAY 79 Ray, N. K., L. Samuels and R. G. Pau, J. Chem. Phys. **70**, 3680 (1979).

RIN 70 Ringström, U., J. Mol. Spectrosc. **36**, 232 (1970).

ROS 70 Rosen, B., *Tables of Constants and Numerical Data* (Pergamon Press, New York, 1970).

ROS 77 Rosmus, P., and W. Meyer, J. Chem. Phys. **66**, 13 (1977).

ROS 78 Rosmus, P., and W. Meyer, J. Chem. Phys. **69**, 2745 (1978).

ROS 81 Rosmus, P., and W. Meyer, J. Chem. Phys. **74**, 4217 (1981).

ROS 87 Ross, A., B. Bussery, G. H. Jeung, M. C. Bacchus-Montabonel and M. Aubert-Frécon, J. Chim. Phys. **84**, 745 (1987).

ROU 74 Roueff, E., J. Phys. B **7**, 185 (1974).

RUP 77 Rupp, M., and R. Ahlrichs, Theoret. Chim. Acta (Berl.) **46**, 117 (1977).

RYD 31 Rydberg, R., Z. Physik **73**, 376 (1931); **80**, 514 (1933); O. Klein, Z. Physik **76**, 226 (1932); and A. L. G. Rees, Proc. Phys. Soc. **59**, 998 (1947).

SAC 75 Sachs, E. S., J. Hinze and N. H. Sabelli, J. Chem. Phys. **62**, 3367 (1975).

SAC 75A Sachs, E. S., J. Hinze and N. H. Sabelli, J. Chem. Phys. **62**, 3377 (1975).

SAC 75B Sachs, E. S., J. Hinze and N. H. Sabelli, J. Chem. Phys. **62**, 3384 (1975).

SAC 75C Sachs, E. S., J. Hinze and N. H. Sabelli, J. Chem. Phys. **62**, 3389 (1975).

SAC 75D Sachs, E. S., J. Hinze and N. H. Sabelli, J. Chem. Phys. **62**, 3393 (1975).

SAK 81 Sakai, Y., H. Tatewaki and S. Huzinaga, J. Comp. Chem. **2**, 108 (1981).

SAS 81 Sastry, K. V. L. N., E. Herbst and F. C. DeLucia, J. Chem. Phys. **75**, 4753 (1981).

SAS 81A Sastry, K. V. L. N., E. Herbst and F. C. DeLucia, Astrophys. J. **248**, L53 (1981).

SAT 82 Sato, T., T. Yabuzaki and T. Ogawa, Jap. J. Appl. Phys. **21**, 1599 (1982).

SAY 81 Sayer, B., M. Ferray, J. Lozingot and J. Berlande, J. Chem. Phys. **75**, 3894 (1981).

SCH 69 Schlachter, A. S., P. J. Bjorkholm, D. H. Loyd, L. W. Anderson and W. Haeberi, Phys. Rev. **177**, 184 (1969).

SCH 78 Scheidt, H., G. Spiess, A. Valance and P. Pradel, J. Phys. B **11**, 2665 (1978).

SCH 80 Schlachter, A. S., K. R. Stalder and J. W. Stearns, Phys. Rev. A **22**, 2494 (1980).

SEL 67 Sellin, I. A., and L. Granoff, Phys. Lett. A **25**, 484 (1967).

SEV 85 Sevin, A., and P. Chaquin, Chem. Phys. **93**, 49 (1985).

SID 78 Sidis, V., and C. Kubach, J. Phys. B **11**, 2687 (1978).

SIN 62 Singh, N. L., and D. C. Jain, Proc. Phys. Soc. **79**, 753 (1962).

SIN 82 Singer, S. J., K. F. Freed and Y. B. Band, Chem. Phys. Lett. **91**, 12 (1982).

SIN 84 Singer, S. J., K. F. Freed and Y. B. Band, J. Chem. Phys. **81**, 3091 (1984).

SOL 67 Solovyov, E. S., R. N. Il'in, V. A. Oparin and N. V. Fedorenko, in *Vth International Conference on the Physics of Electronic and Atomic Collisions* (Abstracts of Papers), I. P. Klaks and E. S. Solovyov, editors (Publishing House "Nauka", Leningrad, 1967), p. 6.

SOL 68 Solov'ev, E. S., R. N. Il'in, V. A. Oparin and N. V. Fedorenko, Sov. Phys. – JETP **26**, 1097 (1968).

SPI 70 Spiess, G., A. Valance and P. Pradel, Phys. Lett. **31**, 434 (1970).

SPI 72 Spiess, G., A. Valance and P. Pradel, Phys. Rev. A **6**, 746 (1972).

STE 81 Stevens, W. J., A. M. Karo and J. R. Hiskes, J. Chem. Phys. **74**, 3989 (1981).

STW 72 Stwalley, W. C., J. Chem. Phys. **56**, 2485 (1972).

STW 75 Stwalley, W. C., J. Chem. Phys. **63**, 3062 (1975).

STW 78 Stwalley, W. C., S. C. Yang, Y. K. Hsieh, F. B. Orth and K. C. Li, J. Chem. Phys. **69**, 1791 (1978).

SUN 85 Sundholm, D., P. Pyykkö and L. Laaksonen, Mol. Phys. **55**, 627 (1985).

SZE 82 Szentpàly, L. von, P. Fuentealba, H. Preuss and H. Stoll, Chem. Phys. Lett. **93**, 555 (1982).

TAM 75 Tam, A. C., G. Moe and W. Happer, Phys. Rev. Lett. **35**, 1630 (1975).

TAM 76 Tam, A. C., and W. Happer, J. Chem. Phys. **64**, 2456 (1976).

TAM 77 Tam, A. C., W. Happer and D. Siano, Chem. Phys. Lett. **49**, 320 (1977).

TAM 89 Tamássy-Lentei, I., and A. Derecskei-Kovács, Intl. J. Quantum Chem. **36**, 277 (1989).
TAN 89 Tanaka, T., T. Mitsui, K. Sugiyama, M. Kitano and T. Yabuzaki, Phys. Rev. Lett. **63**, 1390 (1989).
TEL 84 Telle, H. H., J. Chem. Phys. **81**, 195 (1984).
TEL 86 Telle, H. H., J. Mol. Struc. **143**, 565 (1986).
TUA 74 Tuan, V. N., G. Gautherin and A. S. Schlachter, Phys. Rev. A **9**, 1242 (1974).
VAL 78 Valance, A., Chem. Phys. Lett. **56**, 289 (1978).
VAR 63 Varshni, Y. P., and R. C. Shukla, Rev. Mod. Phys. **35**, 130 (1963).
VAR 88 Varshni, Y. P., Can. J. Chem. **66**, 763 (1988).
VER 82 Verma, K. K., and W. C. Stwalley, J. Chem. Phys. **77**, 2350 (1982).
VID 82 Vidal, C. R., and W. C. Stwalley, J. Chem. Phys. **77**, 883 (1982).
VID 84 Vidal, C. R., and W. C. Stwalley, J. Chem. Phys. **80**, 2697 (1984).
VIS 82 Visticot, J. P., J. Lozingot and B. Sayer, Chem. Phys. Lett. **86**, 425 (1982).
VIS 83 Visticot, J. P., M. Ferray, J. Lozingot and B. Sayer, J. Chem. Phys. **79**, 2839 (1983).
VIS 86 Visticot, J. P., M. Ferray, P. d'Oliveira and B. Sayer, J. Chem. Phys. **84**, 1482 (1986).
WAN 87 Wang, Y., R. L. Champion and L. D. Doverspike, Phys. Rev. A **35**, 1503 (1987).
WAN 87A Wang, Y., R. L. Champion and L. D. Doverspike, Phys. Rev. A **36**, 381 (1987).
WAT 76 Watson, D. K., R. F. Stewart and A. Dalgarno, Mol. Phys. **32**, 1661 (1976).
WIL 63 Wilkinson, P. G., Astrophys. J. **138**, 778 (1963).
WIL 77 Wilson, S., and D. M. Silver, J. Chem. Phys. **66**, 5400 (1977).
YAB 80 Yabuzaki, T., T. Sato and T. Ogawa, J. Chem. Phys. **73**, 2780 (1980).
YAN 80 Yang, S. C., Y. K. Hsieh, K. K. Verma and W. C. Stwalley, J. Mol. Spectrosc. **83**, 304 (1980).
YAN 81 Yang, S. C., Y. K. Hsieh, A. C. Tam, W. T. Zemke, K. K. Verma and W. C. Stwalley, J. Chem. Phys. **75**, 3679 (1981).
YAN 82 Yang, S. C., and W. C. Stwalley, ACS Symp. Ser. **179**, 241 (1982).
YAN 82A Yang, S. C., J. Chem. Phys. **77**, 2884 (1982).
YAN 83 Yang, S. C., D. D. Nelson and W. C. Stwalley, J. Chem. Phys. **78**, 4541 (1983).
ZEM 84 Zemke, W. T., R. E. Olson, K. K. Verma, W. C. Stwalley and B. Liu, J. Chem. Phys. **80**, 356 (1984); **85**, 4209(E) (1986).
ZEM 88 Zemke, W. T., and W. C. Stwalley, Chem. Phys. Lett. **143**, 84 (1988).